Geochemical Fingerprinting of Yellowstone Hotspot Track (YHT) Eruptions from Ash Beds in the Central United States

By
Maggie Graham
The University of Kansas, 2019

Submitted to the graduate degree program in Geology and the Graduate Faculty of the University of Kansas in partial fulfillment of the requirements
for the degree of Master of Science

Chair: Andreas Möller

Greg Ludvigson

Noah McLean

Date Defended: 16 December 2019

The thesis committee for Maggie Graham certifies that this is the approved version of the following thesis:

Geochemical Fingerprinting of Yellowstone Hotspot Track (YHT) Eruptions from Ash Beds in the Central United States

Chair: Andreas Möller

Date Approved: 16 December 2019

ABSTRACT

Volcanic ash beds have been shown to be reliable stratigraphic marker beds because they can be radiometrically dated using magmatic minerals: e.g. zircon, sanidine, etc. This can be utilized in any region containing ash beds and can be especially helpful where beds are laterally discontinuous, such as in the Ogallala Formation in western Kansas and Nebraska and overlying Pliocene and Pleistocene strata. These contain abundant volcanic ashfall beds, but regional correlations of these have so far been limited, due to their non-continuous outcrops and complex stratigraphy. U-Pb dating of zircon by laser ablation inductively coupled plasma mass spectrometry (LA-ICP-MS) at The University of Kansas from several ash outcrops has confirmed the correlation of these ashes with Yellowstone hotspot track (YHT) eruptions.

Volcanic glasses from individual eruptions exhibit unique geochemical signatures, therefore lending each eruption its own distinct geochemical fingerprint. This tephrochronological approach yields robust correlations between the ash beds in the Great Plains strata of Kansas and Nebraska and their YHT source eruptions. The YHT eruptions Lava Creek B (0.6 Ma) and Huckleberry Ridge (2.1 Ma) of the Yellowstone Plateau and the Ibex Hollow (11.93 Ma) eruption of the Bruneau-Jarbidge (10.5-12.7 Ma) eruptive center on the Snake River Plain have previously been correlated to ash beds in western and central Kansas as well as northeastern Nebraska by major and trace element concentrations. Ash samples were collected in Norton, Smith, Jewell, and Meade Counties in Kansas and the Ashfall Fossil Beds State Historical Park in northeastern Nebraska. Trace element data trends of the Norton and Smith county, KS ashes can be correlated to the Ibex Hollow eruption (11.93 Ma) of the Bruneau-Jarbidge YHT eruptive center when compared to published values. Trace elements in volcanic glass shards from an ash bed in Jewell county correlate to Lava Creek B (0.6 Ma). Samples from different locations in Meade County, KS can be correlated with Huckleberry Ridge (2.1 Ma) and Lava Creek B (0.63 Ma), respectively. The sample taken from the basal unit of the deposit in Ashfall Fossil Bed State Historical Park, NE correlates with the Ibex Hollow eruption of the Bruneau Jarbidge eruptive center. Utilizing single shard analysis to generate bivariate elemental plots, chemical trends, and multi-element correlation coefficients proved to be more useful for determining correlations as opposed to comparing average measured values to published average values.

The insight from this research into the provenance of volcanic glass helps to further refine the understanding of dispersal of volcanic ash and other minerals from their associated eruptive centers, and the chronostratigraphy of High Plains, especially the Ogallala Formation. Research discussed here strives to demonstrate advantages in both processing time and overall analytical cost compared to traditional U-Pb techniques. This technique is also applicable to deposits that are too young to be reliably dated using U-Pb dating. The demonstrated high efficiency of the geochemical fingerprinting approach will allow researchers to have a denser coverage of the hundreds of ash deposits throughout the Central United States, and elsewhere, to improve stratigraphic correlations.

ACKNOWLEDGEMENTS

This work was initiated as part of a larger regional study by Dr. Greg Ludvigson and Dr. Jon Smith at the Kansas Geological Survey. The time, attention, and dedication given by Dr. Andreas Moeller, went above and beyond what is expected of an advisor. Special thanks are owed to Dr. Noah McLean and Dr. Greg Ludvigson for lending their time and expertise in mentoring this project as well. Thanks are owed to Dr. Jon Smith, Dr. Tony Layzell, Jason Hallman, and Elijah Turner for collecting and sharing samples and for providing crucial data for this project through their work. Thanks are also owed to Tyrell Tenpenny, Dr. Jeffrey Oalmann, Dr. Joe Andrew and the other KU IGL members who provided invaluable assistance, training, and guidance. Thanks are owed to the Wanner family for granting property access.

Special thanks are given to Brandon Graham, Theodore Graham, Dr. Blair Schneider, Sarah Rupert, Yuri Rupert, Emily Bunse, and Brittany Malone, for their much needed support and motivation. Partial support for this project comes from the University of Kansas, the Kansas Geological Foundation, the Association for Women in Geosciences, and Encana Energy. Logistical and financial support from the KGS was made possible by a USGS STATEMAP grant to the KGS.

TABLE OF CONTENTS

INTRODUCTION

Reconstructing the chronostratigraphy and depositional history of continental basins is a difficult task. Volcanic ash beds play an important role as relative and absolute time markers in many of these studies where biostratigraphy is generally not applicable or does not supply the necessary time resolution, as for example for the Neogene Ogallala Formation of the Central USA and overlying strata (Swinehart, 1974; Sweet, 1999; Ludvigson et al., 2009). The present study uses geochemical "fingerprinting" of individual volcanic glass shards by laser ablation inductively coupled mass spectrometry (LA-ICP-MS) to test the robustness of this approach and methodology, and compares it to the previously used bulk chemical approach of solution ICP-MS (e.g. David, 2009), to Electron Microprobe (EMP) for major and minor elements and X-Ray Fluorescence (XRF) for minor and trace elements (e.g. Perkins 1988, Perkins & Nash 2002), and to the LA-ICP-MS data of Pearce et al. (2004). Geochemical fingerprinting takes advantage of a volcanic eruption's unique chemical signature by comparing multiple major, minor, and trace elements of an unknown ash deposit to the chemistry of an ash deposit of known origin in order to effectively identify an ash deposit of unknown origin (details below). Coupled with physical identification methods (e.g. petrography) and/or mineral ages, geochemical fingerprinting provides robust correlations between ash units (e.g. Lowe, 2011). Methods defined here are applied to the Ogallala Formation in the High Plains region of the US and overlying Pleistocene strata in effort to produce robust chronologic correlations.

The stratigraphy of many continental sedimentary units throughout the central US is difficult to reconstruct due to lack of continuous beds or defined stratigraphic units across wide regions. One such case is the Ogallala Formation in the Central US (Fig 1, Fig 3) and overlying Pleistocene units. These are continental deposits in which classic lithostratigraphy is difficult to perform outside of localized basins or small regions. Bedding is laterally discontinuous, therefore, defining consistently identifiable units for the entire reach of a formation is impossible (Ludvigson et al., 2009). Biostratigraphy can give insights into a specific age range, but the age uncertainty (estimated ~3 Ma for the Ogallala Fm.) associated with this evidence is too high to be of much utility where precise ages of units are needed to understand stratigraphic architecture (Fig 1) (Diffendal, 1982).

Volcanic ash beds can be used as marker beds in many depositional environments, e.g. marine sediments, lacustrine and continental basins (Boellstorff 1976; Perkins et al., 1995; Hannan & Totten, 1996; Perkins 1998; Perkins & Nash, 2002). Assigning a volcanic ash layer to a specific source eruption age allows lateral correlations to be made. Several minerals in these deposits, such as zircon, sanidine, and apatite can be reliably dated using U-Pb or Ar-Ar geochronology (Harley & Kelly 2007; Gehrels 2011; Rivera et al, 2014; Matthews et al, 2015).

Additionally, since each eruption contains a unique geochemical signature, minor and trace element data from volcanic glass shards and minerals found in ash bed deposits can be used to recognize each eruption from a particular eruptive center with relative certainty (e.g. Perkins & Nash, 2002; Pearce et al., 2004; Tomlinson et al., 2010; Lowe, 2011). This method of characterizing volcanic ash deposits is known as geochemical fingerprinting. Geochemical fingerprinting is a method that takes advantage of the unique major and trace element compositions of separate volcanic eruptions. Because no two eruptions - even from the same volcanic center - are the same, we can resolve the differences using their geochemical fingerprint (e.g. Perkins & Nash, 2002; Pearce, 2007; David, 2009; Tomlinson et al., 2010). Studies using this tephrochronological technique have been successful in correlating proximal regions to major volcanic centers, such as those in Wyoming, Montana, and Idaho (e.g. Perkins & Nash, 2002) with respect to the Yellowstone Hotspot Track (YHT) and in many other studies worldwide (e.g. Pearce et al., 2007; Steinhauser et al., 2010; Kraus et al., 2013; Monteath et al., 2019). Geochemical fingerprinting is also useful for ash deposits distal to possible eruption locales and has been successfully performed in regions such as Nebraska, Utah, and the Gulf of Mexico (e.g. Perkins et al., 1998; Perkins and Nash, 2002; Pearce, 2004; Totten et al., 2005). It specifically has utility in locales where stratigraphic correlations have otherwise been difficult to obtain, such as the focus of this study, the Ogallala Formation and overlying Pleistocene units in the Central United States (e.g. David, 2009; Ludvigson et al., 2009). Eruptions of interest for stratigraphic work in near-surface Neogene strata of the Ogallala Formation and overlying Pleistocene units in Kansas and Nebraska include ashes from the Lava Creek B (0.63 Ma), and Huckleberry Ridge (2.1 Ma) eruptions, and from the Bruneau-Jarbidge (10.5-12.7 Ma) eruptive center of the YHT (Fig. 2) (Izett, 1981; David, 2009; Ludvigson et al., 2009). U-Pb geochronology of zircons at The University of Kansas has dated ash beds in the Ogallala Fm. from locations in central Kansas (Hallman, 2015) at 11.7 ± 0.1 Ma, and in NE Nebraska within uncertainty to the same age at 11.86 ± 0.13 Ma (Turner, 2018; Smith et al. 2018). These ages fall into the age range of the Ibex Hollow eruption of the Bruneau-Jarbidge eruptive center of the YHT.

This study focuses on establishing and testing a method and workflow for geochemical fingerprinting of volcanic glass by laser ablation inductively coupled plasma mass spectrometry (LA-ICP-MS) at The University of Kansas. The approach is tested on volcanic glass from ash beds in six selected locations of Kansas and Nebraska, selected based on previously documented ages and chemical analyses (Izett and Wilcox, 1981; Ludvigson, et al., 2009; Wan, 2008, pers. comm. to Ludvigson; David, 2009; Hallman, 2016; Turner, 2017; Smith et al. 2018;) (Table 1). The goal of this research is to take advantage of recorded age and geochemical data to provide robust correlations for the chosen samples. Whether the method is able to yield unique geochemical characteristics for each eruption event that deposited ashes in the central United States will be tested, and also which minor and trace elements are best suited in this approach. It is hypothesized that geochemical fingerprinting of glass shards by LA-ICP-MS is less labor-intensive and therefore faster and less expensive than U-Pb zircon geochronology. The results will help correlate time equivalent units of the Ogallala Fm. and overlying strata across the Central US and to reevaluate the mapped extents of these formations.

The YHT eruptions Lava Creek B (0.6 Ma), Huckleberry Ridge (2.1 Ma) of the Yellowstone Plateau and the Bruneau-Jarbidge (10.5-12.7 Ma) eruptive center of the Snake River Plain, have previously been correlated to ash beds in western and central Kansas using major and trace element concentrations (Pearce et al., 2004; David, 2009; Ludvigson et al., 2009). Ash samples were collected in Norton, Smith, Jewell, and Meade Counties in Kansas and Ashfall Fossil beds State Historical Park in Northeastern Nebraska.

The insight from this research into the provenance of volcanic glass will help further refine the understanding of dispersal of ash and other minerals from their associated eruptive centers, and the Neogene chronostratigraphy of the Central US. The results of this study on geochemical fingerprinting of individual volcanic glass shards by LA-ICP-MS will test three main hypotheses: (1) can distal ash deposits be positively correlated to their source eruptions using LA-ICP-MS analytical methods, (2) can differences in chemistry due to alteration or other petrologic process be identified, (3) can the obtained results be used to make stratigraphic correlations across units that span across large areas, such as the Ogallala Fm. and overlying Pleistocene units in the Central US.

GEOLOGICAL SETTING

Ogallala Formation

The Ogallala Formation consists of fluvial and eolian sediments shed from the uplifting Rocky Mountains onto the Great Plains during the Miocene-earliest Pliocene (Fig. 1). This formation covers the modern-day High Plains region in the central United States extending from New Mexico and Texas in the south to Wyoming and South Dakota in the north (Fenneman, 1917) (Fig 3). The formation is largely made up of gravels, sand, and clays, and contains abundant lenticular ashfall beds of limited extent. Minerals found in ashfall beds make them well-suited for methods related to dating continental deposits (e.g. Swineford, 1963; Frye et al., 1956; Gutentag et al., 1984; Ludvigson, 2009). Most of the volcanic ashes in these units are sourced from large-scale explosive eruptions related to the Yellowstone Hotspot Track (YHT). The Ogallala Formation also hosts the High Plains aquifer, which is the source of much of the drinking and agricultural water used in this expansive region of the central United States (Sophocleous, 2009). The Ogallala is overlain by Pleistocene strata in the Western region of Kansas, which consists of terrace deposits, loess, and dune sands (Kansas Geological Survey, 2008) and locally contain volcanic ash lenses (Ludvigson et al., 2009).

Yellowstone Hotspot Track

The Yellowstone Hotspot Track (YHT) (Pierce & Morgan 1992; Ellis et al, 2013) is defined by a line of volcanic caldera eruptions thought to be caused by a mantle plume under the Northwestern United States. Eruptions began near the Nevada-Oregon border at ca.16.4-16.7 Ma (e.g. Bruesecke et al. 2008; Coble & Mahood, 2012) and occur with a frequency of about 600,000 years. The most recent eruption occurred in the western portion of Wyoming and is called the Lava Creek B eruption, recently re-evaluated to have an age of ca. 630 ka (Matthews et al. 2015). Caldera eruptions are known to be extremely explosive in nature and can produce over 300 km^3 of material in a single eruption (Perkins & Nash, 2002). Ash injected into the stratosphere from these eruptions can travel thousands of kilometers before being deposited in regions far away from any appreciable volcanic activity, i.e. for the YHT eruptions in Kansas and Nebraska (Totten et al., 2005). Ashfall deposits of interest for this study include Ibex Hollow (11.93 Ma), Huckleberry Ridge (2.1 Ma), and Lava Creek B (0.6 Ma). Suspected source eruptions are selected based on previously reported age and geochemical data available for these sample locations (Table 1).

Sample Locations

Volcanic ashes were collected from 5 locations across the state of Kansas and one sample was collected at Ashfall Fossil Beds State Historical Park in Nebraska (Fig 3). The following paragraphs briefly describe the locations, suspected source eruptions, and previously documented information about these locations.

Samples HP14-05b and HP14-07 were initially collected for the zircon U-Pb geochronologic study of Hallman (2016) from the Calvert Ash mine located in Norton County, KS (Fig 3, locality #2). The ash deposit here is light grey and poorly lithified, with abundant glass shards, and a calcrete cement at the top. Sample HP14-07 is a fine-grained vitric ash collected from an abandoned face of the Calvert ash mine (Appendix A, Pic #1). HP14-05b is a massively bedded, fine-grained vitric ash also located at the Calvert ash mine (Appendix A, Pic #2).

This ash deposit is suspected to be sourced from the Bruneau-Jarbidge eruptive center of the YHT (11.93 Ma) (e.g. Swineford, 1963; Potter, 1991; Ludvigson et al., 2009; Smith & Ludvigson, 2011). This is further supported by the zircon U-Pb dating yielding ages of about 11.7 Ma for both HP14-05b and HP14-07 (Hallman, 2016). These samples will serve as a control to help demonstrate the robustness of the correlations determined using the methods outlined in this study.

Sample SCS-KMI-16 was collected in Smith County, KS (Fig 3. locality 3, Pic 4). The exposed deposit is poorly lithified and grey, containing abundant glass shards with a minor amount of calcrete cement. The exposed ash deposit is currently mapped outside of the extent of the Ogallala Formation in Western Kansas, due to bedrock exposure being limited to roadcuts and incised streambeds (Hallman, 2016). Because bedrock exposures are rare in this area, the ash bed has previously been assumed to be part of the Early Miocene sediments that dominate Eastern Kansas (Ludvigson et al., 2009). To test this assumption, we sampled the same ash deposit from the Wanner family ranch outside of Smith Centre in Smith County, KS to determine its origin. Generally, ashfall samples in Kansas found outside of the Ogallala Formation are assumed to correlate with either the Pleistocene Lava Creek B, the Quaternary Huckleberry Ridge eruptions of the YHT or the Quaternary Long Valley caldera (Bishop Tuff) eruption in California (Izett and Wilcox, 1982). However, major and trace element geochemical fingerprinting performed by the USGS tephrochronology lab have verified samples taken in this location to correlate with the Ibex Hollow eruption of the YHT, contradicting the expected age correlation for this location (Ludvigson, 2009).

Sample number AFB-00 is taken from the basal unit of a section of volcanic ash in Ashfall Fossil Beds Historical State Park, near Royal, NE (Fig 3., location 1). This ashfall bed has been correlated to the Bruneau-Jarbidge eruptive center of the YHT (Perkins et al., 1998; Tucker et al., 2014), based on the diverse faunal succession of mammals and plant remains found there. Recent U-Pb zircon dating from the same basal unit sample of the Ashfall deposit (Turner, 2017; Smith et al., 2018) yields an age of 11.86 ± 0.13 Ma, suggesting the likely source eruption for this deposit is also the Ibex Hollow eruption of the YHT.

Sample JCS-KMI-16 was collected in Jewell County, KS from the Mankato Ash Mine (Fig 3, location 4). This ash is mapped outside of the extent of the Ogallala Formation as shown by the most recent surficial map produced by the Kansas Geological survey (KGS, 2008). The ashfall deposit has previously been correlated to the Lava Creek B (0.6 Ma) eruption of the YHT (Wan, 2008, pers. comm. to Ludvigson; David, 2009).

Multiple ash deposits have been identified in Meade County, KS (Bayne, 1976; Izett & Wilcox, 1982; David, 2009; Ludvigson, 2009). Two sample locations were chosen for this study based on their documented volcanic sources (Table 1). These samples were collected as part of an ongoing study by the KGS. Sample number BOR-S2-01 (Fig 3, locality #5), here referred to as Borcher's Badlands (see Table 1), has been correlated with the Huckleberry Ridge (2.1 Ma) YHT eruption based on zircon fission-track ages (Naeser et al., 1973) and geochemical fingerprinting by bulk glass solution ICP-MS (David, 2009). Sample number MC-CA-01 (Fig 3, locality #6), known as the Cudahy Camp ash deposit has been previously correlated to the Lava Creek B (ca. 0.6 Ma) eruption of the YHT, also using bulk glass geochemical fingerprinting (David, 2009) and zircon fission-track ages (Naeser et al., 1973).

METHODS

Seven samples were collected from six field sites with exposed volcanic ash layers throughout Kansas and Nebraska (Fig 3). All ash samples are poorly lithified and samples were dug with a shovel from outcrops after exposing fresh surfaces to avoid surface contamination or contamination from overlying strata.

While volcanic glass is abundant in these ash bed deposits, it is also fragile and subject to alteration and surface contamination (e.g., Pearce et al., 2004; Blockley et al., 2005; Steinhauser & Bichler, 2008). Samples studied here are poorly lithified, so we eliminated the possibility of destroying viable shards by not using hard rock processing techniques (crushing, sieving, aggressive acid etching). Glass shard samples were separated from sediments for laser ablation analysis using techniques similar to those outlined in Blockley et al. (2005). Techniques were modified to be more appropriate for analysis by LA-ICP-MS, as opposed to electron microprobe analysis. Approximately 5 grams of each sample were then treated with 1.5M HCl solution overnight to dissolve any surrounding carbonate cement or surface contamination on glass shards. Samples were then sieved using a 196μm mesh and glass shards were selected from the >196μm size fraction. Shards selected for analysis based on size, transparency and shape (e.g. Fig 4). Shards that were either very thin (<20μm thickness), very curved, cloudy, contained large cracks or bubbles, or with pitted surfaces were not selected for analysis. Between 30-50 glass shards chosen per sample for analysis were mounted on double-sided tape on 1-inch epoxy mounts.

Analysis was performed using a Photon Machines Analyte G2 193nm excimer laser coupled with a Thermo Element2 Inductively Coupled Plasma Mass Spectrometer (LA-ICP-MS). Laser and mass spectrometer settings are defined in Appendix B. Elements selected for analysis include Ca, Ti, V, Mn, Rb, Y, Zr, Nb, Ba, Ce, Nd, Sm, Eu, Gd, Dy, Yb, Hf, Pb, Th, and U, based on their petrological significance to identify source eruptions (Perkins & Nash, 2002; Pearce et al., 2007; Tomlinson et al., 2010). Isotopes chosen for analysis were based on relative abundance and avoidance of significant mass interferences that could occur during analysis (Appendix B).

Data was reduced using Igor Pro and Iolite software packages using the Trace ElementIS data reduction scheme (Paton et al. 2010; 2011). ^{43}Ca is used as internal standard because it is relatively abundant in both the standards and unknown samples and free of major isobaric interferences. ^{43}Ca was chosen as the internal standard based on tests carried out with ^{44}Ca and ^{29}Si as internal standards. Other LA-ICP-MS studies use ^{29}Si as internal standard, but in the case of this study, ^{29}Si produced data that was not reproducible when compared to ATHO-G (Hu et al. 2009, Jochum et al. 2010), possibly due to an isobaric interference with several nitrogen, oxygen, carbon and hydrogen molecules at this mass. Using ^{43}Ca as the internal standard gave results within <5% of published best estimates for the NIST 612 glass (Fig 5a) (Jochum et al, 2011). Values for ATHO-G produced results with ≤10% bias for all reported elements except for Ti (+11.9% bias) and Eu (-12% bias) (Jochum et al, 2006) (Fig 5b). Data generated in these method tests can be found in Appendix C. ^{43}Ca as an internal standard is sensitive to contamination from plagioclase micro inclusions, with significantly higher Ca content than the rhyolitic glass (Pearce et al., 2004). The total CPS yield and calculated ^{44}Ca were monitored and analyses outside of the expected data range were not used for final reporting (see Appendix E for details).

Data were excluded based on duration of analysis, internal standard error, and ^{43}Ca count rates. A combination of calculated similarity coefficients (SC) (Borchardt et al. 1974) and discrimination diagrams are generated to provide correlations between ash samples and literature data. A minimum SC of 0.86 was defined as a positive correlation (Borchardt et al., 1974). Elemental data trends were also compared and evaluated against literature data where possible.

RESULTS

Results for major and trace element concentrations obtained by LA-ICP-MS for seven volcanic ash samples are listed in Appendix E. The results are also presented in sets of element correlation plots and element ratio correlation plots for each set of samples (Figs 6-11). Data were excluded based on duration of analysis, internal standard error, and ^{43}Ca count rates. The sample sets are organized in text sections according to the source eruption they have been correlated with, based on previously published geochemical or geochronological data or stratigraphic correlation assumptions.

Samples assigned to Lava Creek B (JCS-KMI-16 and MC-CA-01)

The two samples discussed in this section (from Jewell County and Meade County, KS) have been designated as sourced from the Lava Creek B eruption based on their previously published geochemistry (David 2009, Ludvigson 2009) (See Table 1). Thirty-five analyses were obtained from JCS-KMI-16 and 40 data points were collected from MC-CA-01. Data are presented as individual data points instead of reporting average values because reporting a singular average value for each element may omit important petrological information, such as correlated concentrations. In the case of these two samples, two distinct populations of glass shards were identified based on Ba concentrations, one with Ba <150ppm and one with >150ppm (here referred to as "high Ba" and "low Ba") (Fig 6a). Nineteen of thirty-five data points for JCS-KMI-16 fell into the low Ba population with the remaining sixteen segregated into the high Ba population. Thirteen of the forty data points for MC-CA-01 fell into the low Ba population with the remaining twenty-seven points falling into the high Ba population. Bimodal element concentrations have also been reported for Lava Creek B ashes by Pearce et al. (2004) based on Fe concentrations, which correlate with the Ba groups. Other element vs. element plots display correlated (6b: Nd-Zr) or anti-correlated (6c: Y-Zr; 6d: Nb-Zr) trends. As a fluid-immobile HFS element that generally increases with fractional crystallization, zircon was chosen for the x-axis of these plots. It is notable that in the Ba-Zr and Nd-Zr plots, the reference average values of Pearce et al. (2004) lie on the same trends as the data presented here, whereas for Nb and Y the concentrations calculated here are significantly higher than the reference average values.

Plots of element concentration against Ce/Zr (because both are weathering-resistant HFS elements increasing with fractional crystallization, the Ce-Zr ratio should be a robust value constant for a particular magma) vs other HFS (Y, Nb, Nd) and LIL (Ba) elements show overlapping data populations for JCS-KMI-16 and MC-CA-01. Fig 7a, c and d show bimodal distributions for Y, Ba, and Nd, respectively. The strongest separation of the modes is in Ba (Fig. 7c) with differences of a factor of 5, whereas differences in Y and Nd are more subtle (ca. 20%). The Nb vs. Ce/Zr plot (Fig. 7b) does not show such a grouping but a positive correlation, similar to the low and high Ba and Fe shard populations (Pearce et al., 2004). Plots presented in figures 6 and 7 show both populations of glass shards (JCS-KMI-16 and MC-CA-01) bear a possible correlation to the Lava Creek B (0.6 Ma) YHT eruption values from Pearce, et al. (2004).

Similarity coefficients (SC) were calculated between the data populations of JCS-KMI-16 and MC-CA-01 and LA-ICP-MS literature data of Pearce et al. (2004) from a sample of Lava Creek B tephra from Idaho (Appendix D). SC was calculated using elemental concentrations of Rb, Zr, Nd, Ba, and Ce. Grain populations for JCS-KMI-16 and MC-CA-01 overlap well with one another and can be correlated to one another. Glass shards from both samples, JCS-KMI-16 and MC-CA-01, in the low Ba population correlate with the >1.6% Fe population of Pearce et al. (2004) (average SC values 0.87 and 0.86, respectively). Glass shards in the high Ba population correlate with the <1.6% Fe population of Pearce et al. (2004), with average SC values 0.89 and 0.86, respectively (See Appendix D).

Samples assigned to the Tuff of Ibex Hollow (HP14-05b, HP14-07, AFB-00, SCS-KMI-16)

Samples described in this section have been interpreted to be sourced from the same eruption, described in the literature as Tuff of Ibex Hollow (Table 1; e.g. Perkins & Nash, 2002). Based on this hypothesis, element vs. element (Fig. 8a-d, Ba, Nb, Y, Rb vs. Zr) and element vs elemental ratio (Fig. 9a-d, Ba, Nb, Y, Rb vs Ce/Zr) plots were generated to compare measured values with literature data (Perkins & Nash, 2002). Thirty viable data points were obtained from HP14-05b, 32 from HP14-07, 43 from AFB-00, and 32 from SCS-KMI-16. Fig 8a and 8d (Zr vs Ba and Rb vs Zr) show no appreciable correlated trend in the data. The 3 samples *HP14-05b, HP14-07 and SCS-KMI-16* show indistinguishable, overlapping data ranges, whereas AFB-00 plots towards higher Ba and within the upper 50% percentile range of Zr. Niobium vs Zr and Y vs Zr (Fig 8b, and 8c, respectively) trends are consistent between all samples, suggesting a common source. Perkins & Nash (2002) data plotted on Fig 8a, b, and d overlap well with experimental data ranges while the lower half of the Y value overlap with experimental data (Fig 8c). Fig 9 also displays experimental data that does not overlap with Perkins & Nash (2002) due to a decreased Ce concentration in our experimental data. Positive correlation trends, especially for Y and Zr for samples from the Calvert ash mine (HP14-05b, HP14-07) in these plots may be related to fractional crystallization processes (Pearce et al., 2004).

Similarity coefficients calculated for all four samples to literature data of Perkins & Nash (2002) obtained by electron microprobe were above 0.86 (Appendix D). Elements used to calculate SC were Ti, Mn, Zr, Nb, Ba, and Th. As observed in other YHT eruptions (Pearce et al., 2004), element vs. element plot trends are interpreted as evidence for fractional crystallization of plagioclase (Fig 8a-d).

Sample assigned to Huckleberry Ridge tephra (BOR-S2-16)

Forty-seven viable data points were collected for sample BOR-S2-16. Element vs. element (Fig. 10) and element vs ratio (Fig. 11) plots were generated to compare measured values with literature data (Pearce et al., 2004) for the Huckleberry Ridge tephra (e.g. 2.003±0.014 Ma, Gansecki et al. 1998; 2.059±0.004 Ma, Lanphere et al. 2002; 2.0794 ± 0.0046 Ma, Riviera et al. 2014) of the YHT. Figure 10 a and d (Ba vs Zr and Nd vs Zr) display a positive correlation trend while fig 10b and c (Nb vs. Zr and Y vs Zr) display a negative correlation. Multiple populations of grains were defined based on Ba values in the same manner as for the Lava Creek B samples described above. These are clearly defined in the distribution of data shown in Fig 11 a. One population of thirty-one grains can be observed at 75-200 ppm, another of sixteen grains at Ba > 200 ppm. Multiple populations of Ba such as this within a sample have been interpreted by the presence of plagioclase microphenocrysts within the glass shard by Pearce et al. (2004). The scatter of data in Fig 11b and 11c. may also be explained by such microphenocrysts.

For illustrative purposes, averages of values for this study are plotted on bivariate element plots along with average values reported in Pearce et al. (2004) (Fig 10a-d). While the plotted averages mostly both fall within the overall population of individual measured values (with the exception of 10d, for which the literature data of Nd are higher than the values reported here), it is apparent that the distribution of the data populations of the individual measured grains strongly influences the reported average value. This demonstrates the problems inherent with only reporting and comparing average values for geochemical fingerprinting.

Similarity coefficients were calculated for BOR-S2-16 compared to a sample from the same geographic location reported in Pearce et al. (2004). Similarity coefficient calculation yielded an average SC=0.87 (Appendix D) positively correlating this ash to the Huckleberry Ridge eruption of the YHT. Elements used to calculate the SC were Rb, Zr, Nb, and U.

DISCUSSION

Using geochronological methods such as U-Pb zircon or Ar-Ar feldspar dating to identify and correlate volcanic ash beds has utility in many instances. However, this can be both expensive and time-consuming because of the need to extract minerals from the volcanic ashes, e.g., by heavy liquid separation techniques. For large regional studies that aim to correlate marker beds/stratigraphic units across large areas, such as the Ogallala Formation and overlying Neogene units in the central US, the geochronology approach is therefore impractical. This study confirms that it is possible to positively correlate volcanic ash beds with their source eruptions using geochemical fingerprinting of individual glass shards via LA-ICP-MS in a relatively quick, cost-effective manner. Separate aspects of this procedure will be discussed in this chapter.

The results of this study on geochemical fingerprinting of individual volcanic glass shards by LA-ICP-MS test three main hypotheses: Using individual shard LA-ICP-MS, (1) can distal ash deposits be positively correlated to their source eruptions, (2) can differences in chemistry due to alteration or other petrologic process be identified, (3) can the obtained results be used to make stratigraphic correlations across units that span across large areas, such as the Ogallala Fm. and overlying Plio-Pleistocene units in the Central US. The following paragraphs explore and discuss the evidence for these hypotheses in the light of published literature.

Correlating Distal Ashes to Source Eruptions

While rhyolitic glasses from different volcanic eruptions generally have inherent geochemical similarities in relative abundance of major elements, every eruption has its own unique geochemical fingerprint of trace elements or combination of major and trace elements (e.g. Pearce et al. 2004), which is the very basic tenet of geochemical fingerprinting applied to volcanic ash deposits (Lowe, 2011). Using individual glass shard analyses, a positive correlation of samples to their source can be made based on their geochemical fingerprints. Elements such as Ti, Mn, Rb, Zr, Nb, Ba, and REEs provide the framework for building fingerprints for unknown ashes. Due to differences in instrumentation, limits of detection, and statistical variations, it is not feasible to simply compare average concentration values to reported literature values. For example, reference data from Perkins & Nash (2002) were obtained using electron microprobe (EMP) analysis and X-ray fluorescence (XRF) spectroscopy. While these methods are typically used to measure major and minor elements, LA-ICP-MS is limited in major element analysis (i.e. cannot measure Fe or K), but it is very useful for measuring minor and trace elements, providing a broader range of elements than XRF and EMP. Instead, comparisons are made by plotting elemental ratios (Figs 7, 9, and 11). Statistical correlations of samples based on multiple elements have been performed using a correlation coefficient calculation approach (Borchardt et al., 1972) (Appendix D).

Earlier studies have demonstrated that multiple eruptions from the same caldera may produce chemical trends that are similar due to the similarities in petrogenesis (Pearce et al., 1999). It can be argued that correlation coefficient calculations may not be enough to definitively correlate ashes to their source eruptions if multiple eruptions of the source volcano of similar composition have to be considered. To test whether samples from the YHT are similar enough to make an incorrect correlation, SC values were calculated for all samples versus all reference data (Appendix D) (Perkins & Nash 2002; Pearce et al., 2004). The calculations (Appendix D) of the correlation coefficients show only one possible 'false positive' correlation of JCS-KMI-16 (high Ba) to Huckleberry Ridge (Pearce et al., 2004). This correlation is likely due to the relatively wide range of the comparative data values for JCS-KMI-16 (Appendix E).

Discerning Multiple Geochemical Shard Populations Within One Sample

In the case of both primary and secondary ash deposits, there is a possibility for material from multiple eruptions being present in one outcrop (i.e. Trapper Creek, Idaho or Borcher's Badlands, Kansas). Analyzing individual shards instead of using bulk geochemical techniques, we were able to discern populations of grains from the same eruption with different trace element geochemical fingerprints. While major element analysis could prove indistinguishable for these glass shards, incompatible elements would be more strongly affected by fractional crystallization processes. Such is the case when caldera eruptions sample both fractionated upper parts and the less evolved deeper parts of a magma chamber (e.g. Pearce et al., 2004). Three samples from this study contain such different glass shard populations, JCS-KMI-16, MC-CA-01, and BOR-S2-01 (see Table 1 for detailed descriptions). Similarly, Pearce et al. (2004) identified two populations in Lava Creek B glass shards from Idaho based on their Fe concentrations. While this study was not able to measure Fe, two populations of grains could be identified using Ba concentrations (Fig. 6a) within both Lava Creek B correlative samples JCS-KMI-16 and MC-CA-01. Using elemental concentrations and similarity coefficient calculations (Appendix D), the low Ba concentration population from this study correlates with the high Fe population from Pearce et al. (2004) and the high Ba data correlates to the low Fe group from that same study.

Although glass is subject to alteration via cation exchange in aqueous solutions (e.g. Steinhauser & Bichler, 2008) the effect of aqueous alteration from depositional environments or during sample preparation (<1% of ion absorption for elements Rb, Ba, La, Ce, Nd, Sm) would not be enough to account for the differences in concentration within the grain populations of this study. In this case, it is surmised that the difference in Ba concentrations is the result of two populations of grains sourced from different phases of the same eruption or different parts of the magma chamber as discussed in previous studies (e.g. Pearce et al., 2004; Leeman et al., 2008; Seligman, 2012).

The ability to observe two (or more) populations of glass shards within an ash sample is an advantage unique to using individual spots instead of bulk methods or simple averaging of results to interpret the data. Any chemical inhomogeneity-including cracks, inclusions, and surface contamination-would also be impossible to detect. Chemical variation due to analysis of micro-inclusions within the glass may also go undetected. Instead reported average values would fall within neither discrete population of grains and would produce a high RSD (>15%). In this study, the average Ba concentration of the two samples correlated with the Lava Creek B eruption would be 130 ppm with 69% RSD for JCS-KMI-16 and 159 ppm with 53% RSD for MC-CA-01. After splitting the results of both samples into high and low Ba populations, the % RSD values are much lower (7.1 and 7.62% for high Ba averages, respectively).

Individual shard analysis may show trends reflective of crystal fractionation. Therefore, the use of element ratio plots may distinguish YHT eruptions from each other more distinctively than bivariate element concentration plots. This lends added robustness to correlations due to eliminating influences from systematic uncertainties in calibrations of absolute concentration. To be fully confident in the produced correlations, a reasonable minimum number of analyses should be performed and included in correlation calculations. For this study, 30-50 individual shard analyses were considered enough to produce a robust dataset.

Applications to Stratigraphic Correlations

Findings of this study support both expected and unexpected correlations with respect to the extent of the Ogallala Formation in Western Kansas and Nebraska, a formation where lithostratigraphic correlations are difficult to perform and correlations rely heavily on the use of expensive radiometric mineral age and relatively imprecise fossil stage data (Ludvigson, 2009). Samples were chosen based on published correlations of their provenance, and their proximity to the mapped edges of the exposed Ogallala Formation. In the following paragraphs, we will discuss the correlations of volcanic ash deposits that have been confirmed by this study and one correlation that contradicts the stratigraphy as it is currently mapped.

The samples taken from Meade County (BOR-S2-01 and MC-CA-01) were collected from units overlying the Ogallala Fm. and were previously correlated with the Huckleberry Ridge (2.1 Ma) and Lava Creek B (0.6 Ma) eruptions, respectively (Izett & Wilcox 1982; Pearce et al., 2004; Ludvigson et al., 2009). Our results confirm these correlations. Sample JCS-KMI-16 from Jewell County was collected from an area beyond the extent of the Ogallala and, like many other ashes in Central and Eastern KS, correlated to the Lava Creek B (0.6 Ma) eruption of the YHT (Izett, 1982; David, 2009; Ludvigson et al., 2009). This was supported by tephrochronologic analysis of a core sample from the same locale done at the USGS Tephrochronology Lab in Menlo Park, California (Wan, 2008, pers. comm. to Ludvigson) of the same outcrop, which agrees with our findings.

We also demonstrate the possibility to use geographically close samples to provide better spatial resolution of geologic unit boundaries. This applies to the samples from Norton (HP14-05b and HP14-07), Smith (SCS-KMI-16) and Jewell (JCS-KMI-16) counties in Kansas. The Smith and Jewell county sites are mapped as being outside of the Ogallala Fm. and should logically correlate to the Lava Creek B YHT eruption (Izett, 1981; David, 2009, Ludvigson, 2009). However, data collected here as well as previously analyzed surface samples support a correlation of the Smith county sample (SCS-KMI-16) with the Ibex Hollow eruption. This supports correlation of the Smith County ash deposits with the Calvert Ash mine in Norton County, KS, a site that lies approximately 55 miles to the West, mapped within the extent of the Ogallala formation. Correlation between these two ash deposits suggests that the erosional extent of the formation might need to be reevaluated.

Similarly, the sample from Ashfall Fossil Beds State Historical Park in Nebraska (AFB-00) is mapped near the northeastern boundary of the Ogallala formation. It correlates well with the results of samples HP14-05b, HP14-07, and SCS-KMI-16 from Norton and Smith county ashes (Fig 08a-d, Fig 09a-d), suggesting these are all derived from the same eruptive source, which is supported by U-Pb zircon ages of ca. 11.9 Ma (Hallman 2015; Turner, 2016; Smith et al., 2018). Previous tephrochronology reports (Wan, 2008, pers. comm. to Ludvigson) and faunal succession correlations for the Ashfall site (Tucker et al., 2014) together with LA-ICP-MS geochemical analyses from this study lead us to correlate these ashes with the Ibex Hollow (11.93 Ma) eruption of the YHT.

This study shows that the approach used here can be used to define the boundaries of the Ogallala Fm. in Kansas and Nebraska more precisely. This may be difficult as outcrop exposures along the edge of the formation are not well exposed and are likely to be only located along stream beds or roadcuts. However, with the detailed ash locality maps previously established (Izett &Wilcox, 1982) and the use of satellite imagery, localities of interest for future stratigraphic work can be carefully chosen. Additionally, because sampling to obtain these ashes is relatively quick and does not require heavy drilling equipment, may make it more likely for property owners to allow sampling.

Limitations of the geochemical fingerprinting approach

Reference literature data for comparison that analyzed the same elements is a limitation of the approach. For the YHT, most of the published data available for correlations are major and minor element concentrations measured using different instrumentation (EMP, XRF, etc.) (e.g. Perkins 1998, Perkins & Nash, 2002, David 2009). Major element analysis can be difficult for high sensitivity LA-ICP-MS configurations, unless minor isotopes can be used, as applied to Si when used as an internal standard (e.g. Tomlinson et al., 2010), so those literature values were not usable for correlations in this study. For the Lava Creek B and Huckleberry Ridge eruptions, there is published LA-ICP-MS data (e.g. Pearce et al., 2004). Collecting vitric ash samples of known origin proximal to the eruption site and analyzing them alongside the distal samples of known and unknown origin, as done by Pearce et al. (2004) was outside the scope of this study but is recommended.

CONCLUSIONS

For Ogallala Formation and overlying Neogene strata in the central US, abundant lenticular ash beds can be used to make stratigraphic correlations across units spanning thousands of kilometers. U-Pb dating of zircons from the units of interest can provide accurate matches to source eruptions (e.g. Hallman 2016; Turner 2017; Smith et al., 2018), but this method involves labor-intensive mineral separation and analytical time and is expensive when regional scale studies require dozens of samples to be correlated. Since the ash bed deposits are found throughout the Ogallala Formation and overlying Neogene strata in Kansas, Nebraska, and Oklahoma, there is utility in having a faster, less expensive way of analyzing samples to make effective correlations between many sites. Geochemical fingerprinting of glass shards from these ash beds can be used to correlate them across Kansas and Nebraska by tracing their provenance back to known large scale eruptions, e.g. along the Yellowstone hotspot track (YHT). Individual volcanic eruptions have been shown to have unique geochemical fingerprints (major and trace element signatures), yielding unique results and robust correlations (e.g. Perkins,1988; Perkins & Nash, 2002; Pearce et al., 2007; Tomlinson et al., 2010; Lowe, 2011). Geochemical fingerprinting of volcanic ashes has been performed with success in other regions of the High Plains (e.g. Perkins, 1998), but few studies have been published about the Kansas Pearlette ash beds (Potter, 1991; David, 2009; Ludvigson et al., 2009). Pearlette ash beds have been defined by Izett & Wilcox (1982) as undifferentiated ash beds with distinctive characteristics (e.g. light grey/white color, finely bedded, poorly lithified).

Previous studies on geochemical fingerprinting of volcanic ash in the area have used bulk methods that produced average values, either by solution ICP-MS (David, 2009) or by atomic absorption spectroscopy (AAS, Potter, 1991). The AAS results did not yield trace element data useful for correlating these ashes to potential source eruptions (Potter, 1991). Solution ICP-MS was successful for some correlations (David, 2009), but the preparation and analysis can be expensive and since this is a bulk analytical technique there is some uncertainty in the assumption that all measured material is from the same eruptive event, and other caveats about using bulk techniques as mentioned above. In the study by David (2009), 20 grams of sample material were required. In the LA-ICP-MS technique, individual glass shards are analyzed, which allows discrimination between potential different shard populations within a deposit, observation of trends of magma fractionation between analyses, or detection of microscopic contamination with K-feldspar, as previously shown by Pearce et al (2004). In summary, the rapid analysis of multiple individual glass shard per sample by LA-ICP-MS allows insights into sample homogeneity and details of magma evolution that are not possible with any bulk technique.

Elemental concentrations from LA-ICP-MS spot analyses were used to construct bivariate and elemental ratio plots. Direct comparisons to reference literature values (mostly given as averages only) proved to be problematic where a range of values were found to be present in the glass shard population (i.e. Ba concentration in Lava Creek B samples). Therefore, similarity coefficient (SC) calculations based on multiple elements were performed for all samples (Appendix D) and matches were determined based on an average SC value >0.86 as recommended by Borchardt (1972). The possibility of false positive correlations was effectively excluded by comparing literature data from ash deposits of different eruptions.

Results produced here correlate three ash beds from Kansas and one from Nebraska (Ashfall Fossil Beds) to the tuff of Ibex Hollow eruption of the Bruneau-Jarbidge eruptive center of the YHT (Fig 02). Independent analysis of a sample from Smith County (Kansas) by the USGS Tephrochronology Lab (Wan 2008, pers comm. to Ludvigson) also determined a correlation to the Ibex Hollow eruption of the YHT. Geochronological evidence provided by U-Pb zircon ages from the Nebraska Ashfall Fossil Beds (Turner, 2016; Smith et al. 2018) and the Calvert Ash mine (Hallman, 2016) support this interpretation.

One sample from Smith County (Kansas) and one sample from Meade County (Kansas) correlate to the Lava Creek B eruptive center of the YHT. Independent analysis of samples from

Smith County by the USGS Tephrochronology Lab (Wan, 2008, pers. comm. to Ludvigson) also determined a correlation to the Lava Creek B eruption of the YHT. One sample from Meade County (Kansas) correlates to the Huckleberry Ridge eruptive center of the YHT. This is confirmed by Pearce, et al. (2004).

Future work toward a large-scale mapping initiative could be very beneficial to correlate and reconstruct the chronostratigraphy and development of the Ogallala Formation in the High Plains region. To improve the accuracy of the correlations proposed here, it would be worthwhile to collect and analyze vitric ash samples taken proximal to the source eruptions of interest in order to build a reference database obtained with the same analytical technique. This would be preferable to comparing with literature values because it would eliminate any complications that may arise in comparing results produced from different analytical methods (e.g. electron microprobe), calibration approaches (e.g. different reference materials, different internal standard elements) or sample preparation techniques.

REFERENCES

Anders, M. H., Saltzman, J. & Hemming, S. R. (2009) Neogene tephra correlations in eastern Idaho and Wyoming: Implications for Yellowstone hotspot-related volcanism and tectonic activity Yellowstone hotspot-related volcanism and tectonic activity. *GSA Bulletin*, *121*(5-6), 837-856.

Bayne, C. K. (1976). *Guidebook: 24th Annual Meeting, Midwestern Friends of the Pleistocene*, *24*. Kansas Geological Survey, University of Kansas.

Blockley, S. P. E., Pyne-O'Donnell, S. D. F., Lowe, J. J., Matthews, I. P., Stone, A., Pollard, A. M., Turney, C.S.M. & Molyneux, E. G. (2005) A new and less destructive laboratory procedure for the physical separation of distal glass tephra shards from sediments. *Quaternary Science Reviews*, *24*(16-17), 1952-1960.

Boellstorff, J. (1976) The succession of late Cenozoic volcanic ashes of the Great Plains: a progress report, *in* Bayne, C.K., ed., Guidebook: 24th Annual Meeting, Midwestern Friends of the Pleistocene: *Kansas Geological Survey Guidebook Series* 1, p. 37-71.

Bonnichsen, B., Leeman, W. P., Honjo, N., McIntosh, W. C. & Godchaux, M. M. (2008) Miocene silicic volcanism in southwestern Idaho: geochronology, geochemistry, and evolution of the central Snake River Plain. *Bulletin of Volcanology*, *70*(3), 315-342.

Borchardt, G. A. (1974). The SIMAN coefficient for similarity analysis. *Classification Society Bulletin*, *3*(2), 1-8.

Borchardt, G. A., Aruscavage, P. J. & Millard, H. J. (1972). Correlation of the Bishop Ash, a Pleistocene marker bed, using instrumental neutron activation analysis. *Journal of Sedimentary Research*, *42*(2), 301-306.

Brueseke, M. E., Hart, W. K. & Heizler, M. T. (2008) Diverse mid-Miocene silicic volcanism associated with the Yellowstone–Newberry thermal anomaly. *Bulletin of Volcanology*, *70*(3), 343-360.

Cathey, H. E. & Nash, B. P. (2004) The Cougar Point Tuff: implications for thermochemical zonation and longevity of high-temperature, large-volume silicic magmas of the Miocene Yellowstone hotspot. *Journal of Petrology*, *45*(1), 27-58.

Coble, M. A. & Mahood, G. A. (2012) Initial impingement of the Yellowstone plume located by widespread silicic volcanism contemporaneous with Columbia River flood basalts. *Geology*, *40*(7), 655-658.

David, B. T. (2009) "Chemical fingerprinting" of volcanic tephra found in Kansas using trace elements [M.S. thesis]: Manhattan, KS, Kansas State University, 115 p.

Diffendal, R. F. (1982) Regional implications of the geology of the Ogallala Group (upper Tertiary) of southwestern Morrill County, Nebraska, and adjacent areas. *Geological Society of America Bulletin*, *93*, 964–976.

Fenneman, N. M. (1917) Physiographic Subdivision of the United States: *Proceedings of the National Academy of Sciences, 3*, p. 17–22.

Frye, J. C., Leonard, A. B. & Swineford, A. (1956) Stratigraphy of the Ogallala Formation (Neogene) of northern Kansas: *Kansas Geological Survey, Bulletin 118*, 92 p.

Gansecki, C. A., Mahood, G. A. & McWilliams, M. (1998) New ages for the climactic eruptions at Yellowstone: single-crystal $^{40}Ar/^{39}Ar$ dating identifies contamination. *Geology*, *26*(4), 343-346.

Gehrels, G. (2011) Detrital zircon U-Pb geochronology: Current methods and new opportunities. ***in*** Busby, C. & Pérez, A.A., eds., *Tectonics of sedimentary basins: Recent advances*, John Wiley & Sons, 45-62.

Gutentag, E. D., Heimes, F. J., Krothe, N. C., Luckey, R. R. & Weeks, J. B. (1984) Geohydrology of the High Plains aquifer in parts of Colorado, Kansas, Nebraska, New Mexico, Oklahoma, South Dakota, Texas, and Wyoming. *U.S. Geological Survey Professional Paper 1400-B*, 63 p.

Hallman, J. A. (2016) Spatial and temporal patterns of Ogallala formation deposition revealed by U-Pb zircon geochronology. [M.S. Thesis]. Lawrence, Kansas. *The University of Kansas.* 101p.

Hanan, M. A. & Totten, M. W. (1996). Analytical techniques for the separation and SEM identification of heavy minerals in mudrocks. *Journal of Sedimentary Research*, *66*(5), 1027-1030.

Harley, S. L. & Kelly, N. M. (2007) Zircon tiny but timely. *Elements*, *3*(1), 13-18.

Hu, Z., Liu, Y., Chen, L., Zhou, L., Li, M., Zong, K., ... & Gao, S. (2011). Contrasting matrix induced elemental fractionation in NIST SRM and rock glasses during laser ablation ICP-MS analysis at high spatial resolution. *Journal of Analytical Atomic Spectrometry*, *26*(2), 425-430.

Izett, G. A. (1981) Volcanic ash beds: Recorders of upper Cenozoic silicic pyroclastic volcanism in the western United States. *Journal of Geophysical Research: Solid Earth*, *86*(B11), 10200-10222.

Izett, G. A. & Wilcox, R. E. (1982) *Map showing localities and inferred distributions of the Huckleberry Ridge, Mesa Falls, and Lava Creek ash beds (Pearlette family ash beds) of Pliocene and Pleistocene age in the western United States and southern Canada* (No. 1325).

Jochum, K. P., Stoll, B., Herwig, K., Willbold, M., Hofmann, A. W., Amini, M., & Raczek, I. (2006). MPI-DING reference glasses for in situ microanalysis: New reference values for element concentrations and isotope ratios. *Geochemistry, Geophysics, Geosystems*, *7*(2).

Jochum, K. P., Wilson, S. A., Abouchami, W., Amini, M., Chmeleff, J., Eisenhauer, A., ... & McDonough, W. F. (2011). GSD-1G and MPI-DING reference glasses for in situ and bulk isotopic determination. *Geostandards and Geoanalytical Research, 35*(2), 193-226.

Jochum, K. P., Weis, U., Stoll, B., Kuzmin, D., Yang, Q., Raczek, I., Jacob, D. E., Stracke, A., Birbaum, K., Frick, D. A., Günther, D. & Enzweiler, J. (2011) Determination of reference values for NIST SRM 610–617 glasses following ISO guidelines: *Geostandards and Geoanalytical Research, v. 35*, p. 397-429.

Kraus, S., Kurbatov, A. & Yates, M. (2013) Geochemical signatures of tephras from Quaternary Antarctic Peninsula volcanoes. *Andean Geology, 40*(1), 1-40.

Lanphere, M. A., Champion, D. E., Christiansen, R. L., Izett, G. A. & Obradovich, J. D. (2002) Revised ages for tuffs of the Yellowstone Plateau volcanic field: Assignment of the Huckleberry Ridge Tuff to a new geomagnetic polarity event. *Geological Society of America Bulletin, 114*(5), 559-568.

Leeman, W. P., Annen, C. & Dufek, J. (2008) Snake River Plain–Yellowstone silicic volcanism: implications for magma genesis and magma fluxes. *Geological Society, London, Special Publications*, *304*(1), 235-259.

Link, P. K. & Phoenix, E. C. (1996) *Rocks Rails & Trails, 2nd Edition: Idaho Museum of Natural History*, 194 p.

Lowe, D. J. (2011) Tephrochronology and its application: a review. *Quaternary Geochronology*, *6*(2), 107-153.

Ludvigson, G. A., Sawin, R. S., Franseen, E. K., Watney, W. L., West, R. R. & Smith, J. J. (2009) *A review of the stratigraphy of the Ogallala Formation and revision of Neogene (" Tertiary") nomenclature in Kansas*. Kansas Geological Survey.

Matthews, N. E., Vazquez, J. A. & Calvert, A. T. (2015) Age of the L ava Creek supereruption and magma chamber assembly at Yellowstone based on $^{40}Ar/^{39}Ar$ and U-Pb dating of sanidine and zircon crystals. *Geochemistry, Geophysics, Geosystems*, *16*(8), 2508-2528.

Monteath, A. J., Hughes, P. D. M. & Wastegård, S. (2019) Evidence for distal transport of reworked Andean tephra: Extending the cryptotephra framework from the Austral volcanic zone. *Quaternary Geochronology, 51*, 64-71.

Naeser, C. W., Izett, G. A. & Wilcox, R. E. (1973). Zircon fission-track ages of Pearlette family ash beds in Meade County, Kansas. *Geology, 1*(2), 93-95.

Paton, C., Woodhead, J. D., Hellstrom, J. C., Hergt, J. M., Greig, A. & Maas, R. (2010). Improved laser ablation U-Pb zircon geochronology through robust downhole fractionation correction. *Geochemistry, Geophysics, Geosystems*, *11*(3).

Paton, C., Hellstrom, J., Paul, B., Woodhead, J. & Hergt, J. (2011). Iolite: Freeware for the visualisation and processing of mass spectrometric data. *Journal of Analytical Atomic Spectrometry*, *26*(12), 2508-2518.

Pearce, N. J., Westgate, J. A., Perkins, W. T. & Preece, S. J. (2004). The application of ICP-MS methods to tephrochronological problems. *Applied Geochemistry*, *19*(3), 289-322.

Pearce, N. J., Denton, J. S., Perkins, W. T., Westgate, J. A. & Alloway, B. V. (2007). Correlation and characterisation of individual glass shards from tephra deposits using trace element laser ablation ICP-MS analyses: current status and future potential. *Journal of Quaternary Science*, *22*(7), 721-736.

Perkins, M. & Nash, B. (2002) Explosive silicic (volcanism of the Yellowstone hotspot: the ash fall tuff record: Geological Society of America Bulletin, 114, 367–381.

Perkins, M. E., Nash, W. P., Brown, F. H. & Fleck, R. J. (1995) Fallout tuffs of Trapper Creek, Idaho—a record of Miocene explosive volcanism in the Snake River Plain volcanic province. *Geological Society of America Bulletin, 107*, 1484-1506.

Perkins, ME., Brown, FH., Nash, WP., McIntosh, W. & Williams, SK. (1998) Sequence, age, and source of silicic fallout tuffs in middle to late Miocene basins of the northern Basin and Range province. *Geological Society of America Bulletin*, *110*, 344-360. 31

Pierce, K. L. & Morgan, L. A. (1992) The track of the Yellowstone hot spot: volcanism, faulting, and uplift, *in* Link, P.K., Kuntz, M.A., and Platt, L.B., eds., Regional Geology of Eastern Idaho and Western Wyoming. *Geological Society of America Memoir 179,* 53 p.

Potter, S. L. (1991) Geologic characteristics of the Calvert ash bed, Ogallala Group (Miocene), western Kansas [M.S. thesis]: Hays, KS, *Fort Hays State University,* 86 p.

Rivera, T. A., Schmitz, M. D., Crowley, J. L. & Storey, M. (2014) Rapid magma evolution constrained by zircon petrochronology and $^{40}Ar/^{39}Ar$ sanidine ages for the Huckleberry Ridge Tuff, Yellowstone, USA. *Geology, 42*(8), 643-646.

Rose, W. I., Riley, C. M. & Dartevelle, S. (2003). Sizes and shapes of 10-Ma distal fall pyroclasts in the Ogallala Group, Nebraska. *The Journal of Geology*, *111*(1), 115-124.

Seligman, A. N. (2012) Generation of Low $\delta^{18}O$ silicic magmas, Bruneau-jarbidge volcanic center, Yellowstone hotspot: evidence from zircons, including oxygen isotopes, U-Th-Pb dating, and melt inclusions. [M.S. Thesis]. *The University of Utah.* 141 p.

Sophocleous, M. (2010) groundwater management practices, challenges, and innovations in the High Plains aquifer, USA—lessons and recommended actions. Hydrogeology Journal, v. 18(3), p. 559-575.

Smith, J. & Ludvigson, G. (2011) A Report to the Calvert Corporation on a Geologic Inspection of the Calvert Volcanic Ash Mine. *Kansas Geological Survey, Open-File Report 2014-3*, 5 p.

Smith, J., Ludvigson, G.A., Harlow, H. & Platt, B. (2014) Ogallala-High Plains aquifer special study phase III: Lithologic calibration of practical saturated thickness in the Ogallala-High Plains aquifer. *Kansas Geological Survey, Open-File Report 2014-2*, 9 p.

Smith, J. J., Turner, E., Möller, A., Joeckel, R. M., & Otto, R. E. (2018). First U-Pb zircon ages for late Miocene Ashfall Konservat-Lagerstätte and Grove Lake ashes from eastern Great Plains, USA. *PloS one*, *13*(11), e0207103.

Steinhauser, G. & Bichler, M. (2008) Adsorption of ions onto high silica volcanic glass. *Applied Radiation and Isotopes*, *66*(1), 1-8.

Steinhauser, G., Sterba, J. H., Oren, E., Foster, M. & Bichler, M. (2010) Provenancing of archeological pumice finds from North Sinai. *Naturwissenschaften*, *97*(4), 403-410.

Sweet, M.L. (1999) Interaction between aeolian, fluvial and playa environments in the Permian

Upper Rotliegend Group, UK southern North Sea. *Sedimentology*, v. 46, p. 171-188.

Swineford, A. (1963). The Pearlette Ash as a stratigraphic marker. *Transactions of the Kansas Academy of Science (1903-)*, *66*(3), 359-362.

Swinehart, J.B., (1974) Ogallala stratigraphy of southwest Nebraska: a proposal. *Nebraska Academy of Science Program*, p. 36-37.

Tomlinson, E. L., Thordarson, T., Müller, W., Thirlwall, M. & Menzies, M. A. (2010) Microanalysis of tephra by LA-ICP-MS—strategies, advantages and limitations assessed using the Thorsmörk Ignimbrite (Southern Iceland). *Chemical Geology*, *279*(3), 73-89.

Totten, M. W., Jurik, M. A. & Hanan, M. A. (2005). The Occurrence and Seismic Expression of Volcanic Ash Beds in the Gulf of Mexico.

Tucker, S. T., Otto, R. E., Joeckel, R. M. & Voorhies, M. R. (2014) The geology and paleontology of Ashfall Fossil Beds, a late Miocene (Clarendonian) mass-death assemblage, Antelope County and adjacent Knox County, Nebraska, USA. *GSA Field Guides*, *36*, p. 1-22.

Turner, E., Smith, JJ., Ludvigson, GA., Layzell, AL. & Möller, A. (2015) Maximum depositional age constraints from U-Pb dating of zircons in Cenozoic deposits of the High Plains Aquifer, southwestern Kansas. *Geological Society of America Abstracts with Programs*, *47*, 801

Wan E. (2008). USGS Tephrochronology Project Report: GL-JCS-KMI and GL-SCS-KMI. *pers. comm.*

FIGURES

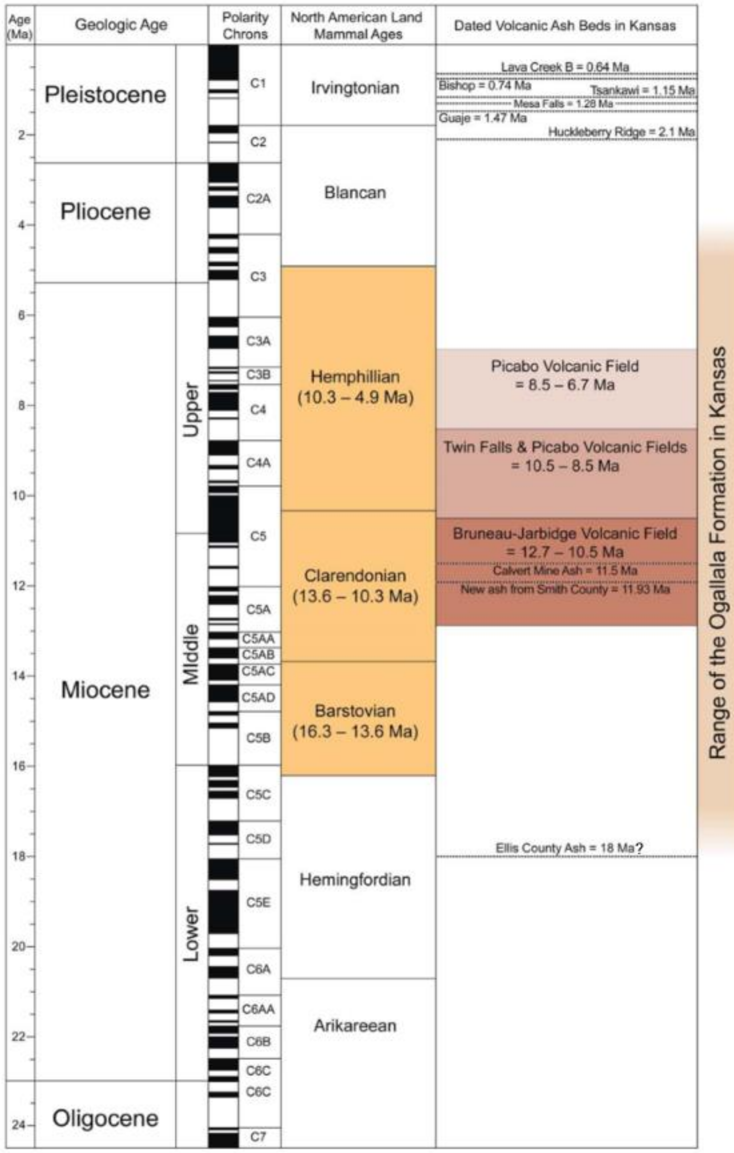

Figure 1. Summary of tephrochronologic and biostratigraphic data constraining the Neogene age of the Ogallala Formation. While the North American Land Mammal Ages (NALMA) are useful for determining a general depositional age range of this formation, the ages ranges are very broad and have been unhelpful in distinguishing different members or performing extensive correlations (Ludvigson et al., 2009) of the Ogallala Fm. throughout the entire High Plains. U-Pb dates from zircons (Hallman, et al 2015; Turner, 2018; Smith et al. 2019) have constrained ash deposits in the region to a more confined age range (12.7-10.5 Ma) that fall into the age range of the Bruneau-Jarbidge YHT eruptions. Modified from Ludvigson et al. (2009).

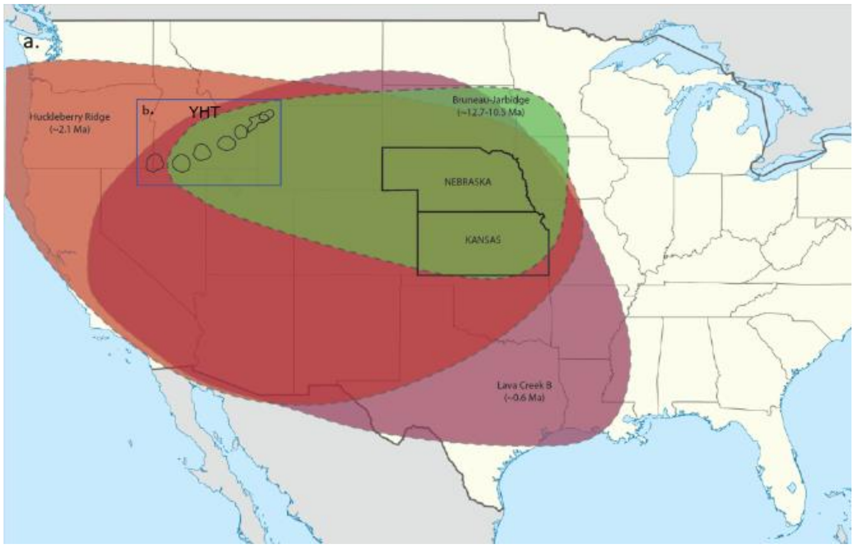

Figure 2a. Map of the estimated ashfall extent of three major YHT eruptions relevant to the study, the Tuff of Ibex Hollow (ca 11.9 Ma) of the Bruneau-Jarbidge eruptive field (green), Huckleberry Ridge (red), and Lava Creek B (purple). Inset (blue rectangle) is shown in Fig. 2b. State borders of Kansas and Nebraska outline broadly the area of study.

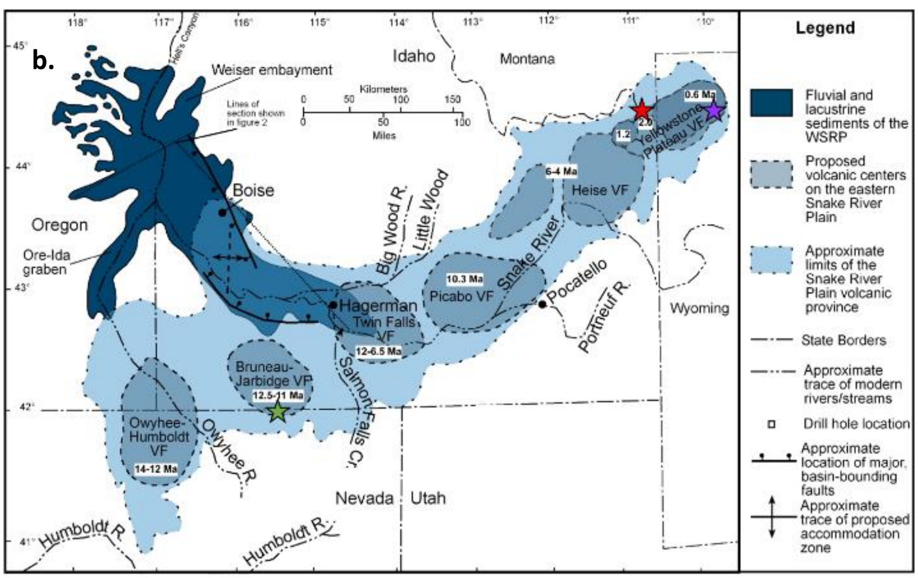

Figure 2b. Subset from Fig. 2a, map of the Yellowstone Hotspot Track (YHT) eruptive centers, from Link & Phoenix (1996) with calderas marked with eruption age ranges. Eruptions are younging from Southwest to Northeast. YHT eruptive centers of interest for this research are Bruneau-Jarbidge (Br-Ja) Huckleberry Ridge (HR) and Lava Creek (LC). Colored stars have been placed near the areas of interest. Modified from Rose and Durant (2009) and Izett and Wilcox (1982).

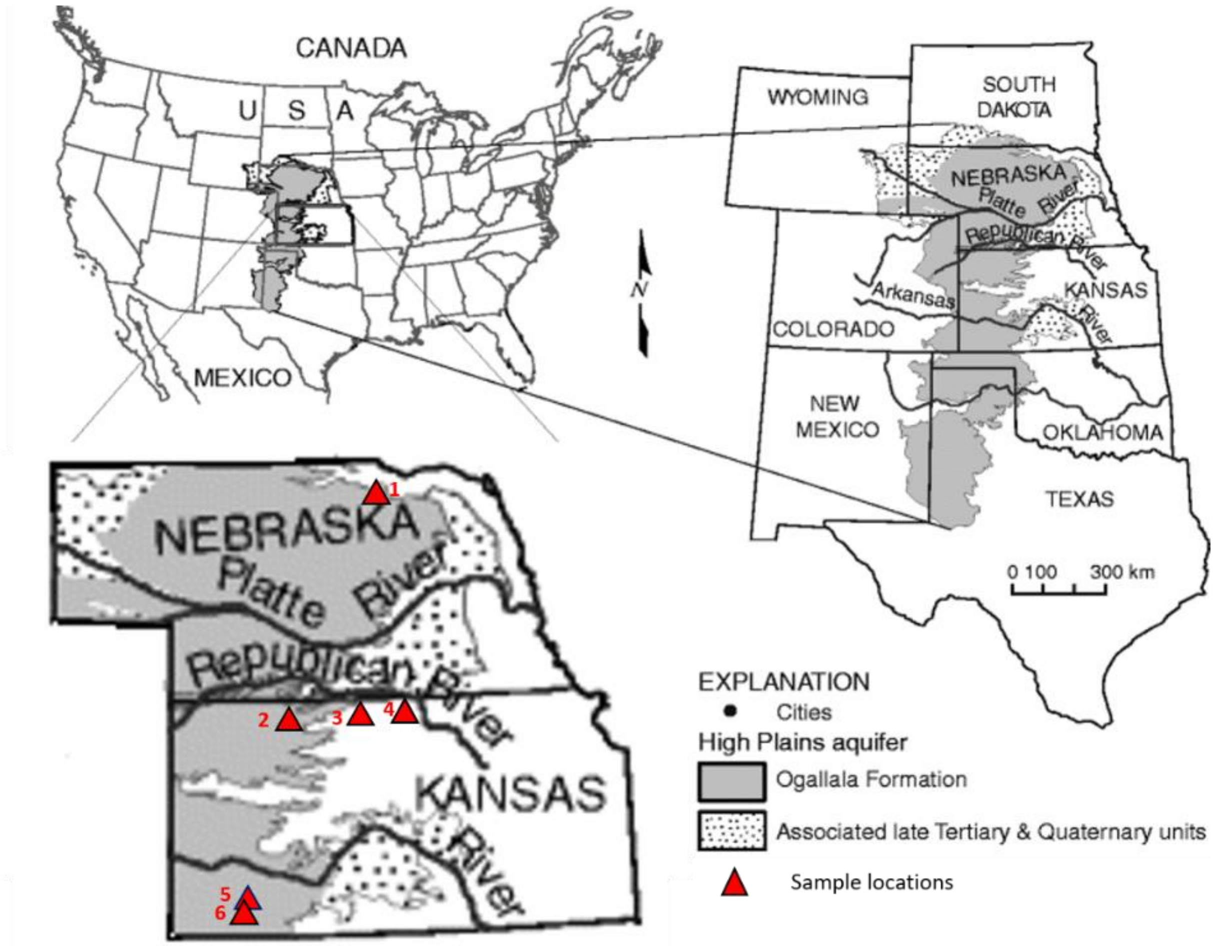

Figure 3. Map of the extent of the Ogallala Formation (grey), associated with late Tertiary and Quaternary units (dappled), and sample locations of this study (red triangles). 1. Nebraska Ashfall Fossil Bed State Park, 2. Calvert Mine 3. Smith County, 4. Jewell County, 5. and 6. Meade County, KS. Modified from Sophocleous (2009).

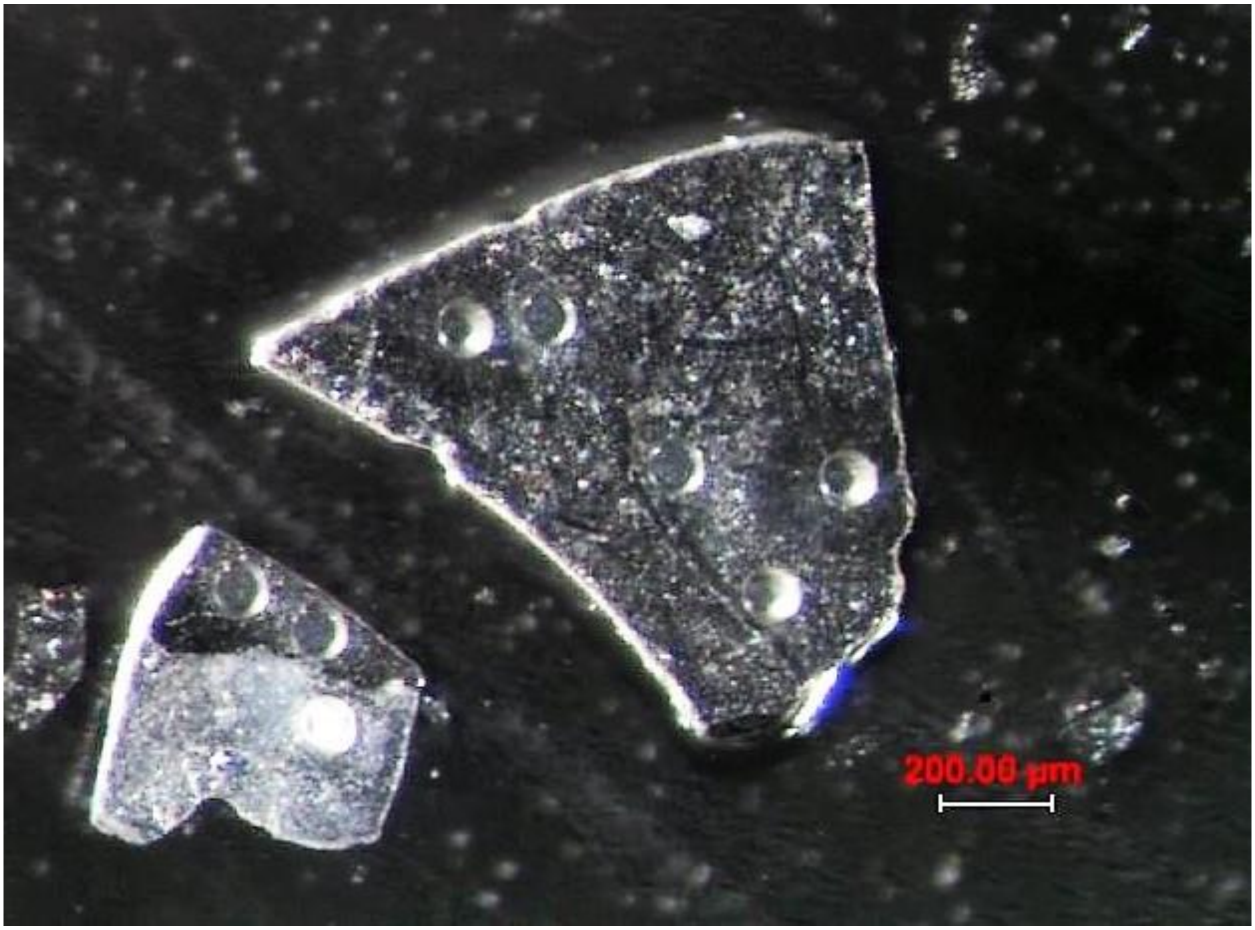

Figure 4. Microscope image of glass shard from sample HP14-07 taken after laser ablation analysis. Shards pictured here were chosen based on size, flatness, and lack of cracks, pits or bubbles. Laser ablation pits are 50µm diameter. Some minor surface dust can be observed, which is eliminated from inclusion in the collected data by three pre-ablation laser shots.

Table 01. Summary of Sample names, ID#, Location, Suspect sources, and supporting literature.

Sample Name	Sample ID #	Location	Suspected source eruption	literature
Calvert Ash	HP14-05b HP14-07	Norton County, KS	Ibex Hollow BJ YHT (ca 11.93 Ma)*	Hallman, 2016 Ludvigson et al., 2009 Izett & Wilcox, 1981 David, 2009 Rose et al, 2003 Swineford,1963 Smith, 2011
Smith County	SCS-KMI-16	Smith County, KS	Ibex Hollow BJ YHT (ca 11.93 Ma)	Ludvigson et al, 2009 Izett & Wilcox, 1981 David, 2009 Wan, E., 2008
Ashfall Fossil Beds State Historical Park	AFB-00	Royal, NE	Ibex Hollow BJ YHT (ca. 11.93 Ma)	Tucker, et al 2014 Perkins & Nash, 2002
Reference for source material: Perkins & Nash, 2002; Pearce et al., 2004				
Mankato Mine	JCS-KMI-16	Jewell County, KS	Lava Creek B YHT (ca 0.6 Ma)	Hallman, 2016 Ludvigson et al, 2009 David, 2009 Diffendal, Wan, 2008, pers. comm. to Ludvigson
Cudahy Camp	MC-CA-01	Meade County, KS	Lava Creek B YHT (ca 0.6 Ma)	Boellstorff, 1976 FOP-lawrence Perkins and Nash, 1995
Borcher's Badlands	BOR-S2-01	Meade County, KS	Huckleberry Ridge (ca 2.1 Ma)	Boellstorff, 1976

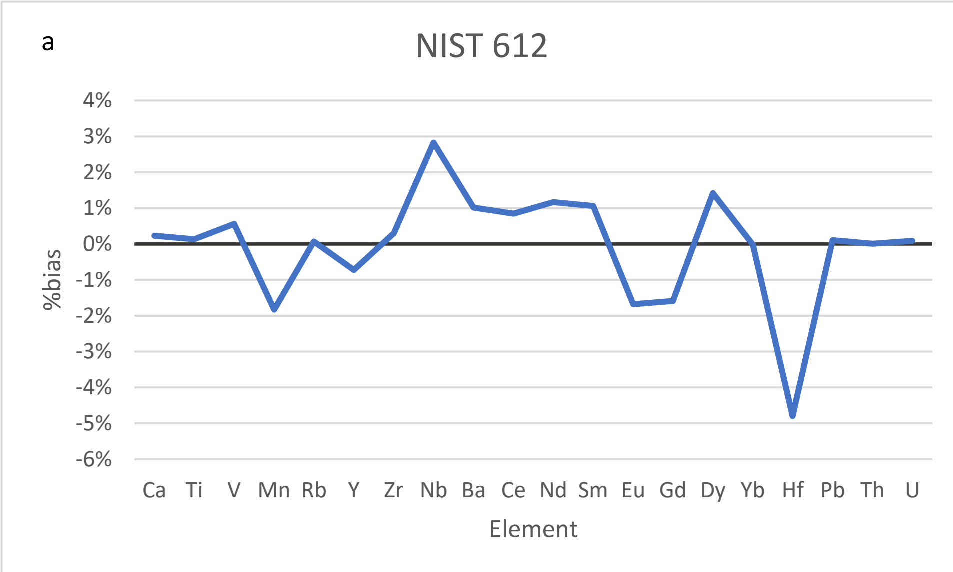

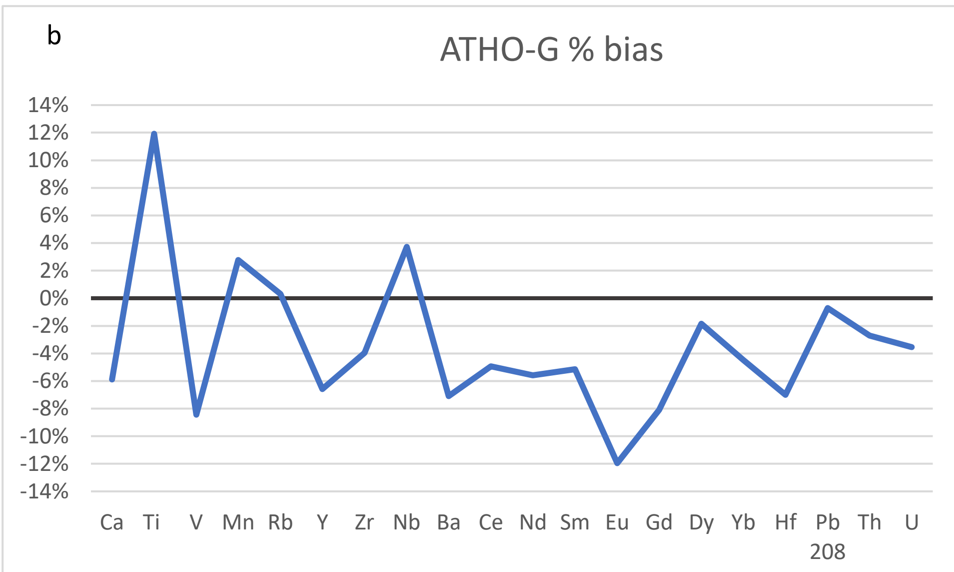

Figure 5 a&b. Reproducibility plots for the primary (NIST 612) and secondary (ATHO-G) reference materials. Fig a. shows %bias values for elements measured agreed with published values within ±5%.Fig b. shows ATHO-G % bias values for elements measured agreed with published values within ±8% with the exception of Ti (+12%) and Eu (-12%).

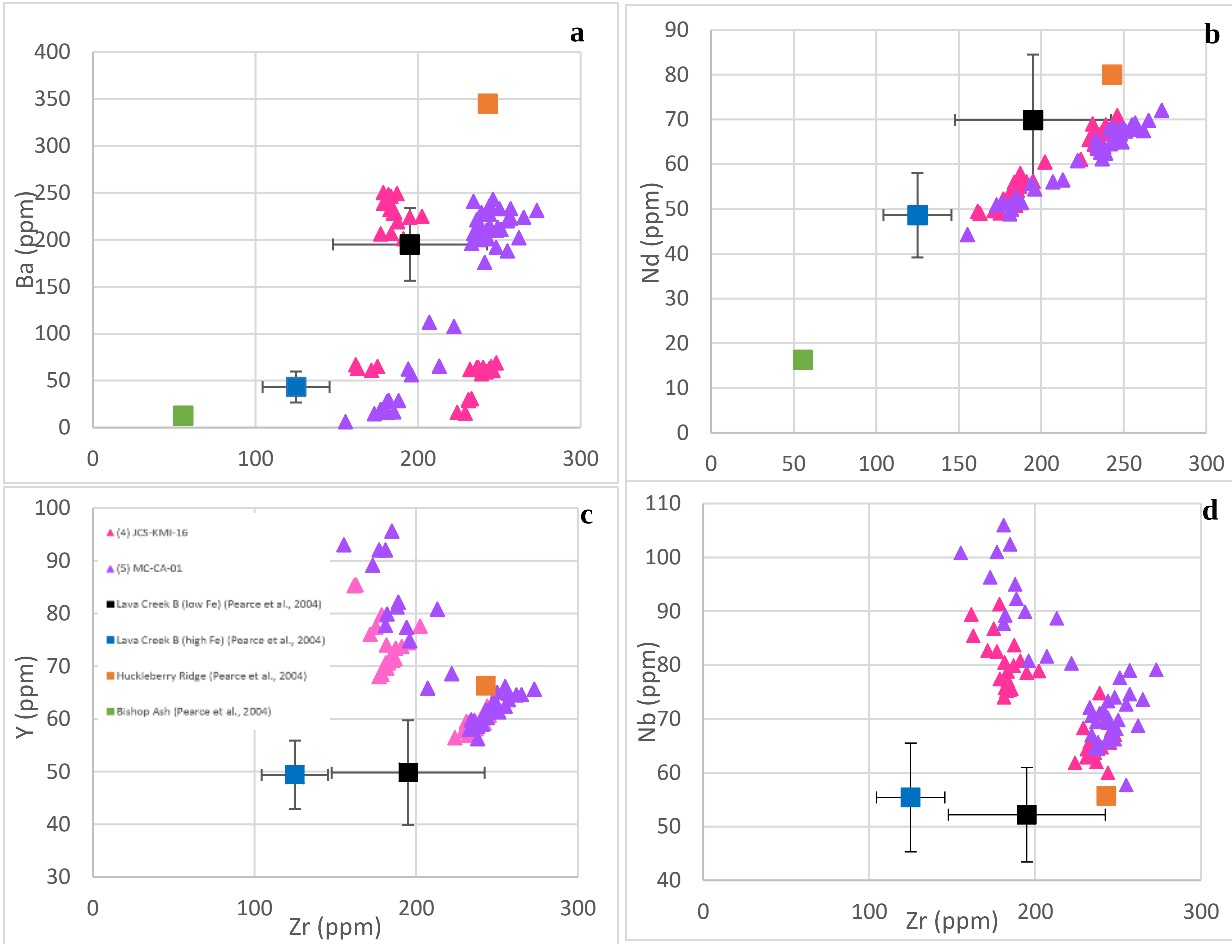

Figure 6a-d. Bivariate element plots (Ba, Nd, Y, Nb vs Zr) for samples suspected to be sourced from the Lava Creek B eruption (0.6 Ma). Published values for Huckleberry Ridge (2.1 Ma) and Bishop Ash (0.76 Ma) are also plotted. Bishop Ash values for Y and Nb were outside of the area of the plots.

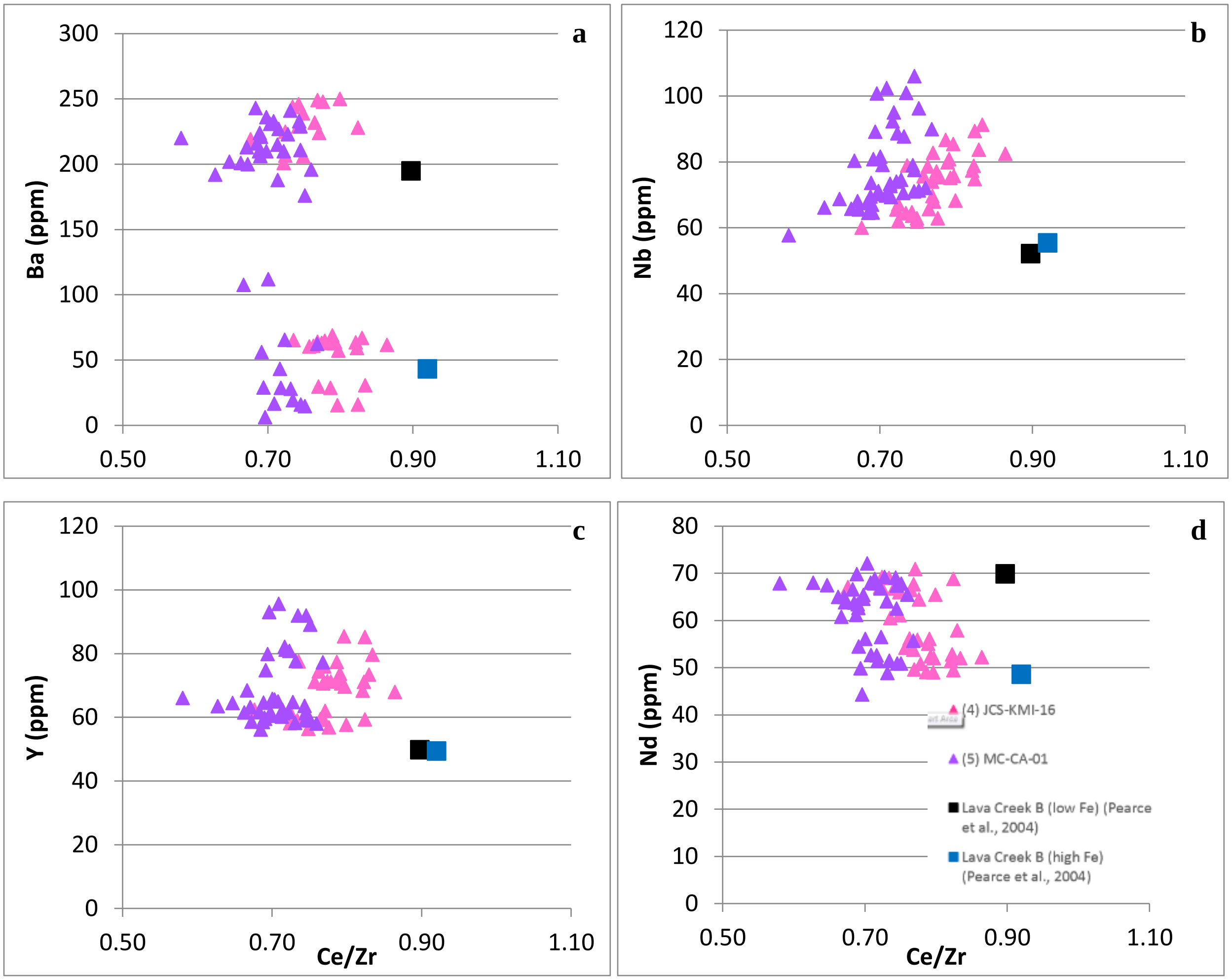

Figure 7a-d. Elemental ratio plots for volcanic ashes suspected to be sourced from the Lava Creek B eruption. Reference data from Pearce et al. (2004).

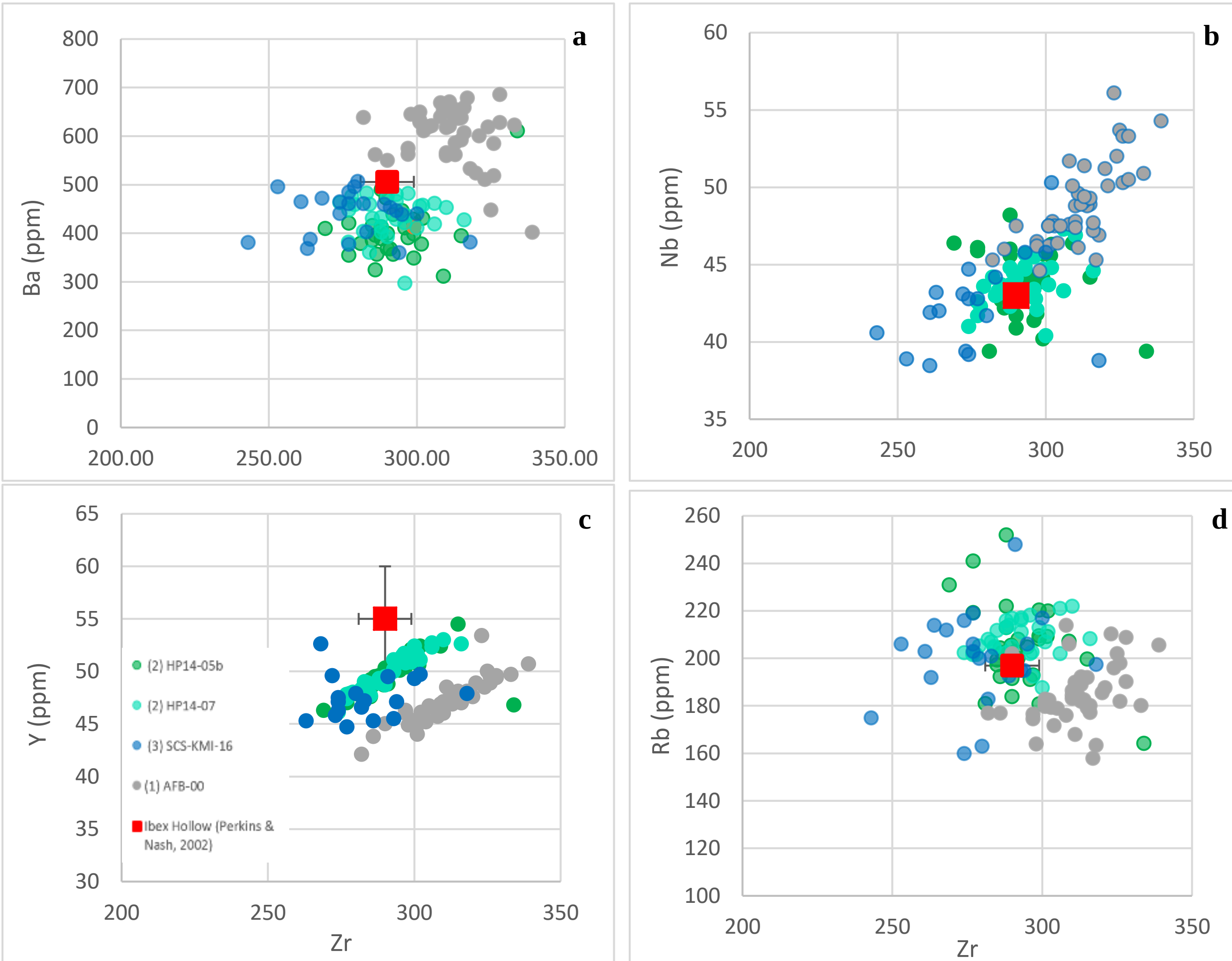

Figure 8a-d. Bivariate element plots- Zr vs. Ba, Nb, Y, and Rb, respectively- for volcanic ashes suspected to be sourced from the Ibex Hollow eruption (see text for discussion). Ibex Hollow reference data averages are from Perkins & Nash, (2002).

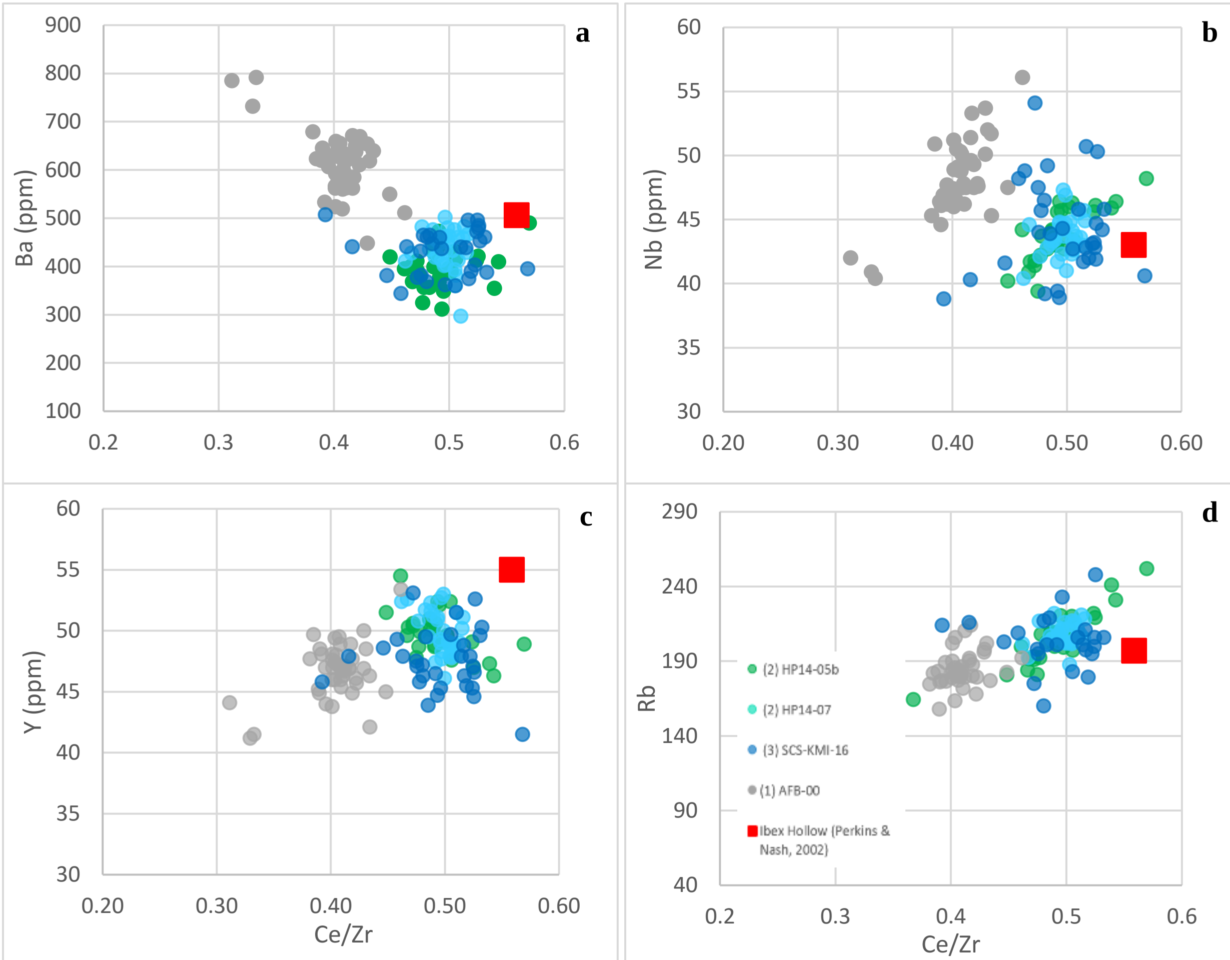

Figure 9a-d. Ce/Zr vs. elemental concentration plots for Ba, Y, Nb, and Nd, respectively. Plots show data from samples of this study and Perkins & Nash (2002) average values for the Bruneau Jarbidge (11.93 Ma) YHT eruption.

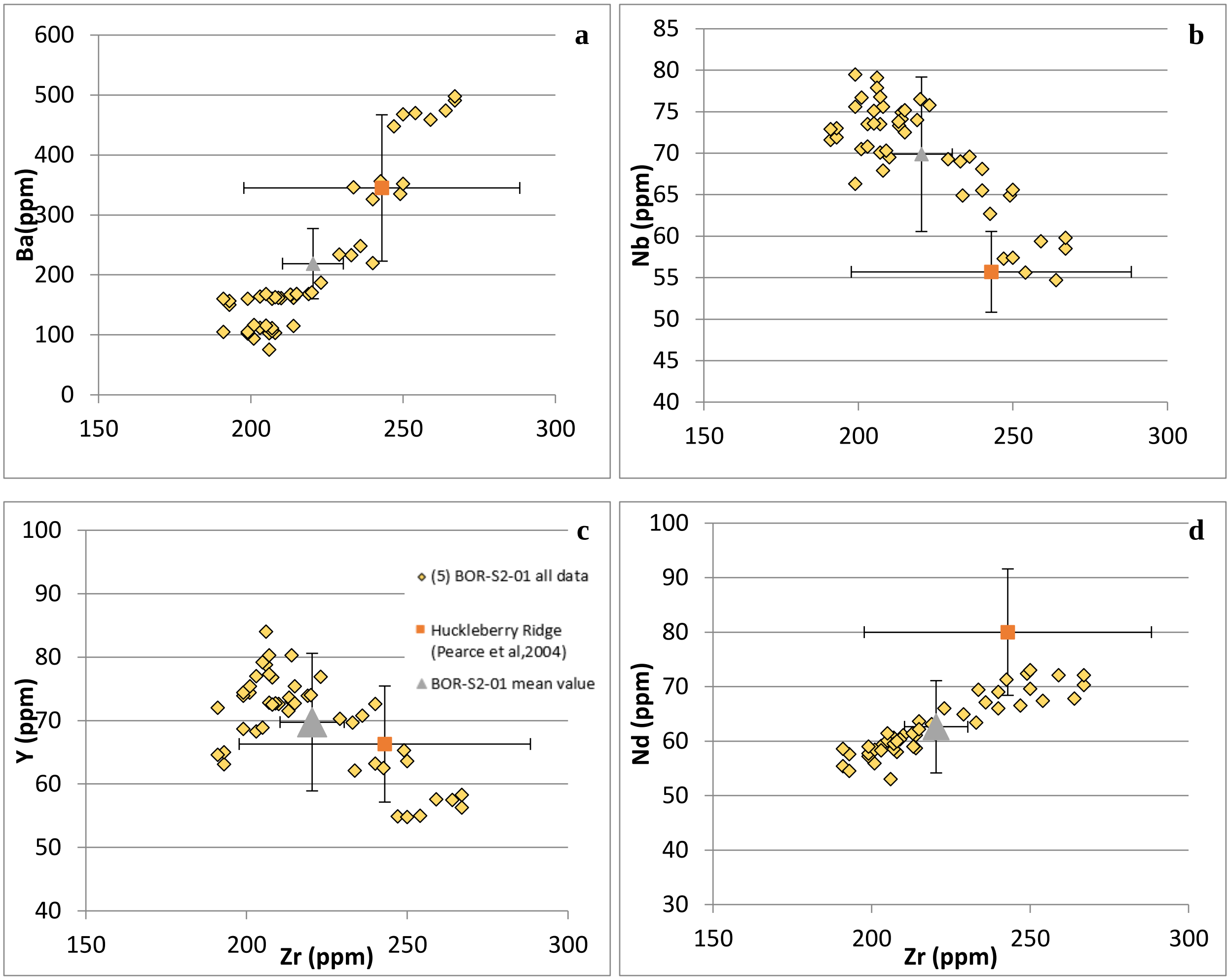

Figure 10a-d. Element vs. element concentration plots for BOR-S2-01 (see locality 5, fig 02) of Zr vs Y, Nb, Ba, and Nd. Average values for sample BOR-S2-16 (Fig 2. Location 5) were plotted against Pearce (2004) reported averages for Huckleberry Ridge tephra.

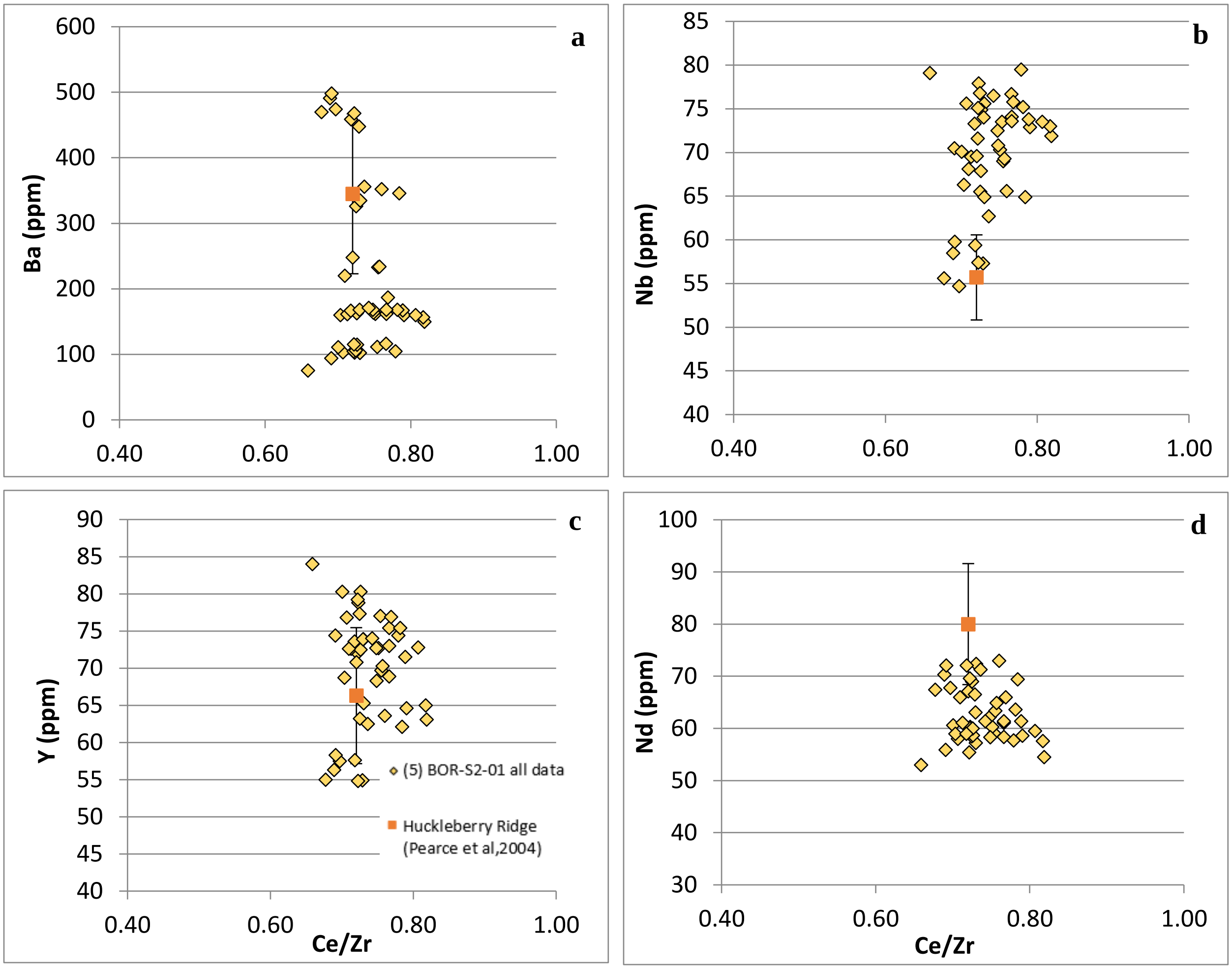

Figure 11 a-d. Ce/Zr vs. Ba, Y, Nb, and Nd (respectively) plots for sample BOR-S2-01 (Fig 2, location 5) and averages reported by Pearce (2004) for Huckleberry Ridge tephra.

APPENDICES

Appendix A: Annotated Outcrop Photographs

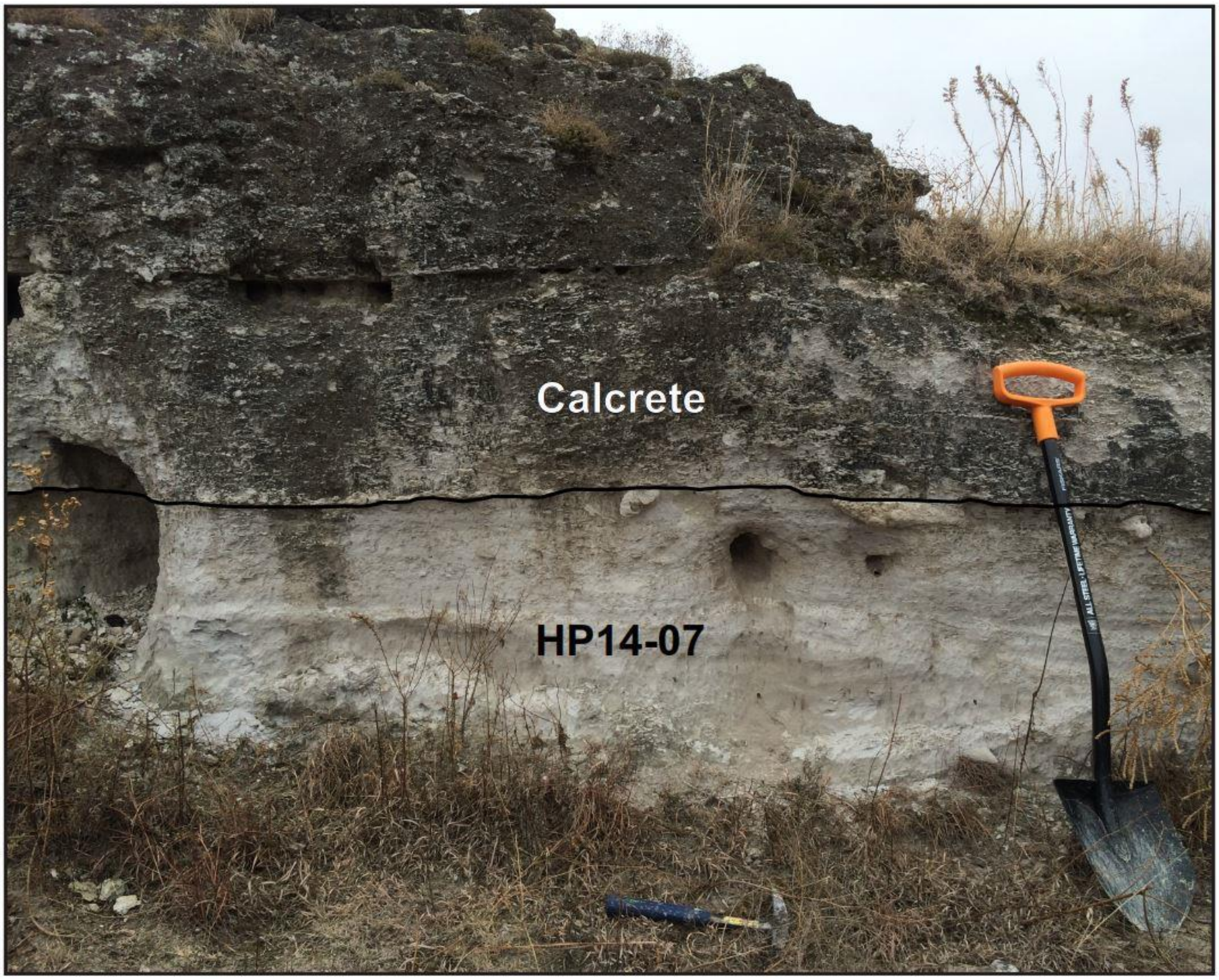

Picture 01. Photo courtesy of Jason Hallman. Sample HP14-07 (Fig 3, locality #2) is a fine-grained vitric ash collected from an abandoned face of the Calvert ash mine.

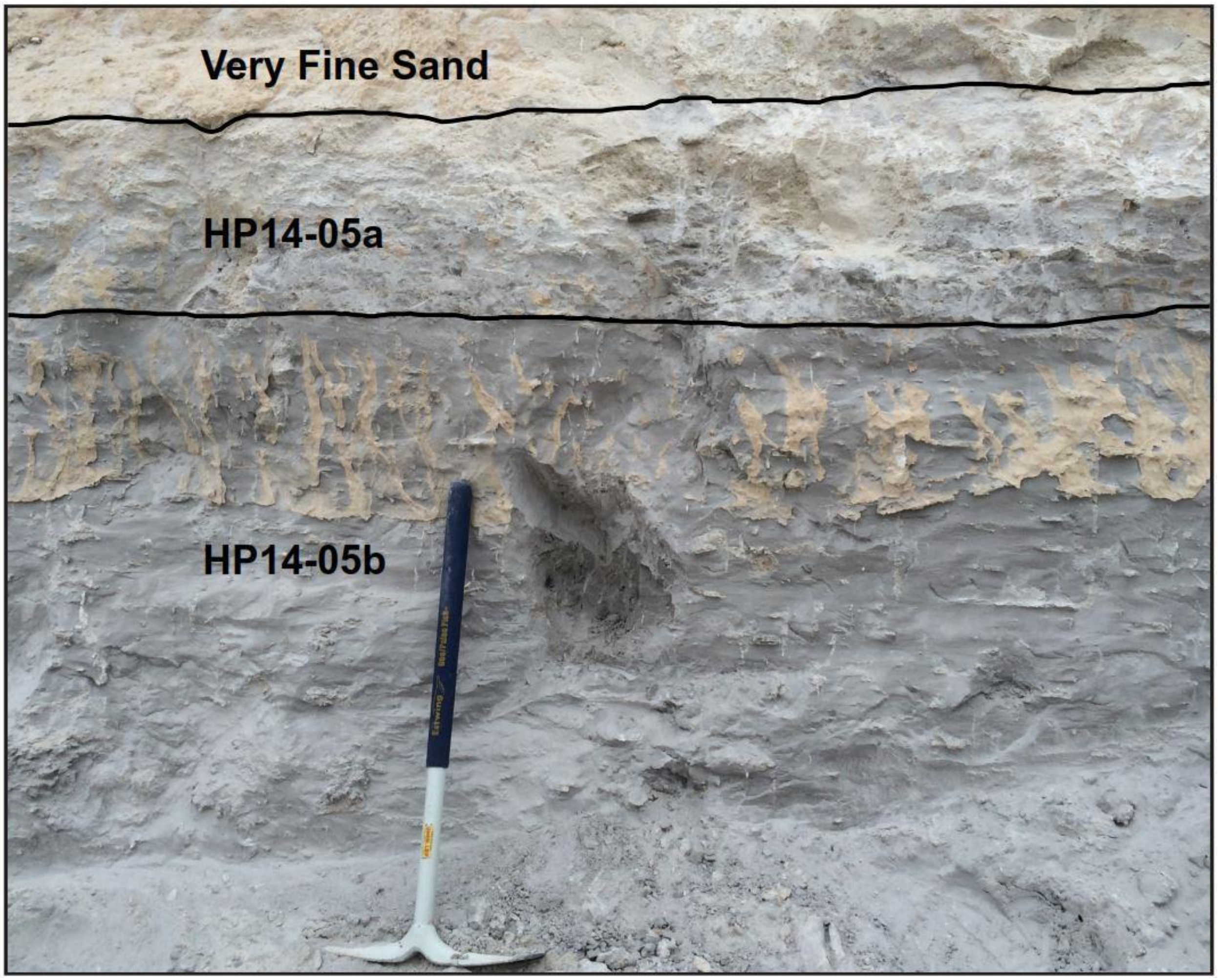

Picture 02. HP14-05b is a massively bedded, fine-grained vitric ash also located at the Calvert ash mine (Fig 3., locality 2). Photo courtesy of Jason Hallman


Picture 03. Fine-grained vitric ash sample MC-CA-01 collected from the Cudahy Camp location (Fig 3, locality 5), Meade County, KS. Photo courtesy John J. Smith.

Picture 04. Fine-grained vitric ash sample SCS-KMI-16 collected from Smith County location (Fig 3, locality 3).

Appendix B. LA-ICP-MS Operational Parameters

Table B-01. Operating parameters for the LA-ICP-MS. Parameters such as spot size, repetition rate, and energy density were chosen to maximize sample collection time and analytical precision without drilling through the thin volcanic glass shards.

LA-ICP-MS operating procedures	
Laser parameters- Photon machines Analyte G2 193nm ArF excimer	
Energy Density	4.0 J/cm^2
Pulse Duration	5 ns
Repetition Rate	5 Hz
Spot size	50 µm
He cell gas flow	0.51 l/min
N_2 cell gas flow	0.5 l/min
Sampling	Spot
ICP-MS settings	Thermo Element2 Sector Field
RF Power	1230 W
Plasma gas flow	0.93 l/min
Carrier gas flow	1.095 l/min
Torch	Garnet
Cones	Garnet
Data acquisition parameters	
Count time on sample	22 sec
Count time on background	20 sec
Sweeps per reading (passes)	1
Replicates (runs)	90
Sample time	42
Isotopes	^{43}Ca, ^{44}Ca, ^{49}Ti, ^{51}V, ^{55}Mn,^{86}Rb, ^{89}Y, ^{90}Zr, ^{93}Nb, ^{137}Ba, ^{140}Ce, ^{146}Nd, ^{147}Sm, ^{153}Eu, ^{157}Gd ^{163}Dy ^{172}Yb ^{178}Hf, ^{208}Pb, ^{232}Th, ^{238}U
External calibration standard	NIST 612, ATHO-G
Comment:	SQUID signal smoothing device used.

Appendix C: LA-ICP-MS Reference Material Validation

Table C-1: Average measured values for NIST-612 for all experiments, listed against reference values from Jochum et al. (2011). Percent bias is calculated in the same manner as Tomlinson et al. 2010.

Element	mean value (ppm)	%standard Deviation	Reference values (Jochum et al., 2011)	%bias
Ca	85200	1.3	85000	0.2%
Ti	44.06	2.9	44	0.1%
V	39.02	1.0	38.8	0.6%
Mn	38.00	1.1	38.7	-0.8%
Rb	31.42	1.2	31.4	0.1%
Y	38.02	1.1	38.3	-0.7%
Zr	38.01	1.4	37.9	0.3%
Nb	40.03	1.1	38.9	2.8%
Ba	39.70	1.6	39.3	1.0%
Ce	38.73	1.2	38.4	0.9%
Nd	35.92	2.2	35.5	1.2%
Sm	38.10	2.2	37.7	1.1%
Eu	35.01	1.0	35.6	-0.7%
Gd	36.72	1.8	37.3	-0.6%
Dy	36.01	1.3	35.5	1.4%
Yb	39.19	1.1	39.2	0.0%
Hf	35.02	1.4	36.7	-0.8%
Pb	38.61	1.7	38.57	0.1%
Th	37.79	1.1	37.79	0.0%
U	37.41	1.4	37.38	0.1%

Table C-2: Average measured values for ATHO-G for all experiments, listed against reference values from Jochum et al, (2006). Percent bias is calculated in the same manner as Tomlinson et al., 2010.

Element	Reference Values (Jochum et al., 2006)	Mean Value (ppm)	% Standard deviation	% bias
Ca	12000	11575.6	4.8	-3.5%
Ti	1528.7	1711	7.3	11.9%
V	3.9	3.58	6.04	-8.4%
Mn	821.1	843.89	5.13	2.8%
Rb	65.3	65.50	6.38	0.3%
Y	94.5	88.27	3.28	-6.6%
Zr	512.0	491.77	2.60	-4.0%
Nb	62.4	64.72	6.61	3.7%
Ba	547.0	508.18	2.71	-7.1%
Ce	121.0	115.04	2.12	-4.9%
Nd	60.9	**57.50**	**3.39**	-5.6%
Sm	14.2	13.47	4.87	-5.1%
Eu	2.8	2.43	3.83	-12.1%
Gd	15.3	14.06	3.43	-8.1%
Dy	16.2	15.90	3.41	-1.8%
Yb	10.5	10.03	3.84	-4.4%
Hf	13.7	12.74	3.71	-7.0%
Pb 208	5.7	5.63	8.50	-0.6%
Th	7.4	7.20	3.02	-2.7%
U	2.4	2.29	6.24	-3.5%

Appendix D: Similarity Coefficient

Similarity coefficient formula used to produce Table E. (Borchardt et al., 1972).

$$d_{(A,B)} = \frac{\sum_{i=1}^{n} R_1}{n}$$

$d_{(A,B)}$ = similarity coefficient for comparison between sample *A* and sample *B*.
i = element number
n = number of elements
$R_i = X_{iA}/X_{iB}$, if $X_{iB} \geq X_{iA}$
$R_i = X_{iB}/X_{iA}$ if $X_{iA} > X_{iB}$
Xi = concentration of element i in sample *A*
Xi = concentration of element i in sample *B*.

Table E-1: Average Similarity Coefficients calculated for measured values vs. reference literature values. Numbers in bold are above the 0.86 threshold for positive correlation defined by Borchardt, et al 1972.

Reference material		Perkins and Nash, 2002	Perkins and Nash, 2002	Perkins and Nash, 2002		Pearce et al., 2004	Pearce et al., 2004	Pearce et al., 2004
Source		YHT	YHT	YHT		YHT	YHT	YHT
Eruption		Tuff of Ibex Hollow	Lava Creek B	Huckleberry Ridge Tuff		Lava Creek B	Lava Creek B	Huckleberry Ridge
Sample name						UA256 (Fe <1.6%)	UA256 (Fe > 1.6%)	UA598
	Elements used				Elements used			
HP14-05b	Ti, Mn, Zr, Nb, Ba, Th	**0.93**	0.65	0.72	Rb, Zr, Nd, Ba, Ce	0.73	0.62	0.81
HP14-07	Ti, Mn, Zr, Nb, Ba, Th	**0.94**	0.64	0.71	Rb, Zr, Nd, Ba, Ce	0.74	0.62	0.81
SCS-KMI-16	Ti, Mn, Zr, Nb, Ba, Th	**0.93**	0.65	0.73	Rb, Zr, Nd, Ba, Ce	0.72	0.64	0.8
AFB-00	Ti, Mn, Zr, Nb, Ba, Th	**0.87**	0.66	0.71	Rb, Zr, Nd, Ba, Ce	0.66	0.62	0.73
JCS-KMI-16 (low Ba)	Ti, Mn, Zr, Nb, Th	0.64	0.83	0.74	Rb, Zr, Nd, Ba, Ce	0.71	**0.87**	0.63
JCS-KMI-16 (high Ba)	Ti, Mn, Zr, Nb, Th	0.70	**0.88**	0.85	Rb, Zr, Nd, Ba, Ce	**0.89**	0.56	**0.87**
MC-CA-01 (low Ba)	Ti, Mn, Zr, Nb, Th	0.53	0.80	0.72	Rb, Zr, Nd, Ba, Ce	0.69	**0.86**	0.61
MC-CA-01 (high Ba)	Ti, Mn, Zr, Nb, Th	0.63	**0.85**	0.84	Rb, Zr, Nd, Ba, Ce	**0.86**	0.56	0.85
BOR-S2-01	Ti, Mn, Zr, Nb, Th	0.63	0.82	**0.86**	Rb, Zr, Nb, U	0.81	0.65	**0.87**

Appendix E. LA-ICP-MS elemental concentration data

Notes on data exclusion: samples were sorted and rejected based on the following criteria

1) *Sample duration <7 seconds were excluded*
2) *^{43}Ca count rates too low or too high (determined on a sample-by-sample basis)*
3) *^{44}Ca concentrations with errors >10%*
4) *Data outliers were also addressed on a sample-by-sample basis*

Table E-1 LA-ICP-MS Elemental Concentration Data: HP14-05 B

Spot #	Duration	Ca43		Ca44		Ti49		V51		Mn55		Rb85		Y89	
	seconds	CPS	Int2SE	ppm	Int2SE	ppm	Int2SE	ppm	Int2SE	ppm	Int2SE	ppm	Int2SE	ppm	Int2SE
1	19.1	14620	850	3680	170	1365	58	0.629	0.039	187.1	8.6	199.7	9.3	54.5	2.5
2	19.1	14830	630	3580	120	1355	50	0.53	0.048	182.4	6.2	205.5	6.4	48.7	1.6
3	19.1	17340	640	3680	150	1317	42	1.359	0.073	203	8	164.3	5.2	46.8	1.6
4	19.1	14520	660	3640	150	1388	53	0.731	0.063	199	10	213	10	49.6	2.1
5	19.1	14070	570	3660	150	1382	51	0.565	0.052	182.7	7.5	204.8	8	50.1	1.8
6	19.1	14830	760	3390	140	1267	47	0.542	0.043	171.2	7.6	191.6	7.8	50.3	2
7	19.1	15360	580	3610	100	1326	39	0.621	0.049	189.3	5.7	202.5	7.4	49.5	1.5
8	15.9	15550	760	3650	180	1345	64	0.646	0.041	191	11	208	12	49.9	2.6
9	19.1	15070	670	3670	140	1336	49	0.568	0.046	189	8.4	209.5	9.6	50.9	2.3
10	19.1	13950	620	3750	180	1426	65	0.676	0.073	207	11	220	11	52.4	2.4
11	19.1	14680	640	3510	140	1356	47	0.63	0.048	192.6	5.9	209.3	6.7	50.6	1.8
12	17.3	15310	560	3540	150	1243	49	0.585	0.05	174	6.5	184	6.7	49.6	1.8
13	15.8	15180	800	3510	150	1347	66	0.67	0.063	184.3	7.9	197.4	8.3	47.6	2
14	6.9	16800	1000	3820	360	1411	80	1.45	0.16	229	17	179	16	43	3.1
15	15.7	12400	670	3850	220	1509	73	0.732	0.069	215	13	252	17	48.9	2.7
16	19.1	11600	620	3640	220	1392	76	0.58	0.068	194	12	241	14	47.3	2.8
17	19.1	12750	470	3580	170	1394	48	0.609	0.07	191.9	7.7	219.3	8.7	47	2.1
18	12.6	13670	930	3730	320	1410	100	0.737	0.086	202	17	231	20	46.3	3.3
19	19.1	15420	700	3600	160	1280	47	0.576	0.041	181.6	6.9	191.2	6.7	50.6	2
20	19.1	15230	690	3440	140	1294	56	0.689	0.058	187	8.3	199.3	9	49.2	2.2
21	19.1	15400	570	3510	130	1218	46	0.564	0.04	171.3	6.3	180.9	6.8	51.5	2
22	13.1	16420	670	3380	140	1215	58	0.609	0.056	172	9.1	181	10	47.8	2.2
23	19.1	14210	610	3760	140	1377	51	0.648	0.062	198.6	9	220.4	8.8	52.1	2
24	19.1	14450	620	3700	160	1325	58	0.638	0.059	192.7	9.2	204.5	9.7	49.1	2.2
25	19.1	13500	500	3720	170	1382	53	0.613	0.057	195.3	9.7	222	10	49.1	1.9
26	19.1	14950	640	3620	140	1331	51	0.686	0.056	191.1	8.9	202.8	9.3	48.8	2.1
27	19.1	15440	600	3460	140	1305	48	0.567	0.056	176.4	6	193	7.1	50.4	2
28	19.1	14290	680	3510	120	1376	45	0.615	0.057	190.5	8	207.3	9.4	52.4	2.3
29	19.1	15900	690	3380	130	1241	46	0.566	0.045	175.8	6.8	192.4	9.2	48.7	2.2
30	19.1	13200	540	3520	170	1327	58	0.51	0.052	180.2	8.6	208.2	9.7	51	2.7
31	19.1	13600	710	3490	170	1314	68	0.568	0.046	179.3	9.6	200	11	50.2	2.5
Average		**14663**		**3599**		**1340**		**1**		**190**		**204**		**49**	
Standard Dev		**1214.14**		**123.02**		**63.52**		**0.20**		**12.79**		**17.97**		**2.14**	
% Standard Dev		**8.28**		**3.42**		**4.74**		**30.27**		**6.75**		**8.79**		**4.32**	

Table E-2 LA-ICP-MS Elemental Concentration Data: HP14-05 B (continued)

Spot #	Zr90		Nb93		Ba137		Ce140		Nd146		Sm147		Eu153	
	ppm	Int2SE	ppm	Int2SE	ppm	Int2SE	ppm	Int2SE	ppm	Int2SE	ppm	Int2SE	ppm	Int2SE
1	315	15	44.2	1.8	395	19	145.2	7.1	55.4	2.6	10.89	0.73	0.645	0.042
2	289.6	9.7	43	1.4	473	15	142.1	4.7	50.2	1.9	9.58	0.79	0.686	0.036
3	334	11	39.4	1.1	611	17	122.7	4.6	48.6	2.2	9.23	0.65	0.806	0.043
4	288	13	46	2.3	389	14	144.5	5.8	52.1	2.1	9.76	0.81	0.615	0.04
5	295	10	44.2	1.8	447	18	143.7	6.3	53.9	2.1	10.01	0.66	0.677	0.038
6	290	12	41.7	1.5	369	17	135.7	5.1	51.6	2.2	9.71	0.7	0.62	0.037
7	286.5	9.6	42.7	1.4	357	12	138.3	4.9	52	2	9.74	0.67	0.598	0.035
8	292	14	43.7	2.2	357	18	139.6	6.5	51.1	2.8	9.86	0.73	0.552	0.035
9	299	13	44.1	1.7	399	16	145.5	6.3	54	2.4	10.3	0.83	0.612	0.038
10	302	14	46.3	2.2	431	22	152.4	8.1	54.5	2.8	10.14	0.64	0.63	0.051
11	301.6	9.4	45.6	1.5	378	13	148.3	6.1	55.9	2	10.27	0.58	0.563	0.039
12	290	11	40.9	1.7	400	14	135.3	4.5	51.5	2	9.79	0.61	0.637	0.041
13	285	12	43.4	1.8	416	20	144.1	7.3	50.9	2.7	9.51	0.97	0.62	0.038
14	304	16	40.4	2.8	536	33	136.5	9.3	50.5	3.6	8.4	1.4	0.731	0.082
15	288	14	48.2	2.5	490	28	164	11	55.9	3.5	9.89	0.75	0.648	0.053
16	277	14	45.9	2.5	355	22	149.3	8.5	49.6	3.1	9.48	0.71	0.567	0.054
17	277	10	46.1	2.2	421	16	145.4	6.5	51.6	2.2	9.47	0.59	0.584	0.035
18	269	17	46.4	3.8	410	28	146	12	51.4	4.2	8.82	0.96	0.652	0.061
19	296	11	41.4	1.5	411	16	139.7	5.6	53.2	2.6	10.22	0.61	0.604	0.039
20	285	11	42.7	1.8	386	17	141.8	6.3	52.2	2.6	9.67	0.62	0.59	0.037
21	299	11	40.2	1.7	420	18	134.1	5.8	53.1	2.3	9.49	0.73	0.656	0.044
22	281	14	39.4	2.1	379	19	133.4	6.5	51.1	3.1	9.78	0.84	0.607	0.03
23	299	11	45.7	1.9	349	14	148	5.7	54.1	2.2	10.24	0.63	0.605	0.039
24	286	12	43.6	1.7	396	17	142.9	6.3	50.6	2.4	9.43	0.63	0.637	0.041
25	288	11	45.6	1.9	413	16	150.8	7.4	54.3	2.7	10.73	0.79	0.619	0.046
26	291	12	43	1.7	368	15	142.9	6.9	50.3	2.6	9.65	0.76	0.635	0.038
27	297	13	41.8	1.5	391	15	140.2	5.4	52.5	2.3	10.53	0.72	0.613	0.043
28	309	13	46.4	2	312	13	152.5	6.6	55.1	2.2	10.79	0.73	0.576	0.039
29	286	13	42.2	2.1	325	15	136.4	6.1	50.6	2.9	10.06	0.61	0.563	0.036
30	299	14	43.9	1.9	429	19	145.5	6.6	54.1	2.9	10.44	0.83	0.631	0.044
31	292	14	43.2	2.2	439	22	143	7.6	55.2	4	10.25	0.83	0.656	0.05
Average	**293**		**44**		**408**		**143**		**52**		**10**		**1**	
Standard Dev	**12.02**		**2.24**		**58.60**		**7.29**		**1.96**		**0.54**		**0.05**	
% Standard Dev	**4.10**		**5.14**		**14.36**		**5.10**		**3.73**		**5.44**		**8.02**	

Table E-3 LA-ICP-MS Elemental Concentration Data: HP14-05 B (continued)

Spot #	Gd157		Dy163		Yb172		Hf178		Pb208		Th232		U238	
	ppm	Int2SE	ppm	Int2SE	ppm	Int2SE	ppm	Int2SE	ppm	Int2SE	ppm	Int2SE	ppm	Int2SE
1	9.31	0.7	9.64	0.57	5.57	0.36	9.15	0.64	28.1	1.1	33.6	1.8	8.28	0.48
2	8.48	0.42	8.92	0.46	5.13	0.23	8.62	0.45	28.2	1.1	31.3	1.2	7.94	0.35
3	8.1	0.44	8.66	0.35	4.94	0.27	9.41	0.41	24.28	0.92	25.18	0.88	6.06	0.21
4	8.29	0.51	9.1	0.55	5.26	0.32	8.79	0.64	31	1.6	31.3	1.4	8.48	0.45
5	8.89	0.47	9.04	0.43	5.49	0.3	8.69	0.51	28.3	1.1	32	1.3	8.01	0.39
6	8.83	0.52	8.97	0.56	5.41	0.33	8.26	0.44	26.2	1.6	31.3	1.4	7.57	0.34
7	8.43	0.47	9.02	0.49	5.16	0.21	8.63	0.51	28	1.2	31.2	1.1	7.97	0.36
8	8.35	0.48	8.47	0.48	5.2	0.37	8.46	0.56	28.8	1.8	30.9	1.6	8.04	0.41
9	8.82	0.57	9.07	0.46	5.35	0.26	9.12	0.53	29.1	1.2	32.3	1.3	7.9	0.32
10	9.49	0.68	9.24	0.55	5.54	0.32	9.36	0.6	31.4	1.6	32.5	1.4	8.7	0.47
11	8.68	0.58	9.14	0.46	5.38	0.3	8.78	0.35	29.4	1.3	31.9	1.3	8.21	0.35
12	8.81	0.51	8.59	0.41	5.19	0.28	8.4	0.4	25.9	1.1	30.7	1.2	7.24	0.28
13	8.75	0.6	8.71	0.45	5.07	0.29	7.97	0.52	28.1	1.4	31.6	1.6	8.13	0.38
14	7.52	0.96	8.32	0.67	4.9	0.53	9.54	0.74	29.6	2.9	25.1	1.8	7.72	0.89
15	8.08	0.71	9.01	0.6	5.24	0.4	8.71	0.67	34.8	2.3	31.3	1.8	9.85	0.5
16	8.18	0.61	8.92	0.65	4.77	0.35	8.01	0.62	33.5	2.1	30.4	1.9	9.22	0.57
17	8.09	0.54	8.18	0.45	4.93	0.24	7.74	0.46	29.7	1.3	30.3	1.2	8.53	0.37
18	7.99	0.85	8.42	0.81	4.62	0.38	7.76	0.59	32.7	3.5	28.7	1.8	9.16	0.73
19	8.82	0.61	9.01	0.49	5.19	0.29	8.54	0.38	26.3	1.1	31.6	1.3	7.36	0.32
20	8.52	0.62	8.9	0.58	5.17	0.31	8.84	0.56	28.7	1.3	31.2	1.5	8.01	0.4
21	8.54	0.41	9.22	0.33	5.23	0.29	8.8	0.4	24.7	1	31.4	1.3	6.91	0.31
22	8.19	0.52	9.41	0.61	5.19	0.26	8.37	0.53	25.1	1.3	30.5	1.5	7.13	0.43
23	8.82	0.51	9.65	0.47	5.49	0.34	9.21	0.5	31.8	1.9	32.9	1.5	8.72	0.43
24	8.43	0.49	9.16	0.57	5.28	0.38	8.4	0.44	29.9	1.3	30.6	1.2	8.17	0.36
25	8.67	0.54	9.15	0.5	5.21	0.26	8.77	0.4	30.8	1.2	32.2	1.4	8.35	0.42
26	8.63	0.41	9.23	0.42	5.14	0.25	8.55	0.43	27.6	1.3	30.2	1.2	7.84	0.3
27	8.53	0.52	9.02	0.44	5.2	0.3	8.86	0.62	26.8	1.3	31.5	1.3	7.48	0.34
28	9.26	0.51	9.73	0.65	5.6	0.26	9.04	0.5	27.1	1.2	33.6	1.6	8.38	0.35
29	8.32	0.52	8.62	0.45	5.12	0.29	8.42	0.5	26.8	1.2	30.4	1.4	7.47	0.32
30	8.81	0.71	8.91	0.56	5.46	0.33	8.67	0.61	29.6	1.4	31.7	1.4	8.11	0.38
31	8.92	0.59	9.52	0.62	5.42	0.31	8.52	0.55	28.2	1.8	32.3	1.8	8	0.46
Average	**9**		**9**		**5**		**9**		**29**		**31**		**8**	
Standard Dev	**0.41**		**0.37**		**0.23**		**0.44**		**2.47**		**1.84**		**0.71**	
% Standard Dev	**4.78**		**4.16**		**4.33**		**5.06**		**8.59**		**5.92**		**8.88**	

Table E-4 LA-ICP-MS Elemental Concentration Data: HP14-07

spot #	Duration seconds	Ca43 CPS	Int2SE	Ca44 ppm	Int2SE	Ti49 ppm	Int2SE	V51 ppm	Int2SE	Mn55 ppm	Int2SE	Rb85 ppm	Int2SE	Y89 ppm	Int2SE
1	19.1	14700	570	3640	160	1351	56	0.55	0.06	183.60	8.90	213.00	11.00	50.90	2.20
2	19.1	14130	610	3560	130	1344	50	0.56	0.05	179.20	7.00	208.30	9.10	52.60	2.30
3	19.1	14990	880	3500	140	1280	47	0.60	0.13	175.10	6.40	192.50	7.60	50.80	2.30
4	19.1	14350	660	3650	150	1364	58	0.79	0.11	199.60	9.50	216.90	8.70	48.70	2.20
5	19.1	14680	540	3550	150	1272	48	0.58	0.04	181.90	7.10	202.40	8.50	46.10	1.90
6	10.1	15890	780	3670	220	1349	74	0.65	0.06	193.00	11.00	202.00	12.00	52.30	2.70
7	19.1	14320	650	3480	130	1318	40	0.59	0.05	189.90	7.00	204.40	7.50	48.90	1.90
8	19.1	13860	690	3730	160	1383	61	0.73	0.05	193.10	7.80	217.00	11.00	50.00	2.20
9	19.1	14660	460	3610	160	1365	58	0.56	0.04	183.20	7.80	202.70	6.30	51.70	2.00
10	19.1	14330	800	3540	150	1322	63	0.57	0.06	181.10	8.10	202.00	9.80	51.20	2.50
11	19.1	13540	670	3890	170	1416	66	0.63	0.05	193.30	9.50	222.00	12.00	53.00	2.60
12	19.1	13110	700	3630	160	1363	55	0.61	0.06	191.80	8.90	216.00	11.00	49.10	2.50
13	19.1	15120	860	3450	150	1234	60	0.60	0.05	174.10	7.90	187.70	9.30	52.40	2.60
14	19.1	12790	550	3480	160	1332	52	1.63	0.26	181.30	6.60	201.60	7.00	47.90	1.80
15	19.1	14760	530	3530	120	1308	41	0.68	0.04	189.10	6.10	201.60	7.30	47.80	1.60
16	19.1	13940	810	3620	170	1336	66	0.64	0.06	189.90	9.80	214.00	12.00	49.00	2.70
17	19.1	13860	500	3630	170	1346	57	0.69	0.06	199.00	10.00	211.80	8.80	47.70	1.80
19	19.1	14840	670	3480	150	1269	46	0.57	0.05	179.80	6.60	202.40	8.20	47.40	1.90
20	19.1	13740	730	3420	170	1320	62	0.58	0.05	182.00	8.70	213.00	11.00	48.90	2.40
21	19.1	14540	810	3530	150	1320	61	0.58	0.06	186.30	9.30	205.00	11.00	49.50	2.70
22	19.1	14000	780	3660	150	1318	58	0.61	0.06	187.70	9.60	207.00	12.00	49.00	2.60
23	19.1	12950	750	3760	200	1433	72	0.65	0.05	198.00	9.40	221.00	11.00	52.70	2.80
24	19.1	13730	540	3620	130	1367	54	0.60	0.05	189.90	7.60	211.10	8.70	51.10	2.00
25	19.1	14140	710	3620	160	1369	54	0.67	0.10	197.90	8.60	218.30	9.40	51.50	2.40
26	19.1	13770	760	3620	160	1360	57	0.68	0.06	190.00	8.80	211.30	9.60	51.10	2.60
27	19.1	14010	780	3620	160	1315	55	0.59	0.05	182.40	7.40	202.40	7.70	49.30	2.10
28	19.1	13890	640	3590	180	1354	53	0.64	0.06	182.90	7.30	207.00	9.00	51.60	2.30
29	19.1	14160	640	3490	110	1315	52	0.63	0.05	183.30	6.90	205.00	8.50	48.30	1.90
30	19.1	12920	570	3690	120	1386	48	0.69	0.07	199.60	7.50	216.20	7.40	50.20	2.00
31	19.1	14220	590	3590	160	1322	50	0.69	0.06	191.00	7.10	205.20	8.80	48.00	2.00
32	19.1	14220	590	3480	130	1325	52	0.68	0.06	194.00	7.90	208.00	10.00	48.30	1.90
Average		**14134.1**		**3591**		**1337**		**0.66**		**187.84**		**208.03**		**49.90**	
Standard deviation		**664.51**		**99**		**41**		**0.19**		**7.04**		**7.73**		**1.80**	
% standard deviation		**4.70**		**2.74**		**3.06**		**27.99**		**3.75**		**3.72**		**3.61**	

Table E-5 LA-ICP-MS Elemental Concentration Data: HP14-07 (continued)

spot	Zr90		Nb93		Ba137		Ce140		Nd146		Sm147		Eu153	
#	**ppm**	**Int2SE**	**ppm**	**Int2SE**	**ppm**	**Int2SE**	**ppm**	**Int2SE**	**ppm**	**Int2SE**	**ppm**	**Int2SE**	**ppm**	**Int2SE**
1	299.00	13.00	44.70	2.10	413.00	19.00	147.50	7.10	54.70	3.00	10.08	0.83	0.61	0.04
2	316.00	14.00	44.60	2.00	428.00	20.00	147.60	7.10	55.90	2.50	10.67	0.61	0.66	0.06
3	297.00	12.00	42.10	1.80	482.00	22.00	141.50	6.20	54.10	2.50	10.23	0.66	0.67	0.04
4	290.00	13.00	44.10	2.10	393.00	18.00	146.40	6.80	53.50	3.10	9.57	0.73	0.66	0.04
5	274.00	10.00	41.00	1.40	463.00	16.00	136.90	5.20	50.40	2.10	9.42	0.66	0.62	0.04
6	306.00	18.00	43.30	2.60	419.00	24.00	149.20	8.70	60.20	4.00	10.32	0.81	0.67	0.05
7	284.00	10.00	43.30	2.00	361.00	12.00	143.40	4.50	53.20	2.60	9.90	0.65	0.58	0.04
8	293.00	14.00	44.70	2.00	480.00	21.00	146.10	6.80	55.80	2.30	9.70	0.65	0.66	0.04
9	296.60	9.50	42.80	1.40	436.00	17.00	143.20	5.50	54.00	2.20	10.47	0.56	0.65	0.05
10	296.00	15.00	43.40	2.30	422.00	21.00	144.90	7.50	55.80	2.70	9.45	0.78	0.66	0.04
11	310.00	15.00	46.90	2.50	453.00	20.00	154.60	8.00	57.30	3.30	11.03	0.83	0.69	0.04
12	288.00	14.00	44.80	2.00	433.00	20.00	144.80	6.70	51.70	2.20	10.19	0.72	0.62	0.04
13	300.00	14.00	40.40	1.90	411.00	20.00	138.60	6.70	55.30	3.00	9.88	0.66	0.62	0.05
14	278.00	11.00	42.30	1.70	476.00	18.00	140.20	6.20	51.10	2.50	9.42	0.74	0.63	0.04
15	276.90	8.80	42.60	1.70	382.00	12.00	140.00	4.90	53.00	2.10	10.37	0.69	0.58	0.04
16	289.00	16.00	44.50	2.30	502.00	26.00	143.40	7.00	52.50	2.70	10.18	0.84	0.67	0.06
17	285.00	11.00	43.70	1.90	431.00	16.00	141.70	5.90	53.60	2.50	9.99	0.66	0.60	0.04
19	277.00	10.00	41.70	1.60	448.00	21.00	136.20	6.50	49.90	2.10	8.99	0.64	0.63	0.05
20	288.00	14.00	43.70	2.30	413.00	21.00	146.20	7.40	53.80	2.60	10.45	0.78	0.60	0.05
21	290.00	17.00	43.10	2.30	476.00	23.00	140.90	6.70	52.90	3.00	9.95	0.86	0.61	0.05
22	283.00	15.00	43.00	2.30	483.00	24.00	145.20	7.70	53.70	2.80	10.00	0.64	0.69	0.04
23	306.00	15.00	47.30	2.30	462.00	24.00	152.00	7.70	55.40	3.00	10.01	0.88	0.64	0.05
24	293.00	11.00	44.90	1.90	466.00	20.00	151.10	6.50	53.50	2.90	9.73	0.78	0.66	0.04
25	296.00	13.00	45.50	2.10	297.00	12.00	150.90	6.30	55.40	2.70	9.90	0.60	0.56	0.03
26	302.00	17.00	44.80	2.30	458.00	23.00	149.10	7.40	56.00	3.60	10.06	0.78	0.63	0.05
27	288.00	13.00	42.30	1.80	402.00	16.00	142.70	5.30	51.40	2.70	9.82	0.69	0.57	0.04
28	301.00	13.00	43.70	1.90	456.00	21.00	146.80	6.60	54.40	2.80	10.67	0.64	0.69	0.05
29	284.00	11.00	43.10	1.70	460.00	17.00	144.00	6.20	52.00	2.20	9.40	0.72	0.63	0.04
30	293.00	12.00	45.70	1.90	429.00	15.00	150.90	5.50	53.60	2.60	10.34	0.65	0.63	0.03
31	279.00	11.00	43.60	1.90	459.00	20.00	142.80	6.20	51.10	2.10	9.33	0.74	0.64	0.04
32	282.00	11.00	44.20	1.80	404.00	16.00	140.20	6.10	49.80	1.90	9.25	0.81	0.58	0.03
Average	**291.63**		**43.74**		**435.42**		**144.81**		**53.71**		**9.96**		**0.63**	
Standard deviation	**10.20**		**1.51**		**41.25**		**4.46**		**2.22**		**0.46**		**0.04**	
% standard deviation	**3.50**		**3.45**		**9.47**		**3.08**		**4.14**		**4.63**		**5.63**	

Table E-6 LA-ICP-MS Elemental Concentration Data: HP14-07 (continued)

spot	Gd157		Dy163		Yb172		Hf178		Pb208		Th232		U238	
#	**ppm**	**Int2SE**	**ppm**	**Int2SE**	**ppm**	**Int2SE**	**ppm**	**Int2SE**	**ppm**	**Int2SE**	**ppm**	**Int2SE**	**ppm**	**Int2SE**
1	8.94	0.52	9.84	0.70	5.41	0.30	9.26	0.47	29.00	1.60	32.20	1.70	8.16	0.41
2	8.97	0.65	9.98	0.58	5.57	0.34	9.17	0.59	27.90	1.30	33.20	1.70	7.93	0.38
3	8.76	0.60	9.32	0.53	5.28	0.35	8.64	0.55	27.20	1.40	32.70	1.80	7.48	0.33
4	9.04	0.58	8.92	0.53	5.26	0.33	8.65	0.51	32.40	1.80	31.30	1.50	8.57	0.41
5	8.04	0.52	8.33	0.46	5.03	0.28	7.93	0.33	28.40	1.10	29.80	1.10	7.86	0.4
6	9.16	0.81	9.35	0.62	5.74	0.43	9.22	0.64	29.30	1.60	33.00	1.90	8.09	0.49
7	8.25	0.47	9.07	0.38	5.36	0.25	8.35	0.51	29.50	1.40	31.00	1.10	8.05	0.35
8	9.03	0.45	9.80	0.58	5.15	0.32	8.78	0.56	30.90	1.50	32.10	1.60	8.26	0.4
9	9.03	0.57	9.19	0.39	5.31	0.28	8.75	0.50	28.60	1.20	31.90	1.20	8.01	0.36
10	8.93	0.60	9.29	0.63	5.44	0.33	8.78	0.55	28.90	1.60	32.00	1.50	8.02	0.41
11	8.94	0.57	9.44	0.53	5.74	0.40	9.22	0.56	30.90	1.60	33.00	1.50	8.85	0.5
12	8.48	0.56	8.71	0.58	5.35	0.31	8.37	0.49	31.00	1.60	31.30	1.60	8.92	0.41
13	8.46	0.53	9.26	0.67	5.54	0.35	8.92	0.57	25.10	1.40	31.70	1.80	7.26	0.41
14	8.70	0.45	8.40	0.49	5.13	0.27	8.18	0.46	29.00	1.50	30.20	1.30	8.06	0.35
15	8.00	0.39	8.72	0.41	5.01	0.31	8.26	0.38	28.80	1.30	30.20	1.20	8.11	0.32
16	8.34	0.55	8.77	0.66	5.05	0.32	8.53	0.50	29.30	1.50	31.00	1.80	8.40	0.46
17	7.94	0.51	8.65	0.42	4.95	0.29	8.41	0.35	30.40	1.90	30.30	1.20	8.20	0.39
19	7.86	0.52	8.45	0.47	5.04	0.26	8.39	0.59	27.60	1.30	29.90	1.60	8.10	0.43
20	8.26	0.64	8.82	0.47	5.18	0.30	8.72	0.74	29.10	1.70	31.10	1.50	8.35	0.42
21	8.70	0.51	8.87	0.46	5.28	0.30	8.32	0.49	28.70	1.50	31.10	1.60	8.36	0.42
22	8.82	0.64	9.27	0.53	5.38	0.38	8.46	0.51	30.60	1.50	30.90	1.40	8.34	0.42
23	9.35	0.56	9.45	0.58	5.34	0.33	9.01	0.60	31.60	1.80	32.50	1.90	8.98	0.5
24	8.82	0.51	9.11	0.60	5.29	0.26	9.33	0.50	29.90	1.50	32.30	1.60	8.41	0.38
25	8.83	0.60	9.24	0.53	5.46	0.27	8.64	0.43	30.30	1.40	32.00	1.10	8.64	0.35
26	8.41	0.55	9.66	0.66	5.52	0.38	8.74	0.57	30.00	1.60	32.40	1.80	8.52	0.44
27	8.34	0.44	9.07	0.53	5.19	0.30	8.34	0.40	28.60	1.50	31.30	1.60	8.05	0.39
28	8.53	0.60	9.34	0.58	5.64	0.28	8.73	0.60	29.40	1.50	32.30	1.50	8.39	0.32
29	8.75	0.56	8.93	0.45	5.00	0.27	8.44	0.49	29.40	1.30	31.20	1.20	8.18	0.34
30	8.66	0.53	9.11	0.52	5.34	0.25	8.56	0.51	30.40	1.30	31.50	1.20	8.62	0.3
31	8.49	0.55	9.10	0.47	5.22	0.28	8.30	0.45	29.20	1.30	30.30	1.20	8.34	0.3
32	8.25	0.40	8.87	0.53	5.18	0.22	8.21	0.55	29.70	1.40	31.30	1.10	8.30	0.37
Average	**8.62**		**9.11**		**5.30**		**8.63**		**29.39**		**31.52**		**8.25**	
Standard deviation	**0.38**		**0.40**		**0.21**		**0.35**		**1.37**		**0.93**		**0.36**	
% standard deviation	**4.36**		**4.41**		**3.94**		**4.07**		**4.68**		**2.94**		**4.38**	

Table E-7 LA-ICP-MS Elemental Concentration Data SCS-KMI-01

Spot	Duration	Ca43		Ca44		Ti49		V51		Mn55		Rb85		Y89	
#	seconds	CPS	Int2SE	ppm	Int2SE	ppm	Int2SE	ppm	Int2SE	ppm	Int2SE	ppm	Int2SE	ppm	Int2SE
2	7.2006	15760	740	3580	230	1314	63	0.644	0.077	196	11	203	11	49.6	3
4	8.9746	16300	1000	3630	200	1308	81	0.665	0.076	194	13	195	13	49.7	3.1
5	5.4265	15210	880	3650	320	1203	60	0.76	0.24	176	10	182.9	9.4	46.3	3.2
6	8.9225	14000	1200	3880	190	1411	96	0.73	0.16	208	14	217	12	51.5	3.3
9	6.0005	16300	1100	3580	250	1330	100	0.692	0.043	185	13	206	19	47.9	3.3
10	6.0005	16700	1600	3660	290	1280	91	0.76	0.2	190	17	201	20	45.5	4.6
12	5.4787	9000	2700	3970	640	1490	230	4.3	2	207	32	211	35	53.4	5.6
13	5.2027	8600	3800	3530	870	1280	340	11.4	7.7	179	53	164	45	48	15
14	12.345	15000	470	3400	170	1279	54	0.669	0.062	192.5	7.4	212	12	45.3	2.1
15	8.6417	15900	740	3590	210	1308	71	0.621	0.072	189	14	200	13	47.1	2.3
20	14.638	16180	690	3490	180	1247	50	0.702	0.063	180.3	7.3	192.7	8.3	46.5	1.9
21	6.5254	15700	1500	3780	240	1331	92	0.85	0.16	200	15	201	15	47.9	4.3
22	6.0845	15900	1100	3490	310	1264	70	1.03	0.55	181	11	194.9	9.4	44.6	2.6
23	7.0545	13140	740	3930	200	1530	110	0.783	0.097	224	15	248	20	52.6	4.7
26	10.494	19000	1300	3550	200	1282	75	1.24	0.14	201	12	163.1	9.4	45.8	3.1
27	6.2609	15100	1100	3780	240	1366	93	0.8	0.12	226	24	214	18	50.3	4.3
29	6.7018	14700	1100	3390	220	1310	120	0.81	0.12	204	20	211	17	41.5	2.4
3	8.2623	10660	760	4260	380	1380	120	0.69	0.13	189	14	192	16	47.2	4.3
4	11.986	9400	590	3660	210	1227	73	0.99	0.15	174	11	160	12	47.9	3.2
5	8.2623	8540	630	4240	300	1480	110	0.76	0.19	214	17	216	18	49.5	4.6
6	7.2149	9760	520	4280	280	1431	67	0.679	0.077	192.5	9.8	201	12	47.5	2.3
7	7.6804	9360	590	4080	220	1459	78	0.77	0.14	203.1	9	198	13	49.3	2.4
8	9.1932	8680	500	4280	270	1508	70	0.72	0.15	198.5	8.2	209	11	47.9	2
13	9.7751	9360	730	4030	320	1420	100	0.84	0.2	195	14	216	16	45.3	3.4
14	12.335	6570	400	4400	370	1580	120	0.95	0.14	219	16	233	16	46.3	3.6
15	18.44	8950	360	4170	210	1381	59	1.21	0.5	185.9	7.8	197.5	9	47.1	2.3
16	7.7968	9350	620	3880	310	1343	92	0.641	0.096	187	12	195	13	43.9	2.5
17	8.7277	8470	650	4610	380	1570	130	0.82	0.13	229	20	219	18	53.1	4.2
18	6.7495	11040	630	3800	250	1287	91	0.91	0.16	198	12	175	13	48.6	2.3
19	6.5167	9320	480	4360	270	1454	83	0.65	0.1	198	8.6	203	13	45.8	2.4
Average				**3864**		**1325**		**1**		**197**		**201**		**48**	
Standard deviation				**330.98**		**81.17**		**1.99**		**14.29**		**18.82**		**2.67**	
% standard dev				**8.56**		**6.12**		**156.68**		**7.25**		**9.36**		**5.59**	

Table E-8 LA-ICP-MS Elemental Concentration Data SCS-KMI-01 (continued)

Spot	Zr90		Nb93		Ba137		Ce140		Nd146		Sm147		Eu153	
#	ppm	Int2SE	ppm	Int2SE	ppm	Int2SE	ppm	Int2SE	ppm	Int2SE	ppm	Int2SE	ppm	Int2SE
2	283	15	44.2	2	461	24	150.2	7.6	50	3.1	8.94	0.77	0.664	0.058
4	291	20	42.7	2.9	360	24	147	11	52.6	3.5	9.6	1	0.534	0.044
5	274	17	39.2	2.5	461	47	131.7	9.3	50.3	3.6	9.6	1.3	0.592	0.066
6	300	18	45.8	2.9	440	27	153	10	54.5	3.4	11.4	1.5	0.668	0.074
9	280	15	41.7	3.2	439	29	144	10	51.3	3.1	8.83	0.87	0.624	0.052
10	264	23	42	3.6	390	31	137	11	50.2	4.4	9.5	1.3	0.602	0.092
12	328	42	45.3	7	501	73	151	27	57.4	7.2	11.9	1.5	0.63	0.12
13	302	87	36.6	8.6	349	85	119	32	45	11	10.2	3.7	0.56	0.18
14	263	10	43.2	2.2	472	18	137.8	5.6	46.7	2.5	8.27	0.58	0.656	0.042
15	274	15	42.8	2.1	496	21	143.7	7.6	52	3	9.4	1.1	0.658	0.064
20	273	13	39.4	1.7	460	17	134.2	6.3	49.4	2.1	9.33	0.69	0.642	0.055
21	272	23	43.1	4	403	29	142	12	50.2	5	8.37	0.82	0.597	0.075
22	261	16	41.9	2.5	480	28	137.1	8.7	47.8	4.5	7.7	1.1	0.611	0.071
23	302	23	50.3	3.1	453	27	159	12	57.3	4.2	11.1	1.2	0.696	0.077
26	318	21	38.8	2.1	507	26	124.8	8.1	47.9	3.6	8.52	0.99	0.645	0.045
27	293	24	45.8	4.4	388	29	156	14	56.1	5.6	10.8	1.2	0.618	0.045
29	243	14	40.6	3.8	395	26	138	13	47	4	8.6	1.3	0.559	0.086
3	277	24	46.5	4.1	369	34	133	12	50.3	5.6	10	1.8	0.538	0.064
4	286	18	40.3	2.7	441	32	118.9	8.1	48.5	4.3	8.5	1	0.612	0.046
5	294	23	49.2	3.4	465	37	142	12	54.7	4.9	10.8	1.5	0.64	0.069
6	282	15	47.5	3	432	20	133.9	8.6	48.3	3.8	8.5	1.2	0.65	0.069
7	300	10	48.2	2.1	344	12	137.4	7.5	52.8	4.3	11.9	1.1	0.63	0.056
8	295	17	48.8	2.8	441	24	136.6	7.9	52.5	4.2	8.7	1.4	0.656	0.081
13	268	20	44.3	3.5	362	25	133	10	46.1	3.5	9.9	1.3	0.589	0.087
14	279	19	50.7	3.9	375	25	144.2	9.4	46.8	3.5	9	1	0.665	0.065
15	277	12	44	2.2	382	20	131.7	5.5	49.5	3.2	8.9	1	0.575	0.048
16	270	23	43.9	3.1	447	31	131	12	48.1	5.2	8.3	1.1	0.665	0.085
17	322	27	54.1	6.4	377	37	152	13	55.6	6	10.6	1.9	0.609	0.053
18	286	15	41.6	3.3	381	20	127.5	7.1	46.6	4.4	9.38	0.83	0.683	0.067
19	289	20	45.7	3.4	465	36	138	12	48.6	4.1	8.7	1.4	0.653	0.049
Average	**285**		**44**		**425**		**139**		**50**		**10**		**1**	
Standard Deviation	**18.41**		**3.90**		**47.70**		**9.88**		**3.37**		**1.11**		**0.04**	
% standard dev	**6.46**		**8.82**		**11.24**		**7.12**		**6.69**		**11.70**		**6.65**	

Table E-9 LA-ICP-MS Elemental Concentration Data SCS-KMI-01 (continued)

Spot	Gd157		Dy163		Yb172		Hf178		Pb208		Th232		U238	
#	ppm	Int2SE	ppm	Int2SE	ppm	Int2SE	ppm	Int2SE	ppm	Int2SE	ppm	Int2SE	ppm	Int2SE
2	8.33	0.68	9.27	0.73	5.19	0.37	8.92	0.45	27.4	1.9	31	1.8	8.18	0.59
4	8.25	0.71	9.2	0.81	5.16	0.48	8.3	0.65	28.1	1.8	31.7	2.2	8.1	0.53
5	7.6	0.71	8.4	0.83	4.88	0.53	8.66	0.93	26	3.1	29.1	1.9	7.21	0.5
6	8.63	0.76	9.57	0.79	5.5	0.43	8.99	0.51	31	2.1	32.8	2.1	8.74	0.66
9	8.18	0.58	8.53	0.6	5.28	0.46	8.42	0.8	30.3	3.2	30.5	2.2	8.13	0.79
10	8.36	0.81	8	1.1	4.86	0.52	8.5	1.1	31.4	3.9	30.5	3.3	8.7	1.1
12	8.8	1.1	9.8	1.2	5.33	0.62	9.2	1.5	28	7.4	31.7	4.5	8	1.5
13	7.7	2.1	8.2	2.4	4.09	0.88	8.6	3.4	19.5	5.7	27.2	8.4	5.9	1.8
14	7.61	0.5	8.6	0.47	4.87	0.25	7.82	0.57	31.7	1.6	29.4	1.1	8.84	0.54
15	7.72	0.63	8.57	0.72	5.24	0.44	7.8	0.54	28.5	1.9	30	1.8	8.11	0.43
20	7.64	0.55	8.71	0.4	4.65	0.32	8.11	0.5	27.3	1.4	29.9	1.4	7.62	0.36
21	8.1	1.1	8.61	0.85	5.27	0.38	7.99	0.6	31.7	3.3	29.7	2.7	8.9	0.85
22	7.96	0.63	8.9	0.8	4.66	0.45	7.75	0.77	29.2	3	29.5	2.4	8.43	0.74
23	9.19	0.79	9.34	0.85	5.19	0.51	8.78	0.77	34.3	2.9	33.4	2.5	10.06	0.83
26	7.87	0.84	8.35	0.59	4.89	0.41	8.74	0.74	24.9	1.9	24.8	1.9	6.53	0.49
27	8.1	1	8.9	1.3	5.23	0.63	8.88	0.88	32.3	3.1	33.2	2.8	8.95	0.83
29	7.05	0.64	8.37	0.89	4.3	0.3	7.64	0.85	28.4	2.7	27.4	1.8	8.6	1.2
3	7.12	0.77	7.8	0.64	5.11	0.6	8.32	0.68	29.90	2.80	29.80	2.60	7.8	0.82
4	8.02	0.98	8.3	0.63	5.09	0.48	8.08	0.69	22.90	1.80	30.80	2.00	6.09	0.43
5	8.35	0.94	9.38	0.59	4.88	0.55	8.35	0.82	31.70	2.40	30.50	2.50	8.69	0.78
6	8.9	1.1	8.71	0.65	5.04	0.46	8.44	0.78	30.50	2.40	30.30	1.70	8.13	0.7
7	10.28	0.86	9.18	0.54	5.48	0.34	8.83	0.45	30.60	2.40	30.80	1.40	7.84	0.44
8	8.68	0.81	8.86	0.55	4.84	0.38	8.48	0.75	33.40	2.70	31.20	2.40	8.41	0.53
13	8.76	0.99	7.82	0.97	4.71	0.42	7.46	0.73	29.2	2.7	28	2.4	8.17	0.89
14	7.6	1	8.23	0.74	5.16	0.41	8.2	1	33.2	2.3	29.5	1.9	9.73	0.82
15	8.57	0.56	8.23	0.38	4.75	0.3	7.99	0.56	29.1	1.7	29.3	1.4	7.57	0.43
16	7.94	0.78	8.51	0.82	5.14	0.54	7.58	0.95	28.5	2.9	28.7	2.6	7.65	0.74
17	9.5	1	9.6	1	5.36	0.38	9.23	0.9	34.7	2.8	33.6	3.4	8.95	0.87
18	7.97	0.82	8.79	0.67	5.15	0.53	7.38	0.56	25	2	29.2	2.1	6.57	0.54
19	9.06	0.88	8.74	0.9	4.76	0.58	8.11	0.94	32.5	2.6	30.5	2.1	8.55	0.77
Average	**8**		**9**		**5**		**8**		**29**		**30**		**8**	
Standard Deviation	**0.69**		**0.51**		**0.32**		**0.50**		**3.33**		**1.85**		**0.94**	
% standard dev	**8.30**		**5.89**		**6.35**		**6.01**		**11.34**		**6.15**		**11.55**	

Table E-10 LA-ICP-MS Elemental Concentration Data AFB-00

Spot #	Duration seconds	Ca43 CPS	Int2SE	Ca44 ppm	±2SE	Ti49 ppm	±2SE	V51 ppm	±2SE	Mn55 ppm	±2SE	Rb85 ppm	±2SE	Y89 ppm	±2SE
1	18.4	10870	620	4150	240.00	1555.00	88.00	0.41	0.04	216.10	9.80	179.00	8.50	46.70	2.30
2	14.1	12330	590	4000	170.00	1532.00	86.00	2.26	0.93	216.00	10.00	171.80	7.90	45.20	2.30
3	18.4	10260	410	4300	220.00	1633.00	70.00	0.37	0.05	225.00	10.00	190.30	8.00	49.40	2.20
4	9.3	10910	630	4010	310.00	1490.00	100.00	1.80	1.00	216.00	14.00	177.00	15.00	42.10	3.00
5	18.4	10730	650	4190	210.00	1620.00	110.00	0.44	0.05	227.00	12.00	182.00	10.00	47.10	2.80
6	11.9	9620	440	4580	200.00	1746.00	72.00	0.52	0.10	250.50	9.80	208.90	8.20	49.60	2.20
7	18.4	9990	560	4370	250.00	1614.00	92.00	0.38	0.05	228.00	14.00	192.00	12.00	47.70	2.60
8	18.4	8460	460	4270	220.00	1640.00	78.00	0.48	0.07	238.00	12.00	196.00	10.00	48.50	2.50
9	18.4	8490	300	4100	160.00	1525.00	73.00	0.57	0.33	220.70	9.30	176.10	9.30	45.70	2.00
10	18.4	10570	410	4010	150.00	1537.00	65.00	0.36	0.03	213.40	8.00	182.90	8.20	45.40	1.60
11	18.4	10340	380	4060	170.00	1588.00	76.00	1.01	0.39	223.00	10.00	181.90	8.40	49.50	2.20
12	7.0	11170	970	4090	360.00	1520.00	140.00	0.45	0.13	218.00	19.00	168.00	13.00	48.50	4.00
13	7.3	11850	410	3970	200.00	1500.00	81.00	0.41	0.07	217.80	9.90	177.00	11.00	43.80	2.40
14	18.4	10740	510	4170	220.00	1549.00	67.00	0.40	0.06	221.90	9.90	184.50	8.90	46.00	2.30
15	18.4	10380	450	4300	180.00	1563.00	58.00	0.37	0.05	220.60	9.90	182.60	7.40	47.20	2.10
17	14.7	9990	400	4190	200.00	1724.00	66.00	0.48	0.10	236.00	11.00	205.60	8.20	50.70	2.20
18	18.4	10030	530	4180	210.00	1571.00	70.00	0.36	0.06	228.00	11.00	189.10	9.50	48.00	2.20
19	11.9	11280	490	4220	190.00	1526.00	56.00	0.38	0.06	222.00	10.00	179.80	9.00	44.00	1.70
21	18.4	10210	450	4290	190.00	1597.00	73.00	0.41	0.05	233.00	11.00	185.50	8.50	47.60	1.90
22	11.1	10360	360	4070	250.00	1581.00	76.00	0.31	0.06	217.10	9.70	180.20	9.40	49.70	2.00
23	18.4	10340	460	4110	200.00	1566.00	72.00	0.33	0.04	213.20	9.10	177.20	8.30	47.00	2.20
24	18.4	10610	440	4180	160.00	1535.00	55.00	0.40	0.05	217.70	7.50	183.20	7.10	46.80	1.60
27	13.8	11070	530	4170	220.00	1555.00	79.00	0.40	0.05	226.00	12.00	179.30	9.30	48.10	2.30
28	11.1	10280	600	3950	200.00	1448.00	86.00	0.54	0.26	206.00	14.00	158.00	11.00	47.70	3.40
29	18.4	10170	460	4250	220.00	1525.00	63.00	0.53	0.22	220.90	9.10	179.40	8.30	46.00	2.00
31	7.2	9840	860	3770	370.00	1610.00	190.00	0.65	0.28	238.00	27.00	202.00	32.00	42.60	4.10
32	14.8	10310	460	4280	210.00	1613.00	75.00	0.44	0.05	233.00	13.00	190.00	10.00	46.90	2.50
34	18.4	9300	510	4250	200.00	1630.00	84.00	0.26	0.05	224.90	9.90	210.40	8.30	53.40	2.60
35	15.7	9510	570	4300	260.00	1660.00	110.00	0.64	0.32	245.00	15.00	198.00	13.00	48.90	3.20
36	18.4	9660	400	4160	210.00	1618.00	66.00	0.37	0.05	221.00	10.00	187.70	9.30	48.90	2.30
37	18.4	11120	410	4130	140.00	1536.00	58.00	0.59	0.27	223.20	9.30	186.50	8.80	47.10	1.80
38	18.4	9910	360	4220	160.00	1631.00	75.00	0.39	0.06	231.00	9.00	192.30	8.60	46.90	1.70
39	18.4	7300	400	4200	290.00	1650.00	100.00	0.73	0.21	236.00	15.00	202.00	15.00	50.00	3.30
40	18.4	10300	520	4120	230.00	1592.00	78.00	0.35	0.05	223.00	11.00	184.30	8.50	47.40	2.40
41	9.0	10540	690	4030	260.00	1532.00	71.00	1.27	0.62	222.80	8.70	176.60	9.50	46.30	2.30
42	14.8	11150	430	4040	120.00	1504.00	48.00	0.33	0.05	214.70	7.90	182.50	6.30	46.10	1.60
43	18.4	11030	500	4220	200.00	1544.00	71.00	0.45	0.05	223.20	9.40	180.20	8.50	47.00	2.40
44	14.7	10580	640	4210	220.00	1539.00	91.00	0.37	0.06	224.00	14.00	181.00	11.00	44.90	2.30
45	16.6	10680	530	4060	190.00	1477.00	63.00	0.41	0.05	217.00	10.00	174.60	8.00	46.00	2.20
46	18.4	9110	580	4430	280.00	1637.00	93.00	0.55	0.11	241.00	16.00	206.00	13.00	46.90	2.60
47	18.4	11110	500	3800	170.00	1447.00	62.00	0.37	0.05	205.80	8.00	164.00	6.90	44.90	1.70
48	18.4	10420	410	3960	180.00	1483.00	60.00	0.36	0.05	207.50	8.30	163.50	6.50	48.10	1.80
50	16.1	8460	500	4550	300.00	1710.00	120.00	2.80	1.80	255.00	14.00	214.00	17.00	46.30	2.70
Average				**4160.70**		**1573.33**		**0.60**		**224.60**		**185.18**		**47.13**	
Standard deviation				**161.90**		**68.23**		**0.51**		**10.80**		**12.52**		**2.10**	
% standard dev				**3.89**		**4.34**		**85.06**		**4.81**		**6.76**		**4.45**	

Table E-11 LA-ICP-MS Elemental Concentration Data AFB-00 (continued)

Spot #	Zr90 ppm	±2SE	Nb93 ppm	±2SE	Ba137 ppm	±2SE	Ce140 ppm	±2SE	Nd146 ppm	±2SE	Sm147 ppm	±2SE	Eu153 ppm	±2SE
1	305.00	16.00	47.50	2.60	622.00	33.00	125.60	6.50	47.40	2.60	9.42	0.88	0.85	0.07
2	304.00	14.00	46.40	2.30	620.00	30.00	118.20	5.40	45.90	3.20	8.35	0.65	0.84	0.06
3	328.00	14.00	50.50	2.50	628.00	29.00	132.40	6.20	49.90	2.70	9.14	0.83	0.86	0.04
4	282.00	19.00	45.30	3.80	639.00	44.00	122.40	7.30	44.90	3.90	8.39	0.93	0.75	0.08
5	313.00	20.00	49.40	3.00	586.00	37.00	129.00	8.10	46.40	3.20	9.17	0.77	0.85	0.06
6	328.00	14.00	53.30	2.40	686.00	23.00	139.80	4.60	49.30	3.20	10.20	1.30	0.84	0.06
7	315.00	17.00	49.30	2.60	638.00	37.00	131.90	8.30	51.50	3.90	9.70	1.00	0.83	0.07
8	324.00	16.00	52.00	2.70	619.00	31.00	139.60	8.00	51.10	3.40	9.62	0.97	0.87	0.07
9	308.00	11.00	47.60	2.10	669.00	26.00	130.10	6.10	47.10	2.70	9.50	1.20	0.87	0.05
10	301.00	13.00	47.50	1.90	633.00	25.00	123.10	5.40	46.20	2.40	9.34	0.80	0.84	0.05
11	326.00	13.00	50.30	2.30	519.00	21.00	132.70	6.20	51.00	2.80	9.14	0.98	0.80	0.06
12	311.00	23.00	46.10	3.40	621.00	47.00	121.40	9.80	48.50	2.70	9.20	1.20	0.92	0.13
13	286.00	12.00	46.00	2.70	562.00	32.00	114.70	6.80	44.40	3.50	8.60	1.00	0.74	0.08
14	310.00	15.00	47.40	2.10	566.00	30.00	124.30	5.90	48.50	3.20	9.64	0.88	0.82	0.06
15	314.00	14.00	48.80	2.40	637.00	29.00	127.60	5.70	49.00	2.40	9.40	1.20	0.85	0.06
17	339.00	13.00	54.30	2.40	402.00	18.00	136.10	6.10	49.30	2.30	9.67	0.81	0.71	0.06
18	313.00	15.00	49.10	2.60	655.00	31.00	126.70	6.30	46.80	2.80	9.11	0.74	0.84	0.06
19	301.00	14.00	46.20	2.10	629.00	30.00	119.10	5.40	45.40	3.70	9.20	1.00	0.77	0.07
21	320.00	14.00	51.20	2.60	524.00	24.00	128.40	5.80	51.20	3.00	9.35	0.78	0.81	0.05
22	333.00	15.00	50.90	2.50	623.00	34.00	128.10	6.10	50.20	3.50	10.10	1.30	0.85	0.07
23	316.00	15.00	47.70	2.30	607.00	33.00	124.90	6.10	49.10	2.80	9.50	0.81	0.79	0.06
24	310.00	12.00	47.80	1.80	618.00	25.00	127.00	5.10	48.10	2.10	9.45	0.83	0.80	0.05
27	315.00	15.00	48.90	2.70	592.00	30.00	126.40	6.50	47.70	2.80	10.15	0.99	0.82	0.06
28	317.00	22.00	45.30	3.70	679.00	54.00	121.00	10.00	49.00	4.30	9.30	1.30	0.81	0.08
29	303.00	14.00	47.50	2.10	619.00	30.00	123.80	5.60	47.70	2.90	9.28	0.65	0.83	0.06
31	289.00	30.00	47.90	5.80	560.00	73.00	124.00	13.00	46.30	4.20	8.90	1.40	0.79	0.10
32	311.00	16.00	49.60	2.80	671.00	38.00	129.40	6.70	48.30	2.90	9.10	1.00	0.90	0.08
34	323.00	14.00	56.10	2.90	511.00	28.00	149.00	8.10	55.40	3.60	10.30	1.00	0.78	0.06
35	326.00	20.00	53.30	3.40	585.00	37.00	136.00	8.30	48.10	3.50	9.81	0.92	0.82	0.08
36	321.00	15.00	50.10	2.40	601.00	32.00	131.00	6.60	50.30	2.80	9.09	0.80	0.82	0.07
37	310.00	11.00	48.80	2.10	560.00	22.00	126.30	5.20	47.10	2.20	8.71	0.72	0.80	0.05
38	313.00	12.00	51.40	2.10	562.00	23.00	130.20	5.60	48.20	2.10	9.24	0.94	0.83	0.06
39	325.00	21.00	53.70	3.30	448.00	30.00	139.40	8.70	51.20	4.50	9.70	1.00	0.73	0.07
40	312.00	17.00	48.90	2.70	646.00	34.00	125.90	6.10	49.10	2.80	8.67	0.79	0.85	0.08
41	297.00	13.00	46.20	2.60	563.00	31.00	121.90	6.50	45.90	2.80	7.83	0.84	0.75	0.06
42	302.30	9.80	47.80	1.90	611.00	21.00	127.50	4.90	47.20	1.40	9.08	0.77	0.82	0.05
43	316.00	15.00	47.20	2.10	659.00	32.00	126.90	6.10	48.00	2.90	9.60	0.85	0.87	0.06
44	301.00	19.00	47.50	2.90	650.00	41.00	126.00	8.30	46.80	3.70	8.50	1.00	0.84	0.07
45	297.00	14.00	46.50	2.50	575.00	26.00	119.80	6.00	46.00	2.20	8.90	0.86	0.79	0.05
46	309.00	19.00	50.10	2.60	654.00	35.00	132.50	8.40	48.30	3.00	9.44	0.97	0.90	0.07
47	298.00	12.00	44.60	2.10	645.00	26.00	116.20	4.40	46.70	2.10	8.67	0.65	0.86	0.06
48	318.00	12.00	46.90	1.90	533.00	21.00	124.60	4.40	47.10	1.80	9.30	0.90	0.76	0.05
50	308.00	17.00	51.70	3.10	640.00	34.00	133.60	8.70	47.00	2.90	8.92	0.98	0.77	0.06
Average	**311.59**		**48.94**		**601.56**		**127.78**		**48.20**		**9.25**		**0.82**	
Standard deviation	**12.03**		**2.62**		**58.65**		**6.71**		**2.08**		**0.51**		**0.05**	

Table E-12 LA-ICP-MS Elemental Concentration Data AFB-00 (continued)

Spot	Gd157		Dy163		Yb172		Hf178		Pb208		Th232		U238	
#	ppm	±2SE	ppm	±2SE	ppm	±2SE	ppm	±2SE	ppm	±2SE	ppm	±2SE	ppm	±2SE
1	8.96	0.68	8.28	0.40	4.83	0.32	8.84	0.63	27.20	1.90	25.50	1.40	6.82	0.38
2	9.11	0.74	7.90	0.60	4.78	0.36	8.45	0.67	25.70	1.30	24.51	0.99	6.53	0.45
3	9.83	0.59	9.05	0.57	5.31	0.35	8.75	0.54	28.40	1.80	28.20	1.50	7.09	0.36
4	8.50	1.20	8.30	0.85	4.58	0.45	7.77	0.73	25.30	1.50	23.60	1.50	6.93	0.70
5	9.23	0.95	9.31	0.74	4.80	0.35	8.38	0.62	27.00	2.00	25.80	1.50	6.81	0.42
6	9.34	0.92	8.95	0.70	5.35	0.34	9.29	0.80	29.10	1.20	27.50	1.50	7.33	0.32
7	8.67	0.66	8.27	0.50	4.93	0.42	8.70	0.77	27.30	1.80	27.40	1.80	7.12	0.45
8	9.20	0.80	9.07	0.56	5.16	0.37	9.27	0.66	28.90	1.80	27.80	1.50	7.87	0.41
9	8.20	0.59	8.69	0.63	4.85	0.29	8.61	0.55	23.70	1.30	26.20	1.10	6.74	0.38
10	8.46	0.79	8.59	0.38	4.75	0.26	8.42	0.52	25.50	1.30	25.40	1.00	6.73	0.29
11	9.38	0.71	9.44	0.54	5.33	0.29	8.93	0.51	26.30	1.50	27.80	1.20	7.13	0.38
12	9.44	0.87	9.21	0.92	4.70	0.39	8.20	0.97	23.90	2.20	25.80	2.50	6.52	0.64
13	8.16	0.76	8.21	0.78	4.52	0.43	8.02	0.60	25.20	1.60	23.90	1.60	6.95	0.53
14	8.38	0.59	8.04	0.59	5.13	0.34	8.90	0.65	27.10	1.50	26.40	1.50	7.18	0.42
15	8.77	0.72	8.53	0.56	5.10	0.35	8.89	0.68	25.70	1.20	26.80	1.20	6.82	0.35
17	9.41	0.84	9.34	0.75	4.96	0.35	9.22	0.54	30.00	1.40	27.80	1.30	7.69	0.44
18	9.49	0.62	8.41	0.69	5.09	0.38	8.59	0.52	27.50	1.50	26.90	1.50	7.17	0.40
19	8.96	0.93	8.19	0.50	4.80	0.34	8.29	0.55	26.70	1.30	25.20	1.10	6.95	0.28
21	9.20	0.62	8.84	0.60	4.91	0.29	8.88	0.62	28.30	1.40	27.70	1.30	7.19	0.45
22	9.29	0.71	9.08	0.53	5.28	0.43	9.42	0.51	26.60	1.50	28.40	1.20	6.97	0.37
23	9.41	0.78	8.37	0.70	4.90	0.34	8.84	0.51	24.60	1.30	26.50	1.40	6.74	0.36
24	8.66	0.52	8.43	0.38	4.62	0.24	8.80	0.64	26.10	1.10	26.60	1.00	6.96	0.29
27	9.24	0.80	8.98	0.74	5.15	0.35	8.59	0.48	27.00	1.60	26.60	1.60	6.89	0.45
28	8.40	1.10	7.76	0.70	4.99	0.48	8.57	0.95	21.90	1.80	27.20	2.30	6.07	0.49
29	8.17	0.78	8.71	0.63	5.06	0.32	8.39	0.54	26.30	1.30	26.10	1.40	6.69	0.36
31	8.30	1.30	7.68	0.86	4.56	0.43	7.87	0.77	27.60	4.40	23.90	2.30	7.30	1.10
32	8.49	0.99	8.72	0.66	4.87	0.35	8.07	0.79	27.30	1.40	26.00	1.30	7.04	0.38
34	10.27	0.85	9.94	0.59	5.62	0.42	9.53	0.69	31.40	1.80	31.60	2.00	8.17	0.47
35	9.36	0.69	8.99	0.73	5.12	0.35	8.59	0.70	29.10	1.70	27.20	1.60	7.85	0.49
36	9.61	0.61	8.60	0.60	5.00	0.36	8.89	0.59	26.90	1.80	27.30	1.40	6.85	0.36
37	8.40	0.53	8.59	0.49	4.88	0.28	8.51	0.41	27.12	0.96	26.50	1.10	6.87	0.33
38	9.73	0.74	8.55	0.44	4.95	0.29	8.83	0.49	27.70	1.40	27.10	1.20	7.17	0.36
39	9.60	0.92	8.73	0.58	5.27	0.45	8.63	0.76	30.20	2.20	29.20	2.10	8.01	0.63
40	9.27	0.70	8.59	0.68	5.21	0.34	8.52	0.61	25.80	1.40	26.70	1.40	6.81	0.36
41	8.55	0.92	8.05	0.49	4.81	0.24	8.25	0.74	25.90	2.50	25.40	1.60	6.44	0.54
42	8.38	0.43	8.09	0.39	4.87	0.31	8.65	0.60	25.36	0.97	26.26	0.95	6.86	0.25
43	9.12	0.77	8.66	0.40	5.04	0.35	9.10	0.61	26.60	1.50	26.40	1.40	6.82	0.35
44	8.50	0.83	8.12	0.66	4.85	0.48	8.14	0.65	27.20	2.10	25.30	1.80	6.85	0.46
45	8.22	0.71	8.48	0.48	4.88	0.40	8.54	0.60	25.80	1.50	25.50	1.50	6.45	0.40
46	8.96	0.91	8.76	0.52	4.92	0.33	8.91	0.77	29.70	2.20	26.60	1.60	7.88	0.56
47	8.03	0.59	8.04	0.39	4.80	0.29	7.86	0.57	23.60	1.40	24.50	1.00	6.22	0.30
48	9.10	0.64	9.28	0.60	5.00	0.29	8.71	0.66	22.76	0.84	27.20	1.20	6.29	0.27
50	8.52	0.87	8.72	0.73	5.13	0.35	8.09	0.50	32.40	2.90	26.10	1.40	8.72	0.84
Average	**8.94**		**8.62**		**4.97**		**8.62**		**26.83**		**26.52**		**7.03**	
Standard deviation	**0.53**		**0.48**		**0.23**		**0.41**		**2.12**		**1.45**		**0.53**	
% standard dev	**5.98**		**5.55**		**4.61**		**4.77**		**7.91**		**5.46**		**7.51**	

Table E-13 LA-ICP-MS Elemental Concentration Data: BOR-S2-01

Spot #	Duration Seconds	Ca43 ppm	Int2SE	Ca44 ppm	Int2SE	Ti49 ppm	Int2SE	V51 ppm	Int2SE	Mn55 ppm	Int2SE	Rb85 ppm	Int2SE	Y89 ppm	Int2SE
1	18.4	7110	330	4630	250	860	42	0.025	0.03	287	14	222	11	74	3.8
2	14.9	7360	380	4420	250	805	43	0.14	0.069	268	14	210	12	72.7	3.8
3	9.8	8210	420	4480	310	755	34	0.099	0.063	271	13	218.2	9.2	73.9	4.1
5	18.4	5770	450	4220	370	997	91	0.57	0.13	307	29	155	18	55	4
6	15.2	8240	550	4280	240	896	50	0.058	0.037	276	16	188	10	70.8	4
7	18.4	6980	390	4520	240	834	42	0.055	0.047	296	17	235	16	65	3.5
8	18.4	7940	540	4220	290	726	45	0.087	0.045	249	17	206	14	72	5.1
10	15.1	8240	390	4270	190	992	56	0.097	0.035	296	15	185.4	8.1	63.6	3.3
11	18.4	8150	400	4340	200	766	40	0.06	0.031	271	14	239	12	78.8	4.4
12	18.4	7610	420	4400	250	855	51	0.076	0.031	284	15	231	14	73	4.5
13	9.4	7270	540	4670	460	882	88	0.115	0.048	311	25	239	23	63.1	3.8
14	12.1	7980	360	4390	230	817	46	0.043	0.05	271	13	205.6	9.6	72.7	3.6
15	18.4	7770	430	4190	220	773	46	0.41	0.17	247	12	195	11	68.7	3.6
16	13.8	9080	570	4220	300	1016	65	0.126	0.041	294	21	158	10	54.9	4
17	18.4	8300	390	4530	220	1070	61	0.154	0.042	304	15	177.6	6.7	57.6	3.2
18	10.2	8030	290	4560	250	830	45	0.09	0.059	275	13	214.7	9.9	73.6	2.6
19	18.4	8000	370	4490	260	831	41	0.096	0.042	275	12	212.4	9.8	73.9	4.2
20	7.2	8180	770	4210	420	1040	100	0.156	0.048	299	33	158	19	57.5	5.7
21	18.4	6760	360	4310	260	705	41	0.129	0.041	256	13	248	16	84	4.4
23	13.0	7660	530	4550	390	833	64	0.093	0.032	285	20	219	18	72.8	5.1
24	14.3	7820	410	4420	250	756	45	0.129	0.076	271	14	226	12	80.3	4
25	18.4	7420	450	4690	260	872	54	0.033	0.035	290	16	237	16	75.4	5.1
26	18.4	7990	410	4400	270	873	49	0.142	0.052	268	12	190.9	9.6	72.6	3.7
27	13.6	7350	470	4580	360	840	58	0.114	0.066	298	22	218	17	71.5	5.4
28	18.4	8230	410	4180	200	1021	51	0.34	0.19	295	13	158.3	8.3	56.3	2.9
29	18.4	5320	440	4370	310	776	58	0.27	0.086	267	18	228	17	77	5
30	17.1	5990	490	4000	290	704	47	0.44	0.2	259	16	202	15	80.3	5
31	8.0	7680	620	4620	310	787	59	0.053	0.055	283	20	242	19	75.4	5.3
32	16.1	7120	490	4170	290	1158	93	0.69	0.1	260	17	212	15	68.3	4.8
33	16.6	7360	500	4400	310	894	63	0.123	0.042	284	19	193	13	69.7	4.6
34	18.4	8280	330	4360	190	983	43	0.095	0.039	288	12	180.6	7.2	62.1	2.8
35	18.4	8470	390	4330	240	1039	56	0.132	0.035	301	15	161.6	9.5	54.8	2.8
36	13.4	6560	480	4480	390	823	89	1.1	0.64	279	20	234	19	76.8	6.6
37	11.3	7320	510	4660	420	847	74	0.039	0.04	304	26	265	23	74.4	5.7
38	18.4	8180	410	4380	280	1032	63	0.204	0.064	293	16	164.8	9.1	58.3	2.9
39	10.4	8090	430	4490	300	960	54	0.097	0.062	280	14	167.2	8.2	65.3	3.5
40	18.4	8970	400	4140	220	766	32	0.095	0.035	257	13	195.6	9.1	72.6	3.7
41	18.4	7990	360	4430	220	830	34	0.08	0.038	283	13	222.4	9.8	68.9	3.2
42	18.4	7790	430	4640	200	867	42	0.082	0.038	290	13	233.1	9.2	76.9	4.3
43	18.4	8680	340	4190	210	998	43	0.251	0.053	307	13	170.3	7.8	62.5	2.4
44	18.4	8320	530	4480	250	787	51	0.062	0.038	271	15	230	14	77.3	4.2
45	11.5	8660	450	4230	190	715	36	0.095	0.071	249	12	208.2	9.5	74.4	3.5
46	14.1	9150	640	4130	240	764	51	0.04	0.051	253	16	197	12	72.5	4.2
47	18.4	7240	500	4330	230	768	45	0.064	0.024	267	16	226	15	79.2	5
48	18.4	7640	390	4400	250	908	46	0.074	0.032	279	12	192.7	9.8	70.3	3.6
49	18.4	8240	460	4370	270	943	57	0.41	0.48	281	17	179	10	63.2	3.7

Table E-14 LA-ICP-MS Elemental Concentration Data: BOR-S2-01 (continued)

Spot #	Zr90 ppm	Int2SE	Nb93 ppm	Int2SE	Ba137 ppm	Int2SE	Ce140 ppm	Int2SE	Nd146 ppm	Int2SE	Sm147 ppm	Int2SE	Eu153 ppm	Int2SE
1	220	10	76.5	4.4	171	7.5	163.3	9.2	61.4	3.7	13.3	1.1	0.571	0.044
2	209	10	70.3	3.8	162	9.9	157	10	60.3	3.9	12	1.3	0.576	0.069
3	199	11	75.6	3.6	102.5	5	145.3	8	57.2	4.8	12.9	1.4	0.443	0.064
5	254	19	55.6	5	470	36	172	17	67.4	4.2	12	1.3	0.844	0.077
6	236	14	69.6	3.8	248	14	170	11	67.1	5	13.6	1.1	0.659	0.041
7	193	12	73	4.5	156.4	8.4	157.7	8.7	57.6	3.5	11.2	1.3	0.498	0.042
8	191	13	71.6	4.8	104.7	7.3	137.8	9.9	55.4	4.2	12.3	1.1	0.44	0.057
10	250	13	65.6	3	352	15	190	11	73	4.1	13.9	1.3	0.813	0.064
11	206	10	77.9	4.1	102.7	6	148.9	8.2	60.3	4	12.9	1.4	0.433	0.039
12	214	12	74.1	4.3	162	10	164	11	61.1	4.4	13.3	1.4	0.582	0.032
13	193	17	71.9	6	150	12	158	12	54.5	4.1	11.1	1.4	0.516	0.069
14	215	12	72.5	4.2	168.3	9.4	160.8	8.2	62.2	4.8	13.3	1.1	0.573	0.061
15	199	10	66.3	3.7	160.2	8.2	140	7.3	59	3.6	13	1.4	0.536	0.05
16	247	15	57.3	3.8	448	29	180	11	66.5	4.4	13.3	1.4	0.904	0.09
17	259	13	59.4	3.1	459	25	186	11	72.1	4.8	13.4	1.3	0.832	0.056
18	213.2	8.3	73.3	3.6	166.5	6.8	153	7.8	59	4	12.5	1.4	0.554	0.053
19	219	10	74	3.4	168	9.4	159.8	8.1	63.1	3.7	12.1	1	0.588	0.049
20	264	29	54.7	4.8	474	56	184	21	67.8	6.5	12.9	2.4	0.851	0.089
21	206	11	79.1	4.2	75.6	4.3	135.7	7.9	53	2.7	13.7	1.6	0.367	0.045
23	207	14	73.5	5.7	160	12	167	13	59.5	4.2	11.8	1	0.538	0.036
24	214	12	74.9	4.1	114.7	6.3	155.4	9.2	58.7	3.8	13.2	1	0.451	0.038
25	215	14	75.2	5.4	168	12	168	12	63.6	5	12.7	1.2	0.564	0.06
26	240	13	68.1	3.4	220	13	170.3	8	66	3.7	13.1	1.5	0.674	0.064
27	213	16	73.8	5.3	167	12	168	12	61.4	4.8	12.9	1.7	0.566	0.065
28	267	14	58.5	3.4	491	26	184	10	70.3	4.7	13.1	1.1	0.897	0.067
29	203	14	73.5	5.2	111.6	9	153	11	59.1	5.6	12.4	1.3	0.448	0.052
30	207	12	70.1	4.4	111.2	7.4	145	9.7	60.6	3.9	13.6	1.4	0.463	0.05
31	201	17	76.7	6.3	116.3	6.3	154	12	58.4	3.3	12.7	2.1	0.46	0.069
32	203	15	70.8	5.3	164	13	152	12	58.3	5.1	13.2	1.3	0.536	0.076
33	233	17	69	4.5	233	16	176	11	63.4	5	13.2	1.6	0.666	0.069
34	233.7	9.8	64.9	2.8	346	13	183.3	9.1	69.4	3.3	13.9	1.2	0.718	0.067
35	250	13	57.4	2.7	468	22	180.6	8.9	69.6	4.6	12.2	1.3	0.901	0.077
36	208	17	75.6	5.5	103.5	9.3	147	11	58	5.9	13	1.6	0.465	0.067
37	199	16	79.5	6	104.8	9.4	155	13	57.7	5.4	12.5	1.2	0.442	0.054
38	267	15	59.8	3	498	24	184.6	9.9	72.1	5.4	14.2	1.3	0.932	0.077
39	249	13	64.9	4.1	335	15	181.9	9.2	72.4	4.3	14.2	1.5	0.805	0.074
40	210	10	69.5	3.3	161.5	7.9	149.7	7.2	61.1	3.1	12.2	1.2	0.496	0.043
41	205	8.8	73.6	3.5	168.3	7.6	157.1	8.1	61.4	3.2	12.6	1.1	0.512	0.042
42	223	11	75.8	3.2	187	10	171.4	9.7	66	3.9	14.8	1.4	0.557	0.06
43	242.6	9.4	62.7	2.5	356	15	178.6	7.7	71.3	3	14.2	1.5	0.766	0.054
44	207	12	76.8	5	106.3	7.5	150	10	58.5	4.1	12.7	1.1	0.531	0.065
45	200.9	9.8	70.5	2.7	94	5.7	138.8	6.9	55.9	4.5	11.8	1.6	0.41	0.041
46	208	13	67.9	4.4	163	12	151	10	60	4.4	12.5	1.1	0.551	0.063
47	205	13	75.1	4.5	115.3	7.3	148	10	60.1	4.3	12.2	1.1	0.459	0.049
48	229	11	69.3	4	234	12	173.3	9.5	64.9	4.2	14.2	1.4	0.684	0.045
49	240	14	65.5	4.1	326	20	174	11	69	4.6	13.7	1.1	0.727	0.067

Table E-15 LA-ICP-MS Elemental Concentration Data: BOR-S2-01 (continued)

Spot #	Gd157 ppm	Int2SE	Dy163 ppm	Int2SE	Yb172 ppm	Int2SE	Hf178 ppm	Int2SE	Pb208 ppm	Int2SE	Th232 ppm	Int2SE	U238 ppm	Int2SE
1	13.1	1.2	13.43	0.82	7.63	0.48	8.46	0.67	40.5	2	28.3	1.5	7.71	0.44
2	11.63	0.8	12.7	1	7.28	0.49	8.05	0.77	36.8	2.2	27.5	1.6	6.74	0.41
3	11.73	0.95	13.06	0.92	7.78	0.33	7.9	0.64	40.6	2.8	28.4	1.4	8.15	0.5
5	12.3	1.3	10.29	0.82	5.59	0.56	8.33	0.73	28.6	2.8	23.6	1.7	4.67	0.56
6	12.3	1.1	13.1	1.1	6.88	0.58	8.53	0.61	33.8	2.2	28.8	1.8	6.53	0.44
7	10.53	0.84	12.3	1.1	6.73	0.58	7.66	0.66	42.2	2.6	25.5	1.5	8.3	0.62
8	11.2	1	12.8	1	7.57	0.76	7.34	0.81	36.6	2.5	27.3	2	7.09	0.55
10	12.27	0.91	11.98	0.91	6.21	0.46	8.58	0.5	34.9	1.8	26.9	1.5	6.08	0.31
11	11.8	0.89	14.15	0.99	8.2	0.73	8.63	0.8	43	2.7	30.4	1.9	8	0.47
12	12.5	1.2	13.14	0.74	7.38	0.54	7.85	0.64	41.4	2.8	28.3	1.8	7.49	0.46
13	10.9	1.2	12.5	1.3	6.86	0.69	7.1	1	48.3	5.8	25.7	2.1	8.7	1.1
14	12.31	0.99	13.4	1.2	7.6	0.62	7.9	0.73	38.1	2.4	29.2	1.9	7.29	0.48
15	11	1	12.58	0.87	6.63	0.4	7.84	0.69	38	2.1	26.5	1.5	6.45	0.37
16	12	1.3	10.82	0.85	5.12	0.42	7.65	0.66	30.1	1.9	23.6	1.5	5.14	0.32
17	11.7	0.96	10.9	0.84	5.95	0.38	8.64	0.58	31.8	1.8	24.1	1.3	5.53	0.33
18	12.2	1.1	13.03	0.79	7.02	0.65	8.76	0.69	35.7	2.2	27.7	1.2	7.46	0.39
19	13	1.1	13.8	1.1	7.39	0.52	7.86	0.58	38.8	2	29.6	1.7	7.5	0.39
20	12.3	1.7	11.3	1.6	5.74	0.97	7.8	1.1	31	3.6	24.2	2.7	4.98	0.69
21	13.8	1	14.64	0.91	8.52	0.59	8.77	0.62	45.6	2.9	30.3	1.7	8.1	0.47
23	12.6	1.1	13.7	1.2	6.7	0.61	7.63	0.77	40.8	3.6	28.8	2.3	7.81	0.57
24	12.19	0.9	14.14	0.92	7.99	0.61	8.61	0.85	40.5	2.9	29.9	1.9	7.53	0.57
25	12.6	1.2	13.2	1.1	7.5	0.59	8.45	0.78	43.7	3.5	29.6	2.4	7.94	0.61
26	13.2	1.3	13.27	0.94	7.56	0.51	9.2	0.6	34.8	2.1	29	1.6	6.33	0.31
27	11.64	0.9	12.8	1	7.12	0.52	7.62	0.69	41.8	2.8	28.3	2.1	8.08	0.68
28	10.76	0.91	10.82	0.73	5.68	0.46	8.03	0.46	30.3	1.9	24.6	1.2	5.12	0.28
29	11.3	1	14.2	1.3	8.08	0.87	8.2	1	41.4	3.3	29.6	2.1	8.19	0.58
30	11.98	0.89	15.4	1.1	8.18	0.67	7.83	0.68	34.4	2.9	29.3	1.9	6.92	0.57
31	11.3	1.3	13.2	1.3	7.36	0.57	6.76	0.76	44.9	3.6	28.3	2.3	8.59	0.7
32	12.3	1.2	12.44	0.97	7.02	0.58	7.81	0.63	42.3	3.4	28	2.2	7.35	0.6
33	12.3	1.1	12.59	0.97	6.72	0.65	7.98	0.63	36.9	2.6	28.2	1.7	6.65	0.55
34	12	1	11.47	0.79	6.31	0.44	7.84	0.68	32.9	1.8	25.7	1.2	5.98	0.34
35	11.11	0.72	10.66	0.63	5.59	0.41	8.22	0.64	30.8	2.1	23.5	1.3	5.1	0.31
36	12.5	1.2	14.1	1.4	8.12	0.74	7.87	0.67	42.9	3.8	29	2.6	8.3	0.72
37	11.3	1.5	13.1	1.1	7.93	0.82	8.01	0.82	48	4.4	28.9	2	9.33	0.65
38	12.2	1	10.9	0.49	6.05	0.39	8.71	0.66	30	1.6	24.5	1.4	5.14	0.34
39	12.8	1.2	12.7	1.1	6.51	0.75	8.08	0.65	32.1	2.2	26.6	1.8	5.73	0.36
40	11.53	0.97	13.8	0.87	7	0.38	7.62	0.45	36.1	1.9	27.6	1.5	6.75	0.37
41	10.96	0.71	13.29	0.87	7.05	0.4	7.55	0.48	40.8	2.2	26.9	1.3	7.46	0.37
42	13.81	0.82	13.79	0.9	7.76	0.51	8.04	0.57	44.3	2.5	30.2	1.8	8.02	0.43
43	12.12	0.99	11.59	0.45	5.99	0.43	7.76	0.5	32.8	1.7	25.9	1.1	5.52	0.35
44	12.5	1.3	13.6	1.1	7.9	0.62	7.87	0.67	42.2	2.9	29.5	2.1	7.92	0.58
45	12.2	1.4	13.8	1.2	8.01	0.61	8.06	0.59	37.4	2.1	29	1.5	7.16	0.35
46	12.3	1.1	13.3	1.2	7.7	0.48	8.35	0.69	36.3	2.4	27.4	1.8	6.65	0.44
47	12.2	1.2	13.87	0.97	7.86	0.63	7.85	0.69	40.7	3	29.4	1.9	7.95	0.54
48	12.17	0.87	12.21	0.96	6.72	0.47	8.24	0.53	35.1	2.1	27.6	1.6	6.55	0.4
49	12.33	0.83	11.76	0.73	6.63	0.51	8.21	0.71	31.9	1.6	26	1.4	5.72	0.36

Table E-16 LA-ICP-MS Elemental Concentration Data: JCS-KMI-16

Spot	Duration	Ca43		Ca44		Ti49		V51		Mn55		Rb85		Y89	
#	seconds	CPS	Int2SE	ppm	Int2SE	ppm	Int2SE	ppm	Int2SE	ppm	Int2SE	ppm	Int2SE	ppm	Int2SE
2	19.1	10750	450	3530	170	770	33	0.27	0.18	266	10	232	10	78	3.2
3	17.8	9600	480	3490	260	824	51	0.60	0.38	296	20	269	22	68	4.4
5	19.1	8480	560	3720	240	788	47	0.25	0.28	316	18	321	22	80	4.4
6	19.1	11770	550	3380	170	736	36	0.04	0.039	262	12	226	11	71	3.2
7	19.1	11420	560	3340	150	734	28	0.02	0.031	258.6	9.9	227	9.6	71	3.3
11	19.1	10400	690	3340	200	621	41	0.11	0.058	278	19	299	18	85	5.5
12	19.1	9610	500	3540	230	795	44	0.14	0.14	278	12	244	15	71	4
15	19.1	11590	620	3350	170	725	34	0.07	0.034	259	12	222	11	71	3.9
18	19.1	11110	500	3520	160	766	33	0.13	0.086	268	12	228	12	74	3.4
19	16.0	10190	520	3650	270	799	46	0.19	0.12	279	17	247	16	74	3.8
20	17.0	9670	710	3700	270	734	52	0.20	0.19	285	23	283	19	77	5.6
21	19.1	10190	600	3440	190	790	45	0.09	0.071	275	13	240	14	68	3.9
22	19.1	10440	570	3440	160	594	27	0.07	0.057	267	11	283	15	85	4.1
23	19.1	10420	620	3360	150	700	31	0.02	0.037	265	13	265	12	76	3.7
24	15.0	11510	690	3350	200	758	44	0.22	0.18	267	17	232	13	70	4.1
25	19.1	9720	490	3750	230	811	45	0.07	0.039	288	15	263	16	73	3.5
26	19.1	10420	480	3520	140	785	35	0.21	0.16	273	14	244	15	71	4
29	19.1	11370	560	3440	180	740	36	0.22	0.23	259	13	230	11	71	3.4
30	19.1	11590	580	3350	150	746	35	0.03	0.032	265	12	230	13	71	3.8
1	14.5	11930	570	3220	140	902	38	0.28	0.36	277	14	160	7	58	2.8
4	19.1	11650	420	3320	130	893	31	0.23	0.16	268.9	9.9	167	8	59	2.7
8	19.1	10920	580	3730	180	956	48	0.13	0.052	303	16	180	10	62	3.4
9	19.1	12070	530	3310	130	886	38	0.12	0.048	281	13	160	7.2	61	2.4
10	13.8	11770	720	3250	210	883	54	0.18	0.08	269	15	167	13	56	3.5
13	11.6	11380	880	3690	330	970	73	0.19	0.095	302	26	193	16	59	4.5
14	11.0	12100	720	3480	250	899	54	0.07	0.042	284	14	169	8.3	60	4.1
16	19.1	9240	500	3210	170	861	59	0.97	0.26	252	15	140	8.3	62	3.7
17	19.1	11730	440	3540	190	929	43	0.33	0.31	288	12	176	9.1	62	2.7
27	12.3	10490	530	3670	290	1068	70	1.40	1.6	354	18	202	8.1	59	2.5
28	9.7	11890	740	3300	200	912	59	1.00	0.83	283	19	168	14	57	3.6
31	19.1	10910	550	3560	200	931	50	0.21	0.12	294	16	169	7.5	59	2.9
32	13.1	9910	600	3670	330	1014	72	0.36	0.19	297	20	182	13	58	4.3
34	19.1	11470	540	3420	170	912	39	0.09	0.031	283	16	174	10	60	3.5
35	11.9	11920	610	3480	180	888	37	0.16	0.057	284	14	169	7.5	60	2.9

Table E-17 LA-ICP-MS Elemental Concentration Data: JCS-KMI-16 (continued)

Spot	Zr90		Nb93		Ba137		Ce140		Nd146		Sm147		Eu153	
#	ppm	Int2SE	ppm	Int2SE	ppm	Int2SE	ppm	Int2SE	ppm	Int2SE	ppm	Int2SE	ppm	Int2SE
2	202	8.8	79	3.2	65	2.9	149	6.5	61	2.8	14.1	1	0.30	0.029
3	177	11	83	6	62	4.7	153	12	52	3.8	10.9	0.84	0.28	0.029
5	179	9.9	91	5.7	31	1.9	149	8.3	52	3.4	11.6	1.1	0.23	0.028
6	186	9.1	76	3.6	61	3.1	141	6.1	54	3.3	11.6	0.97	0.29	0.018
7	184	7	77	3.5	63	2.8	142	6.4	56	2.7	11.7	0.88	0.31	0.026
11	162	9.7	89	5.6	16	1.2	133	8	50	3.3	11.9	1.1	0.13	0.021
12	183	9.8	79	3.9	59	3.5	151	6.8	53	3	12.8	1	0.29	0.032
15	181	9.9	74	3.9	64	3.6	139	7.5	54	3.5	11.7	0.96	0.31	0.032
18	195	8.6	79	3.7	61	3.2	149	7.5	56	3.1	12.2	0.93	0.30	0.025
19	191	10	81	5.3	63	3.9	151	11	56	3.6	12.8	1.4	0.31	0.041
20	175	12	87	6.4	29	1.8	138	9.8	49	3.8	11.4	0.82	0.20	0.027
21	179	9.4	77	4.5	64	4	147	9.5	51	3.1	11.8	1.1	0.26	0.026
22	163	8.1	85	4.1	15	0.99	130	6.3	49	2.5	12.4	0.85	0.15	0.017
23	171	8	83	4	30	1.5	132	5.8	50	2.7	11.9	1	0.19	0.02
24	182	9.5	76	4	57	3	145	7.1	52	3.2	11.7	0.9	0.30	0.031
25	187	9	84	4.5	67	3.6	156	9	58	3.4	12.8	0.99	0.32	0.023
26	187	10	80	4.5	69	3.7	148	7.7	55	2.5	11.8	0.99	0.30	0.026
29	185	9	75	3.6	65	3.3	144	7.4	51	2.6	12.2	1.2	0.32	0.026
30	183	8.7	75	3.7	64	4.3	145	7.6	52	3.1	12.4	0.93	0.29	0.025
1	237	10	62	2.6	207	8.5	172	6.7	67	3.4	12.0	0.76	0.61	0.047
4	231	8.7	64	3.2	244	12	170	7.4	69	3.5	12.5	0.84	0.64	0.038
8	246	12	68	4	224	12	190	9.1	71	4.4	13.7	1.1	0.66	0.051
9	245	11	66	3.2	201	8.8	177	7.4	67	3.4	12.9	0.86	0.59	0.028
10	224	13	62	4	206	13	168	9.5	61	3.9	12.4	1.3	0.59	0.052
13	242	19	70	5.6	249	20	186	14	68	5.7	13.7	1.4	0.65	0.065
14	240	13	65	3.8	229	13	178	10	67	4.3	11.9	0.9	0.64	0.054
16	244	15	60	3.5	219	14	165	11	67	4.5	13.1	1.2	0.60	0.042
17	248	10	67	3.2	225	10	180	8.2	69	2.9	13.5	0.79	0.66	0.045
27	239	13	75	4.7	228	13	197	10	69	4.7	14.0	0.89	0.65	0.059
28	232	14	63	3.7	248	12	180	11	65	3.2	13.4	1.3	0.65	0.041
31	233	11	66	2.9	232	11	178	9	67	3.7	12.2	0.95	0.61	0.039
32	229	14	68	4.5	250	16	183	13	66	5.5	12.2	1.2	0.61	0.069
34	236	14	64	3.3	246	12	175	8.2	67	3	14.0	1.3	0.64	0.052
35	231	10	63	3.5	239	12	173	8.1	66	3.8	11.7	0.63	0.66	0.051

Table E-18 LA-ICP-MS Elemental Concentration Data: JCS-KMI-16 (continued)

Spot	Gd157		Dy163		Yb172		Hf178		Pb208		Th232		U238	
#	ppm	Int2SE	ppm	Int2SE	ppm	Int2SE	ppm	Int2SE	ppm	Int2SE	ppm	Int2SE	ppm	Int2SE
2	11.9	0.75	14.4	0.58	8.0	0.5	7.7	0.45	36.3	1.8	29.4	1.3	8.0	0.34
3	10.3	0.73	12.5	1	7.2	0.63	6.7	0.54	45.5	3.8	26.0	1.7	9.0	0.7
5	12.0	0.78	13.9	0.97	8.1	0.56	7.3	0.53	43.9	2.8	30.5	2	10.9	0.78
6	11.1	0.75	13.1	0.64	7.1	0.42	7.4	0.49	35.1	1.8	27.4	1.5	7.8	0.4
7	11.3	0.8	12.9	0.62	7.4	0.43	7.3	0.41	36.0	1.5	27.5	1.3	7.4	0.34
11	11.5	0.98	14.7	1.1	8.8	0.68	7.0	0.54	42.7	2.8	31.7	1.9	10.3	0.64
12	11.1	0.62	12.2	0.68	7.4	0.55	6.8	0.53	36.7	2.4	27.8	1.6	8.5	0.47
15	10.9	0.85	12.6	0.93	7.1	0.53	7.1	0.53	34.7	2.4	26.9	1.6	7.4	0.41
18	11.7	0.79	13.6	0.73	7.7	0.47	7.8	0.52	37.0	1.8	28.8	1.3	7.9	0.46
19	11.8	0.88	13.4	0.75	7.5	0.59	7.9	0.57	38.9	2.8	28.2	1.9	8.7	0.62
20	11.3	0.98	13.8	1.1	8.0	0.63	7.0	0.52	40.4	3.2	29.6	2	9.7	0.64
21	10.9	0.86	13.1	0.94	7.1	0.43	7.1	0.47	36.8	2.2	26.4	1.5	8.2	0.51
22	11.8	0.77	14.8	0.89	9.1	0.46	7.2	0.45	38.8	2	31.4	1.6	9.5	0.52
23	11.9	0.81	13.8	0.85	8.2	0.47	7.4	0.48	40.5	2.1	29.4	1.5	9.0	0.46
24	10.6	0.83	12.4	0.83	7.0	0.4	7.0	0.43	36.6	2.2	27.1	1.3	7.5	0.42
25	12.1	0.88	12.8	0.87	7.5	0.42	7.1	0.41	40.0	3.1	28.3	1.5	8.5	0.58
26	11.6	0.85	13.2	0.78	7.7	0.53	7.4	0.55	38.5	2	28.6	1.6	8.0	0.4
29	10.9	0.79	12.6	0.75	7.3	0.41	7.5	0.36	35.2	1.9	26.8	1.3	7.5	0.4
30	11.1	0.77	12.6	0.62	7.5	0.38	7.1	0.59	36.2	2.5	27.2	1.7	7.5	0.48
1	11.1	0.74	11.2	0.7	6.1	0.38	7.6	0.41	27.0	1.3	24.3	1	5.2	0.25
4	11.2	0.73	11.1	0.65	6.0	0.34	7.9	0.41	27.4	1.5	23.8	0.98	5.6	0.29
8	11.4	0.72	11.8	0.73	6.4	0.45	8.0	0.61	31.5	1.6	25.5	1.3	5.8	0.32
9	10.9	0.53	11.3	0.59	5.9	0.33	7.7	0.44	27.3	1.5	24.9	1.3	5.3	0.28
10	10.1	0.82	10.6	0.73	5.6	0.43	7.5	0.55	27.1	1.9	22.7	1.4	5.4	0.38
13	11.0	1	11.4	1	6.0	0.53	7.8	0.77	31.5	3.3	24.6	1.9	5.8	0.55
14	11.3	1.1	11.1	0.9	6.1	0.51	7.8	0.47	27.6	1.8	24.0	1.6	5.4	0.42
16	11.7	0.82	11.9	0.84	6.4	0.52	8.2	0.52	23.2	1.5	25.1	1.6	4.9	0.37
17	11.7	0.51	11.8	0.75	6.4	0.35	8.2	0.36	29.1	1.5	25.2	1.1	5.6	0.32
27	10.9	1.1	11.7	0.9	6.2	0.48	8.1	0.72	34.2	2.1	25.6	1.4	6.8	0.48
28	10.7	0.77	11.2	1	6.3	0.6	8.1	0.89	29.0	3.3	23.4	2	5.2	0.41
31	11.2	0.73	11.2	0.71	5.9	0.26	7.8	0.43	28.9	1.7	23.8	1	5.3	0.3
32	10.6	0.82	10.5	0.93	6.0	0.44	7.5	0.62	30.8	2.6	23.5	1.5	6.5	0.65
34	10.6	0.84	11.2	0.81	6.1	0.37	8.3	0.54	30.3	1.7	24.1	1.3	5.5	0.29
35	11.0	0.87	11.3	0.71	6.0	0.49	7.7	0.7	26.7	1.4	24.1	1.3	5.3	0.31

Table E-19 LA-ICP-MS Elemental Concentration Data: MC-CA-01

Spot	Duration	Ca43		Ca44		Ti49		V51		Mn55		Rb85		Y89	
#	seconds	CPS	Int2SE	ppm	Int2SE	ppm	Int2SE	ppm	Int2SE	ppm	Int2SE	ppm	Int2SE	ppm	Int2SE
3	18.4	5680	480	4190	390	1036	94	0.221	0.059	305	27	231	22	65.8	5.3
8	18.4	7260	430	4300	220	837	43	0.014	0.029	276	14	225	11	80.8	4.5
11	18.4	6020	390	4380	300	707	47	0.05	0.033	295	17	310	18	92	6.2
13	17.1	6490	380	3860	240	566	35	-0.008	0.03	266	15	291	15	93	5.3
16	5.2	6310	830	3900	360	720	100	0.011	0.066	284	35	320	46	92	13
17	12.8	6050	330	4210	260	671	44	0.038	0.046	273	13	293	18	89.1	5.3
20	14.4	4160	400	4490	430	818	77	0.16	0.2	310	26	306	31	81.2	8.7
21	18.5	5690	360	4340	290	704	69	0.173	0.05	284	18	257	16	95.6	5.9
25	15.6	6440	340	4150	220	760	43	0.013	0.037	266	15	261	16	79.9	4.6
32	18.4	6210	350	4040	270	745	50	0.023	0.049	266	17	269	19	77.7	4.5
37	18.4	6360	380	4050	260	800	43	0.061	0.041	253	12	223	11	74.8	3.4
43	12.0	7230	500	4210	350	920	66	0.018	0.039	280	21	214	15	68.5	5.7
47	11.2	6660	400	4290	330	872	61	0.011	0.05	280	16	248	13	77.3	5
1	18.4	6720	360	4290	250	1049	61	0.111	0.051	301	18	185	12	61.7	3.7
2	18.4	4410	320	4140	280	1011	70	0.168	0.062	305	19	165	11	58.5	3.8
4	8.1	7510	600	3860	280	894	61	0.8	0.36	276	19	153	13	63.5	5.2
5	8.1	9320	500	3810	290	956	60	0.117	0.059	278	13	149	10	61.5	3.7
6	16.3	6180	300	4030	250	982	47	0.367	0.054	280	13	162.3	7.9	60.5	3.5
7	12.5	6930	430	4160	320	994	58	0.152	0.052	293	17	184	13	60.2	4.1
9	18.4	8470	440	4030	210	985	48	0.081	0.035	284	14	163.4	8.6	61.3	3.3
10	18.4	6770	400	4220	180	1065	60	0.11	0.035	303	17	184.6	8	64.8	3.5
12	8.0	6890	560	4660	350	1100	100	0.185	0.095	331	29	188	18	61.3	5.4
14	9.1	7240	520	3730	250	907	62	0.2	0.13	283	20	171	13	56.2	3.8
15	7.8	7560	500	4080	340	975	51	0.068	0.049	293	15	168	11	65	3.8
18	14.5	8170	340	3980	190	935	49	0.084	0.038	270	12	167.2	5.9	59.8	2.5
22	11.9	6870	510	4300	370	1004	76	0.105	0.05	312	26	180	14	58.2	3.6
23	18.4	7550	330	4040	210	999	41	0.086	0.035	286	14	166.5	7.8	61.5	3.3
24	8.0	6040	710	3550	350	840	120	0.077	0.081	262	35	133	17	66.1	7.2
28	18.4	7010	350	3920	210	948	43	0.218	0.061	277	13	159.8	8.1	64.5	3.1
29	18.4	7060	300	4200	230	1039	54	0.107	0.028	295	14	169.5	7.7	64.6	3.4
30	7.3	6740	620	4140	390	1070	100	0.14	0.14	312	30	184	21	59.2	4.5
31	7.8	7120	660	4280	410	1020	130	0.137	0.06	307	34	195	22	59	6
36	14.7	7040	440	4470	280	1027	76	0.121	0.049	309	20	183	13	58	3.1
38	10.2	6620	550	4170	300	1054	87	0.135	0.061	314	20	185	14	62.4	4.8
39	12.1	6400	430	4730	400	1130	79	0.131	0.047	328	24	199	14	63.6	5
40	13.4	6250	360	4540	350	1091	63	0.117	0.07	324	19	193	12	65.6	3.8
45	18.5	7190	490	3970	270	974	68	0.165	0.041	270	17	163.2	9.5	61.6	4.2
46	10.5	8530	470	3790	250	932	56	0.083	0.041	258	15	152.4	9.2	63.2	3.9
48	5.5	8620	500	3910	200	911	48	0.089	0.072	249	11	144	10	59.5	3.7
49	11.6	7080	610	3750	310	939	76	0.37	0.2	254	19	144	10	58.6	4.5

Table E-20 LA-ICP-MS Elemental Concentration Data: MC-CA-01 (continued)

Spot	Zr90		Nb93		Ba137		Ce140		Nd146		Sm147		Eu153	
#	ppm	Int2SE	ppm	Int2SE	ppm	Int2SE	ppm	Int2SE	ppm	Int2SE	ppm	Int2SE	ppm	Int2SE
3	207	18	81.6	7.6	112	12	145	15	56.1	6	11.6	1.7	0.381	0.053
8	213	12	88.7	4.2	65.4	3.6	154	8	56.5	3.6	11.44	0.86	0.339	0.029
11	181	11	106	6.1	16	1.1	134.9	8	50.9	3.9	12.11	0.96	0.14	0.022
13	155.3	8.7	100.8	6	6.31	0.61	108.1	6.1	44.3	3.1	11.3	1.2	0.097	0.016
16	177	23	101	14	19.3	3.5	130	16	51.5	9.3	11.8	2.8	0.123	0.042
17	173	10	96.3	5.3	14.8	1.7	129.9	7.5	50.9	5.2	12	1.5	0.119	0.025
20	188	19	95	6.7	28.8	4.2	135	14	51.4	6.3	10.2	1.5	0.221	0.028
21	185	12	102.4	7.1	16.7	1.6	131.1	8.9	52.7	4.1	12.4	1.4	0.168	0.028
25	182	11	89.2	5.9	29	2.3	126.3	7.4	49.9	4.1	10.7	1.2	0.228	0.033
32	181	13	87.7	5.4	28.1	2.4	132.4	8.6	48.9	3.7	10.7	1.1	0.219	0.044
37	196	10	80.8	4.4	56.1	3.8	135.5	7	54.5	3.4	10.8	1	0.303	0.032
43	222	16	80.3	7.2	107.7	8.7	148	11	60.8	6.2	11.5	1.2	0.428	0.057
47	194	12	89.9	5.8	62.3	4.3	149	10	55.7	2.7	11.8	1.2	0.358	0.057
1	248	13	74	4.6	210	11	179	10	66.8	4.4	13.6	1.5	0.597	0.062
2	237	16	69.5	4.8	210	15	163	11	61.2	4.1	10.5	1.3	0.58	0.066
4	248	19	66.2	4.5	192	14	155.6	9.2	68	7	14.1	1.7	0.58	0.1
5	243	13	65.8	4.3	201	12	161	11	65	4.4	12	1.2	0.635	0.077
6	242	13	71.1	4.3	210	11	168.9	8.7	64.6	3.4	11.8	1.5	0.604	0.039
7	244	15	73.3	4.9	215	13	174	11	67.9	5.5	13.9	1.7	0.627	0.055
9	244	13	69.3	3.4	227	12	174.4	9.7	68.2	4.2	12.8	1.2	0.598	0.047
10	257	14	74.6	3.8	223	12	187	10	69.2	4.6	12.5	1	0.6	0.049
12	251	24	77.6	7.7	211	26	187	19	67.4	5.6	14	2.4	0.64	0.11
14	238	16	64.5	4.3	216	19	163	15	63.8	6.2	11.9	1.5	0.618	0.097
15	250	15	69.8	4.8	233	13	177	11	68	5.1	13.9	1.4	0.706	0.087
18	234	11	67	2.9	206.4	9.2	161.4	7.8	63.5	2.7	12.6	1.3	0.576	0.047
22	234	15	70.6	5.4	241	18	171	12	64.1	4.7	12.1	1.7	0.66	0.064
23	244	12	70.2	3	236	13	170.3	7.7	65.4	3.7	13.7	1.2	0.663	0.06
24	255	26	57.7	6.8	220	29	148	17	67.9	8.3	14.7	2.7	0.62	0.1
28	262	12	68.7	3.3	202	11	169.5	8.7	67.5	3.7	13.4	1.2	0.589	0.057
29	265	13	73.6	4.1	224	12	182.5	8.2	69.8	3.9	12.84	0.85	0.659	0.055
30	239	25	71	7.6	229	21	178	21	62.5	6.9	13	3.2	0.68	0.11
31	241	26	71.3	7.8	176	17	181	23	67.8	9.2	11	1.6	0.562	0.059
36	233	15	72.1	4.3	196	13	177	11	65.5	3.6	11.4	1.3	0.585	0.053
38	255	16	72.7	5.8	188	11	182	15	68.8	7.2	11.61	0.95	0.663	0.081
39	257	19	79	5.5	233	15	191	14	69.1	5.4	13.1	2	0.579	0.056
40	273	15	79.1	4.1	231	16	192	13	72.1	6.1	14.4	1.7	0.708	0.067
45	246	16	67.5	4.1	243	16	168	11	66.6	5.2	13.7	1.5	0.647	0.056
46	249	16	68.1	4.5	213	14	167	11	65	4.6	14.1	1.3	0.599	0.061
48	236	15	64.6	4.5	221	15	163	13	62.7	5.1	12.2	2	0.67	0.13
49	238	19	65.6	5.1	200	17	160	13	63.9	5.9	11.8	1.5	0.596	0.082

Table E-21 LA-ICP-MS Elemental Concentration Data: MC-CA-01 (continued)

Spot	Gd157		Dy163		Yb172		Hf178		Pb208		Th232		U238	
#	ppm	Int2SE	ppm	Int2SE	ppm	Int2SE	ppm	Int2SE	ppm	Int2SE	ppm	Int2SE	ppm	Int2SE
3	10.8	1.3	11.9	1.2	6.99	0.75	7.76	0.99	34.7	3.8	26	2.5	7.07	0.38
8	11.43	0.63	14	1	8.28	0.53	7.86	0.51	39.7	2	31.2	1.5	7.94	0.49
11	12.5	1	16.6	1.2	9.64	0.85	7.97	0.56	48.6	2.9	33.8	2.4	10.9	0.38
13	11.98	0.92	15.57	0.85	9.28	0.69	7.28	0.59	41.3	2.7	33.8	2.2	10.15	0.9
16	14.6	3.1	15.2	2	9.1	1.6	7.3	1.9	45.7	4.5	31.3	3.4	10.1	0.4
17	13	1.2	14.9	1.1	9.3	0.81	7.35	0.72	45.3	3	32.8	2.2	10.29	1.4
20	12.8	2.2	14.4	1.8	8.32	0.96	6.66	0.81	48.3	6.1	30	3.1	10.3	0.44
21	12.69	0.93	16.2	1.4	9.72	0.86	8.06	0.74	44.4	3.1	35.2	2.4	10.05	1.2
25	12.4	1.1	15.1	1.3	7.92	0.64	7.26	0.81	40.2	2.7	29.3	1.8	8.88	0.61
32	11.7	1.2	13.6	0.98	7.95	0.61	7.75	0.68	40.7	2.8	28.4	1.7	8.58	0.71
37	12.4	1	13.7	1.2	7.93	0.52	7.64	0.69	37.7	2	27.7	1.6	7.22	0.42
43	12.1	1.2	12	1	6.88	0.62	7.43	0.87	36.1	3.8	25.1	2.2	7.05	0.86
47	11.5	1.3	14.5	1.6	8.41	0.8	7.8	1	40.6	2.8	29.2	2.3	8.22	0.35
1	11.9	1	11.31	0.89	6.4	0.55	7.86	0.61	32.8	2.4	25.4	1.6	6.15	0.47
2	11.1	1.2	11.2	1.1	6.4	0.67	7.89	0.71	27.6	2.1	23.1	1.5	5.13	0.47
4	11.6	1.7	11.7	1.3	6.1	0.69	8.3	1.1	29	3.8	24.7	1.9	4.61	0.73
5	11.52	0.72	10.45	0.72	5.91	0.59	7.49	0.73	26.5	2.4	23.8	1.6	4.69	0.48
6	11.14	0.77	10.73	0.66	6.09	0.49	7.76	0.58	29.9	2	24.5	1.5	5.16	0.41
7	11.4	1.3	12.5	1.3	6.26	0.65	7.67	0.71	31.7	2.4	25.1	1.7	5.42	0.32
9	11.7	1.1	11.7	0.79	6.08	0.48	7.97	0.48	30	1.7	24.8	1.4	5.26	0.46
10	11.3	1.1	12.49	0.91	6.5	0.42	8.64	0.69	32.6	1.9	26.7	1.3	6.12	0.32
12	9.9	1.6	11.8	1.5	6.02	0.65	7.9	1	37	4.7	25.6	3.1	6.81	0.7
14	11.3	1.1	11.2	1.1	5.52	0.56	7.72	0.81	29.8	2.8	22.8	1.7	5.05	0.68
15	11.6	1.3	11.94	0.89	6.41	0.46	8.27	0.82	29.5	2.1	24.8	1.4	5.18	0.46
18	11.37	0.99	10.44	0.65	5.63	0.4	8.16	0.56	28.5	1.9	23.4	1.1	5.1	0.6
22	12.1	1.1	10.8	0.94	5.38	0.5	7.72	0.85	33.4	2.9	22.9	1.5	5.76	0.72
23	11.96	0.82	11.54	0.96	5.87	0.38	7.74	0.57	30.3	1.9	23.7	1.1	5.35	0.44
24	12.1	1.3	12.6	1.7	6.64	0.93	8.5	1	23.6	3.6	24.5	2.5	3.85	0.28
28	11.68	0.78	11.57	0.79	6.58	0.54	8.5	0.6	26.8	1.7	25.7	1.3	5.2	0.35
29	12.2	0.87	11.85	0.57	6.82	0.49	8.84	0.6	31.7	1.6	25.9	1.2	5.39	0.31
30	10.8	1.7	11	1.8	5.8	0.67	8.4	1.5	32.2	4.4	24	3.1	5.55	0.3
31	10.8	1.7	10.9	1.2	5.74	0.67	6.99	0.61	34.6	3.1	24.8	2.8	6.16	0.92
36	11.3	1.2	10.87	0.9	6.3	0.62	7.86	0.73	32.6	2.6	24	1.8	5.75	1.4
38	11.51	0.99	10.66	0.88	6.16	0.74	7.9	1.1	33.9	2.9	26	2	5.74	0.45
39	11.5	1.2	12.1	1.1	5.92	0.56	8.73	0.88	36.6	2.5	25	1.6	6.51	0.55
40	13.5	1.5	12.4	1	6.72	0.51	9.19	0.77	35.2	2.5	26.7	1.8	6.27	0.39
45	11.1	1.1	11.39	0.73	5.85	0.46	7.97	0.71	29.7	2.2	24.3	1.6	4.88	1.4
46	11.2	1	11.22	0.99	6.4	0.4	7.96	0.71	26.7	2.7	24.8	1.7	4.95	0.32
48	10.53	0.84	11.4	1.2	6.2	0.93	8.2	1	23.7	2.7	24	2.5	4.76	0.52
49	10.7	1.5	11.5	1.1	5.82	0.43	7.58	0.82	25	2.4	23.3	1.6	4.81	0.55